Åbo Akademi University

Carl-Erik Lange

Hybridisation of pulp fibres with LDH for applications in composites and lightweight fibrous foam

Fibre and cellulose technology

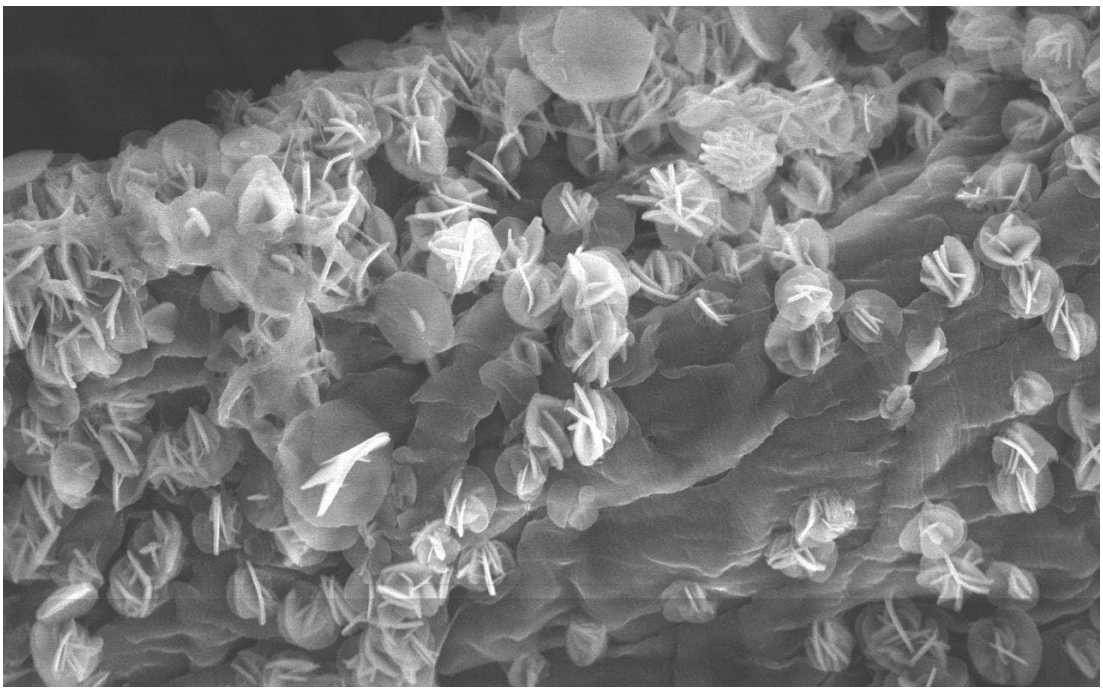

Carl-Erik Lange (Born 1976)

Studies and exams

Masters in University of Turku 2009

Batchelor in University of Turku 2008

PhD dissertation defence in Åbo Akademi 2017

Åbo Akademi University Press
Tavastgatan 13, FI-20500 Åbo, Finland
Tel. +358 (0)2 215 3478
E-mail: forlaget@abo.fi

Sales and distribution:
Åbo Akademi University Library
Domkyrkogatan 2–4, FI-20500 Åbo, Finland
Tel. +358 (0)2 -215 4190
E-mail: publikationer@abo.fi

Hybridisation of pulp fibres with LDH for applications in composites and lightweight fibrous foam

Carl-Erik Lange

Laboratory of Fiber and Cellulose Technology
Faculty of Science and Engineering
Åbo Akademi
Åbo, Finland, 2017

ISBN 978-952-12-3571-9
Painosalama Oy – Turku, Finland 2017

Supervisor

Professor Pedro Edson Fardim
Laboratory of Fibre and Cellulose Technology
Faculty of Science and Engineering
Åbo Akademi University, Finland
&
Department of Chemical Engineering
Faculty of Engineering Science
KU Leuven, Belgium

Opponent

Professor Anil Netravali
Cornell University
Department of Forest Science and Apparel Design
9 St. Joseph Lane, Ithaca, NY, 14850
USA

Reviewers

Professor Anil Netravali
Cornell University
Department of Forest Science and Apparel Design
9 St. Joseph Lane, Ithaca, NY, 14850
USA

Professor Thaddeus Maloney
Aalto University
School of Chemical Engineering
Department of Bioproducts and Biosysytems
Vuorimiehentie 1A, PO.Box 16300, FI-00076 AAL,
FINLAND

Abstract

Carl Lange
Hybridisation of pulp fibres with LDH for applications in composites and lightweight fibrous foam

Thesis for Doctor of Philosophy in Chemical Engineering
Åbo Akademi University, Faculty of Science and Engineering, Turku, Finland, 2017: 82 pages, 46 figures and 16 tables.

The work was carried out under supervision of Professor Pedro Fardim at the Laboratory of Fibre and Cellulose Technology, Åbo Akademi University, Porthansgatan 3-5, 20500, Turku, Finland

Keywords: adsorption, bleached pulp, chemical pulp, combustion, composite, fibre foam, flame retardant, hydrotalcite, layered double hydroxide, mineralisation, nanoparticle, polypropylene, surface engineering, thermogravimetry, thermomechanical pulp.

The research around the pulp and paper (P&P) sector has changed dramatically during the past 15 years. P&P industry is particularly keen to find new solutions for the raw-materials they provide as well as explore novel process technologies. This thesis is a step towards engineering of hybrid materials from pulp fibres and synthetic hydrotalcite (LDH). The purpose was to gain knowledge from the different *in situ* synthesis techniques of LDH with pulp fibres, properties of the prepared hybrid materials and how the hybridised fibres behave in different applications, specifically in a composite and a lightweight fibrous foam.

The hybrid material prepared in this work consisted of either a sulphate pulp (Kraft) or a thermomechanical pulp (TMP), and synthetic LDH particles from hydrated magnesium and aluminium salts. Hybridisation was conducted by three different *in situ* synthesis routes that followed either the preparation of a high super saturated (*hss*) or low super saturated (*lss*) aqueous pulp suspension, or, by the aid of urea hydrolysis (*Uhyd*). It was noted that the hybridisation of hydrogen peroxide bleached TMP pulp of spruce (*Picea abies*) was successful and that the functionalisation of the hybridised fibres with sodium dodecyl sulphate (SDS) was possible if $Mg(NO_3)_2$ and $Al(NO_3)_3$ were applied as LDH precursors. The apparent contact angle (θ) of a sessile water droplet reached 135° upon functionalisation. It is noteworthy that the LDH particle size on fibre surface varied from 70 nm up to 5 µm depending on the synthesis route. Hybridisation of Kraft fibres by urea hydrolysis produced mineralised fibres that expressed lower compliance than the other two synthesis routes. Absorption studies with methylene blue and metanil yellow probe molecules showed that the *lss* route retained most of the fibres' original cationic capacity, but also provided the highest capacity for anions suggesting an ampholytic character of the hybrid fibres. The relatively short aliphatic hydrocarbon chain of SDS on LDH surface was not able to improve the coupling of fibres and polymer matrix in a polypropylene composite. The bottleneck was in particle cohesion. In the lightweight fibrous foam, the *in situ* synthesis of LDH was engineered to include both micron and nano-sized particles by applying *lss* and *Uhyd* synthesis routes. The pulp contained approximately 34% w/w of LDH. Under combustion the amount of CO_2 and soot and the peak heat release rate (PHRR) were reduced significantly. The *in situ* synthesised LDH particles shielded the fibres from external heat by reducing liberation of volatile gases. Effective charring was observed on the surface of LDH nanoparticles.

Synthetic LDH appears as a promising platform to functionalise fibre surfaces. It equips pulp fibres giving them an ampholytic character and reduces liberated heat under forced burning. LDH is also able to mineralise Kraft fibres if the synthesis route is correctly chosen. These characteristics can be further exploited in diverse applications where fibres require ability to absorb both cationic and anionic substances. On the other hand, flammability issues are important whenever the fibres are used in-house applications. Pulp fibre industry can readily apply LDH synthesis into the existing processes and take advantage of the proposed hybridisation. LDH may also be useful in more general terms in fibre technology. The key issue is that LDH formation does not require complex chemistry.

Sammanfattning

Carl Lange
Hybridisering av fibermassa med LDH och dess användning i kompositer och lättviktsfiberskum

Avhandling för doktorsexamen i kemiteknik
Åbo Akademi Universitet, Fakulteten för Naturvetenskap och Teknik, Åbo, Finland, 2017: 82 sidor, 46 figurer and 16 tabeller.

Arbetet utfördes under handledning av Professor Pedro Fardim vid Laboratoriet för Fiber- och Cellulosateknologi, Åbo Akademi Universitet, Porthansgatan 3-5, 20500, Åbo, Finland

Nyckelord: adsorption, blekt massa, fiberskum, flamskydd, hydrotalcit, komposit, sulfatmassa, mineralisering, polypropen, skiktad dubbelhydroxid, termomekanisk massa.

Forskning kring massa- och pappersteknologi (P&P) har ändrat sig betydligt under de senaste 15 åren. Massa- och pappersindustrin har varit särskilt intresserad av att hitta nya lösningar till sitt råmaterial och utveckla nya processteknologier. Detta arbete ger ett tillägg i kunskap till forskningen om hybrid-material innehållande skiktad dubbelhydroxid (LDH) och massafibrer. Avsikten har varit att samla ihop kunskap från olika LDH syntesstrategier med massafibrer, förstå de preparerade hybridmaterialens egenskaper och hur de fungerar i olika användningsändamål, speciellt i kompositer och lättviktsfiberskum.

Hybrid-materialen preparerade i detta arbete innehöll blekt kemisk (sulfat) massa eller termomekanisk (TMP) barrvedsmassa och LDH-partiklar syntetiserade av magnesium och aluminium-hydratsalter, d.v.s. syntetisk hydrotalcit. Experimenten genomfördes med tre olika *in situ* syntesmetoder, d.v.s. låg övermättning (*lss*), hög övermättning (*hss*) och hydrolys med urea (*Uhyd*). Mätningarna visade att hybridisering av väteperoxidblekt TMP-massa av gran (Picea abies) lyckades med den låga övermättningsmetoden (*lss*) och att funktionalisering av hybrida fibrer med surfaktanten natriumdodecylsulfat (SDS) var möjligt om $Mg(NO_3)_2$ och $Al(NO_3)_3$ användes i syntetiseringen. LDH-partiklarnas storlek på fiberytan varierade mellan 70 nm och 5 µm och den största uppmätta kontaktvinkeln för en orörlig vattendroppe uppnådde θ = 135°. Hybridisering av sulfatmassa med *Uhyd*-metoden förorsakade mineralisering så att fibrerns böjstyvhet ökade. Fibrernas karboxylgrupper och aktivt alkali på LDH-ytan kvantifierades med adsorptionsanalyser med metylenblå (MB) och metanilgul (MY) som probmolekyler. Syntetisering av LDH partiklar med lss-metoden behöll det flesta av fibrernas karboxylgrupper som fria men men möjliggjorde också den högsta MY adsorptionskapaciteten vilket påvisade att hybridfibrerna hade en amfolytiska karaktärer. En relativ kort alifatisk ytaktiv kolvätekedja var inte förmögen att stärka bindningen n mellan kompositmaterialets polypropylen och de hybridiserade fibrerna. Flaskhalsen var i partiklarnas låga kohesion. Lättviktsfiberskumet var planerat att innehålla LDH partiklar i både mikroskala och nanoskala. Det var möjligt att inkludera nästan 34 % (vikt/vikt) av LDH till materialet. Mängden av CO_2, den termisk energins frigörningstakt och mängden rök under förbränning minskade betydligt. De in-situ syntetiserade LDH-partiklarna skyddade fibrerna från extern värme genom att minska frigörningen av brännbara gaser. En effektiv förkolning notiserades också vid gränsytan mellan LDH-nanopartiklar och fibrer. Syntetisk LDH framstår som lovande plattform för att funktionalisera fiberytor. Den förser fibermassan med en amfolytisk karaktär och minskar den termiska energin vid förbränning. LDH kan också mineralisera sulfatmassafibrer om syntesmetoden är korrekt vald. Dessa egenskaper kan användas i olika applikationer där fibrer är modifierade för att absorbera katjoner och anjoner. Förbränningsegenskaper är också viktigt att ta i beaktandet när fibrer ska användas inomhus. Det bör poängteras att det är möjligt att implementera LDH-syntesen till redan existerande massateknologi och utnyttja hybridisering. En av LDH-syntesens fördelar är å ena sidan att den inte kräver komplicerad organisk kemi för att implementeras till produktion och å andra sidan fibertyans växelverkan med anjoniska och katjoniska komponenter, med vilka man kan modifiera fiberns ytenergi för att skapa önskade egenskaper.

Tiivistelmä

Carl Lange
Kuitumassan hybridisointi LDH:lla ja sen käyttö komposiitissa ja kevytrakenteisessa vaahtomateriaalissa.

Väitöskirja luonnontieteen filosofiasta kemiatekniikassa
Åbo Akademi, Luonnontieteiden ja tekniikan tiedekunta, Turku, Suomi, 2017: 82 sivua, 46 kuvaa ja 16 taulukkoa

Väitöstyö on laadittu professori Pedro Fardimin alaisuudessa Åbo Akademissa, Kuitu- ja Selluloosateknologian laboratoriossa, Porthaninkatu 3-5, 20500 Turku, Finland

Avainsanat: adsorptio, hydrotalsiitti, kalorimetri, komposiitti, kuituvaahto, mineralisaatio, palaminen, palonesto, polypropeeni, sellu, taivutuslujuus, termogravimetria, termomekaaninen massa

---

Massa ja paperi teknologia (P&P) on satsannut tutkimukseen merkittäviä resursseja viimeisten 15 vuoden aikana. Teollisuus on ollut erityisen kiinnostunut löytämään uusia mahdollisuuksia tuottamalleen raaka-aineelle ja etsimään uusia prosessiteknisiä ratkaisuja. Tämä väitös on askel kuitumassan ja synteettisen hydrotalsiitin (LDH) muodostaman hybridimateriaalin tutkimukselle. Tietoa on luotu erilaisten LDH:n synteesireittien mahdollisuuksista kuitumassan kanssa ja samalla tutkittu miten hybridimateriaali käyttäytyy eri sovellutuksissa, erityisesti komposiitissa ja kuituvaahdossa.

Tutkimuksessa käytettiin sekä kemiallista massaa (Kraft) että termomekaanista massaa (TMP) ja LDH synteesi toteutettiin pääasiassa käyttäen alhaisen ylikylläisen liuoksen tekniikkaa (*lss*), korkean ylikylläisen liuoksen tekniikkaa (*hss)* ja urea hydrolyysia (*Uhyd*). Hybridisaation havaittiin onnistuvan kuusipuusta (*Picea abies*) valmistetulla TMP kuiduilla *lss* tekniikan avulla käyttäen $Mg(NO_3)_2$ ja $Al(NO_3)_3$ lähtöaineita, mikä mahdollisti massan jatkofunktionalisoinnin pinta-aktiivisella natriumdodekyylisulfaatilla (SDS). Funktionaalisoidusta kuitumassasta valmistetun paperiarkin vesikontaktikulma saavutti parhaimmillaan 135°:en suuruuden. On huomionarvoista, että partikkelikokojakauma kuitumassan pinnalla vaihteli 70 nm:n ja 5 µm:n välillä synteesireitistä riippuen. Urea hydrolyysin avulla kemiallisen massan kuidut olivat mineralisoituneet. Kuitujen taivutusjäykkyys kasvoi hybridisaation seurauksena. Absorptio metyleenin sinisellä (MB) ja metaniilin keltaisella (MY) osoitti kuitujen olleen amfolyyttisiä. Anionisten ja kationisten molekyylien absorptiokapasiteetti oli korkein *lss* synteesireittiä hyväksi käyttäen. Suhteellisen lyhyen alifaattisen surfaktantin käyttö hybridisoitujen kuitujen pinnalla ei merkittävästi parantanut kuitujen ja komposiittimatriisin välistä voimansiirtoa vetorasituksessa. Pullonkaulaksi osoittautui partikkelien alhainen koheesio. Kuituvaahto valmistettiin kuitumassasta, johon oli pyritty syntetisoimaan sekä mikro että nanokokoluokan LDH partikkeleita. Kahdessa vaiheessa suoritetun synteesin tuloksena kuitumassan painosta noin 34% oli mineraalia. Palotesteissä kuituvaahdon vapauttama CO_2 määrä, nokipartikkelit sekä savun määrä alenivat merkittävästi. Myös vapautuvan lämpöenergian maksimi oli vertailunäytettä selvästi alhaisempi. LDH partikkelien pinnalla havaittiin hiiltymistä.

Synteettinen LDH on lupaava mineraali kuitumassan ominaisuuksien muokkaamiseksi. Kuidut saavat mm. amfolyyttisen karaktäärin ja tulevat vaikeammin palaviksi. Toisaalta kuitujen jäykkyyteen voidaan vaikuttaa LDH synteesireitistä riippuen. Sovellutuskohteet joissa tarvitaan sekä anionien että kationien absorboitumista materiaaliin voivat käyttää esitettyä menetelmää hyödyksi. Palamisominaisuudet on otettava huomioon, mikäli materiaalia käytetään sisätiloissa. On merkillepantavaa, että esitetty LDH synteesi ja kuitujen hybridisaatio on mahdollista liittää jo olemassa olevaan massatuotantoon sellaisenaan. Avainasemassa ovat LDH synteesin soveltuminen tuotantoon ilman monimutkaista orgaanista kemiaa ja kuidun pinnan aktiivisuus anionisille ja kationisille yhdisteille joilla voidaan muokata mm. kuitujen pinta-energiaa.

List of publications and authors contribution

I Lange, C. & Hultholm, T. & Fardim, P. (2012) *Hydrophobisation of mechanical pulp fibres with sodium dodecyl sulphate functionalised layer double hydroxide particles*, Holzforschung 66:433-441.

II Lange, C. & Touaiti, F. & Fardim, P. (2013) *Hybrid clay functionalised biofibres for composite analysis*, Composites Part B: Engineering 47, 260-266.

III Lange, C-E. & Lastusaari, M. & Reza, M. & Latifi, S.K. & Kallio, P. & Fardim P. (2015) *In situ Hybridisation of Pulp Fibres Using Mg-Al Layered Double Hydroxides*, Fibers 3, 103-133.

IV Lange, C. & Eriksson, J.E. & Lehmonen, J. & Tuominen, M. & Ek, P. & Fardim, P. (2016) *Nanoengineering of Hybrid Lightweight Cellulosic Fibre Foams for better Flame Resistance*, Journal of Nanoscience with Advanced Technology 1(3), 1-13.

contribution: All parts, including writing the manuscripts, excluding experimentation and analysis performed with confocal microscope, ICP-MS, XRD, TEM, single fibre compliance tests, XPS, cone calorimeter and preparation of the micro injection moulded samples and the foamed structures.

List of figures

List of tables

Nomenclature

List of used abbreviations

Abbreviation	*Explanation*
BKraft	bleached chemical pulp (see; Kraft)
BTMP	bleached thermomechanical pulp (see; TMP)
CC	cone calorimeter
CDE	cupriethylene diamine
CTMP	chemi-thermomechanical pulp
DMC	dimethyl carbonate
DP	degree of polymerisation
EDS	energy dispersive spectrum
FCT	Laboratory of Fibre and Cellulose Technology
FRPs	fibre reinforced polymers
FTIR	Fourier Transform Infrared (spectrometer)
GalA	galacturonic acid
H	hexagonal (atomic orientation within a mineral)
HexA	hexenuronic acid
HOMO	highest occupied molecular orbital
hss	high super saturation
HsVid	high speed video recorder
I	intercellular layer, middle lamella
Kraft	chemical pulp, sulphate pulp
L	fibre lumen
LDH	layered double hydroxide
LUKE	Natural Resources Institute of Finland
lss	low super saturation
LDH-lwFF	LDH containing low weight fibre foam
lwFF	low weight fibre foam
MA	maleated co-polymer
MB	methylene blue
MeGluA	4-*O*-methylglucuronic acid
Mg-Al LDH	LDH synthesised from Mg^{2+} and Al^{3+} ions
METLA	Forest Research Institute (now LUKE)
MY	metanil yellow
NPs	nanoparticles
P	primary layer
P&P	pulp and paper
PaPSaT	Pulp and Paper Science and Technology
R	rhombohedral (atomic orientation within a mineral)
R_{MgAl}	magnesium to aluminium atomic ratio
S1…S4	secondary cell walls in a fibre numbered from 1 through 4
SCC	single cation component
SEM	Scanning Electron Microscope

SDS	sodium dodecyl sulphate
Tekes	Finnish Funding Agency for Innovation
TG	Thermogravimetry
TMP	thermomechanical pulp
ToF SIMS	Time of Flight Secondary Ion Mass Spectrometer
Uhyd	urea hydrolysis
w	Wart layer
WPC	wood plastic composite
XPS	x-ray photoelectron spectroscopy
ÅAU	Åbo Akademi University

List of physical symbols

Symbol	*Explanation*	Units
$\Delta_m H_f^\circ$	*standard molar heat of formation*	J
$\Delta_{fus} H_m$	*molar fusion enthalpy*	J
$\Delta_f G_m^\circ$	*standard molar Gibbs free energy of formation*	J
$c(M_{tot}^{z+})$	*total metal ion concentration*	$mol \cdot dm^{-3}$
d	*thickness*	m
ε	*stretch, strain*	%
E_y	*Young's modulus (also: Y_E)*	Pa
F	*force*	N
h	*viscometer constant*	s^{-1}
HRR	*heat release rate*	$kW \cdot m^{-2}$
l	*length*	m
μ	*ionic concentration*	mol
M_w	*molar weight*	$g \cdot mol^{-1}$
mp	*melting point*	°C
n	amount	mol
PHRR	*peak heat release rate*	$kW \cdot m^{-2}$
ρ	*density*	$kg \cdot m^{-3}$
R	*atomic ratio*, *resistivity*	%, Ω
RH	*relative humidity*	%
σ	*strain*	Pa
θ	*surface coverage*	%
T	*temperature*	°C
t	*time*	s
w	*weight*	g
Y_{max}	*deflection limit*	m

Table of Contents

Preface & Acknowledgements

We live in a pragmatic world. The first time I came across that fact was in France in 2005. I had been granted a short-term position in a small cosmetics company C.C.W. Sarl in picturesque Dreux that produced and distributed raw materials to bigger companies such as L'Oréal, Lancôme and others. In one occasion when I was asked to interpret the data from their product my boss came to me with an annoyed expression on his face and said, 'would your wife understand the things that you have written here?' I had mistakenly used in-depth scientific language to explain the rheological properties of their new lipstick base material. So, my boss demanded me to write a cooking recipe for the customers and continued, 'people are pragmatic, Carl!' Thus, I turned my attention to ketchup and honey, yet another embarrassing mistake I am sure. However, that statement remained in the back of my head as a paradigm of our society.

Science is in the core of the researcher's life, but equal significance should be put on one's capability to convey the knowledge to fellow students, professors, colleagues and experts, just as it is important to explain the intricacies of a product to customers in business. Understanding the practicalities of teamwork and collaboration in a multicultural environment will impact to the outcome of the research. The same can be said from time and project management skills and the discussions with industrial representatives and partners.

The scientific work itself is one piece in a big puzzle and a challenge that often emanates from the current economic status and foreshadows the imaginary production trends. There is something the researchers are hoping for the industry to produce and apply in their process or finance in the foreseeable future – this is the imaginary aspect. And the selling pitch is expected to be ambitious. Regardless what the projects proposal says, it ultimately reflects on the one hand the responsibility of a researcher to the partners and the consortium's responsibility towards the society on the other. In such an interphase, it becomes extremely important for the scientist to be able to communicate the results in a meaningful way to everyone. The milestone meetings may be loaded with expectations and, to aggravate, there are two parallel standpoints to conduct the discussions. Either one answers to the questions 'when can we have it?' and 'how much does it cost?' or to the questions 'how does it work?' and 'why does it work?' The former takes the industrial point of view while the latter is of course for academics.

It might well be that the industry nowadays begins to move towards a sturdier attitude and exercise their power through finance as new proposals are being created to obtain answers they like to have. Competition is fierce and the money hunt through grants plays a crucial role in academic life. I thankfully acknowledge that due to our professor I skipped most part of the money hunt, so I never really needed to trouble my head with that issue. However, even if the industrial involvement in academic research is expected and a necessity *de facto*, capital acts like a two-edged sword. I am fully aware of the implications of the power relations involving economics and what they might do for the academic education and to the

freedom of research, but I am also deeply grateful for the industrial partners that invested into my work and made my research possible. The partners in alphabetical order were: Metsä Group, UPM, SAPPI and Stora Enso.

To be honest, somewhere in between the social meaningfulness and roundtable discussion, I sometimes felt that I was left with nothing but a magic-8 ball in my hand to go on. 'Is there any future for what I do?' I asked. 'Ask again later!' seemed to be the answer. A complete blackout of ideas may surmise when a mature technology seeks for innovative approaches and there is no one else to turn to besides oneself. The current situation in academic world would, in my opinion, benefit from rationalisation of the mega trends and from lateral co-operation with the existing resources and infrastructure, but also from implementing synectics into research. In that sense, a fresh breath of air is still needed. Thus, my message to early stage researchers is to build up a good, open and trustworthy communication line with all the partners at the initial stage before going any further with the research. Be fluent with the framework that has been bestowed for you and trust your own instincts and follow the guidelines given by the professor. Be bold, not ignorant.

The experimental work in this thesis was carried out in the laboratory of Fiber and Cellulose Technology at Åbo Akademi University during 2009-2015. I was appointed researcher in the SmartFibre project coordinated by ERA-Net framework and funded by the Finnish Funding Agency for Innovation in 2009. Three years later I was granted a position in the International Doctoral Programme in Bioproducts Technology that was funded for 2012-2015 by the Ministry of Education and the Academy of Finland. The research themes were divided to include the bio-refinery concept, natural fibre products, novel packaging materials, nanotechnology in bio-products, energy applications and process management. My subject was included in fibre products and nanotechnology. From 2013 onwards the experimental work was partially funded by the project PowerBonds, in co-ordination with the WoodWisdom-Net 2 research program, in which I was appointed as a deputy leader for work package one.

The gratitude for my thesis goes to Prof. Dr. Pedro Edson Fardim who was bold enough to take me into his team after my graduation from the University of Turku in 2009. My background being in materials chemistry and chemical analysis I was concentrating in my education on electrochemistry – still a highly relevant and interesting field I must admit – and had little knowledge about pulp and paper engineering. The very first task Prof. Fardim granted me with, as I entered his laboratory, can be summarised with a short Swedish sentence, *från ved till papper*, from a log of wood to paper. Needless to say, I learnt the intricacies of pulp and paper manufacturing through practical work. Prof. Fardim has the ability to encourage and inspire his students. He gives freedom for the "green" scientist to spread out one's wings and he shares the enthusiasm in the advent of new possibilities yet unexplored. In due course, he keeps the student on the ground by reminding that the doctorate work is his or hers own. Indeed, that is an important and practical piece of information from time to time.

I wish to extend my gratitude to several co-workers and colleagues as well. Had I not received help from all of you, I would not have been able to do the necessary work for my thesis. Occasional discussions with Ph.D. Jani Trygg, whom I shared an office with, were refreshing. I am fully aware that those moments when ideas and

questions are thrown impromptu up into thin air may carry a potential distraction within, but I was glad to notice Jani gradually lived up to my example. Some of the colleagues were leaving FCT soon after I entered there, but were nevertheless important in sharing the practical knowledge involved in pulp and paper science. Special thanks for the help during that pivotal transition time go to Ph.D. Risto Korpinen.

Finally, I would like to make a remark that I have taken far too many liberties from my family life in my quest for a doctorate degree. My sincere hope is that I have not robbed too much time from the love of my life, Heidi, and from our two adorable children, Sarah and Ralph.

Turku, Finland, 15.4.2017
C.-E. Lange

1. Introduction

The introduction, or the map if you will, that is provided for the reader expands the items that are presented during the *lectio praecursoriae* and aims to serve as a guide to get acquainted with the big picture behind this scientific work. This thesis is a step towards engineering hybrid materials from pulp fibres and synthetic hydrotalcite. Its background is in P&P technology. While the engineering aspects of chemistry are at the heart of the work, there is also the pragmatic socio-economic context surrounding it. That context is the framework against which the purpose and the reason of the research will become appreciated. Therefore, attention in the following chapters will be first directed to the challenges that were always present and paramount in importance in the life of a chemical engineer, but appear often in the distance for the reader – the big picture.

1.1. Research landscape – the big picture

1.1.1. Academic framework

Åbo Akademi University (ÅAU) has a relatively long history in providing higher education in wood chemistry. The university itself was founded in 1918 and soon after, in 1921, Professor Erik Hägglund established The Forest Products Chemistry. Thirty years later in 1951, Waldemar Jensen was appointed professor in Wood Chemistry at ÅAU and the institute tied up its research to P&P industry through close collaboration with Ralph Erik Serlachius (1901–1980). Serlachius' family were pioneers in paper manufacturing in 19th century Finland and we all remember them by the Serla tissue paper that can still be found on the shelves in supermarkets.

The institute began to grow in a large scale in the early 1970's and by the mid 1980's it had professors in three laboratories. Paper Chemistry was led by Dan Eklund, Forest Products Chemistry by Bjarne Holmbom and the Chemical Pulping Technology by Bruno Lönnberg. All three professors became internationally well-known forest industry researchers, especially Professor Holmbom who received the Wallenberg Prise that was handed over to him and at the same time to Christer Eckerman by King Carl XVI Gustav in 2008.

During the 1980's and 1990's the pulping sector focused mainly on mechanical process and sulphate cooking. These two well-established industrial processes received little attention in the early 2000 that ultimately led to the renewal of the laboratory of Chemical Pulping Technology that changed its name to Laboratory of Fibre and Cellulose Technology (FCT) in 2006. Pedro E. Fardim took over the research with more contemporary focus to match the industrial trends and became the appointed professor after the retirement of Prof. Lönnberg.

FCT has changed markedly since then. Conventional technology with facilities to grind the wood and use chemical cooking to produce paper has transformed by taking bold steps towards more challenging areas. With the aid of state of the art spectroscopic, chromatographic and nanoparticle synthesis instrumentations the current research penetrates fields such as composites, nanoparticles, drug delivery

systems, biomass fractionation and stimuli responsive surfaces still keeping the wood derived fibres in its focus.

The consensus at EU level research and development in 2009 was that bio-based materials should replace, at least in part, the crude oil derived counterparts. Motivation was drawn from the climate change and waste management and, to some degree, from the assumptions of global oil reserves. Studies were concentrating on polysaccharides and particularly on cellulose either in nano-, micro-fibrillated or some derivative form. Therefore, all natural based materials were about to receive unprecedented attention from funding agencies and companies in the EU. Everything was pointing towards long-term sustainability, valorisation of biomass and circulatory economy, and they still are.

In the closer regime, a five-year plan for the Biomass Refinery concept was about to be launched under the ERA-NET collaboration, as a part of a Forest Cluster framework. In one project initiative that was partially funded by the Finnish Funding Agency for Innovation (Tekes), the forest industries were introduced with a SmartFibre concept that aimed to search high-value added products for the P&P sector. The question was whether modern pulping would be able to find novel systems to functionalise fibre surfaces *on site* without tedious chemistry that requires additional installations and investments. The project was carried out in collaboration with FCT and a group from Tampere University of Technology led by Prof. Pasi Kallio who developed a micro robotic instrument to manipulate single wood fibres.

The Smart Fibre concept was aiming to find innovative ways to provide the pulp fibres with stimuli responsive properties and new characteristics. Initial questions were dealing functionalisation in a typical pulp and paper (P&P) production line. For example, which synthesis process steps could be used? How refining and bleaching stages would be affected and which properties could be envisaged for pulp fibres with the given system?

The boundary conditions in paper manufacturing process require low toxicity, aqueous environment and, preferably, FDA approved chemicals. Synthesis kinetics should also match with the station in the production line. Initially the idea was to apply the chemicals at the so-called wet end station. In practice, for example, the additives in paper manufacturing are applied to the pulp sludge during the mixing before the machine screen that precedes the headbox spraying the diluted pulp sludge onto the wire where fibre web forms. Another possibility was to functionalise the pulp fibres at the end of a pulp production line. The system would allow some flexibility in kinetics since a batch process could be envisaged. Also, the functionalised pulp would not need to be used for paper or board alone but in other applications with greater value. Limitations with toxicity would not be as strict as they would be in paper production. Organic solvents and complex chemistry, however, were out of the scope due to large production volumes.

Keeping the manufacturing process preferences in mind, the engineering challenges culminated to hybrid structures that comprise of organic and inorganic phases. The organic moiety carries the function to the system while the inorganic counterpart provides structural features gluing the organic function to fibre surface. Inorganic particles are typically applied with retention aid polymers, but we began to look for a system that could be applied without them. Thus, the main problem

translated into a process that involved *in situ* synthesis of inorganic particles on fibre surface in a batch process.

1.1.2. Economic framework

The operation costs of Åbo Akademi University just as in all the Finnish universities were funded from the governmental budget until 2010. Allocated statutory funds were withdrawn by the government and since then the university administration has been subject to public law. To make the situation easier for the universities they were given a matching fund option for the transition period 2009–2011. For each euro, the universities could collect the government guaranteed 2.5 euros in return. ÅAU was able to gather approximately 5% from the total returns, matching some 34 million euros. The state has announced a considerably smaller total share of 150 million euros for the next funding round that will last until 2017. The change in legislation has pressed universities to actively seek new funding options especially from the EU. It is not a surprise that the research, which eventually receives a "green light" from a funding agency, mirrors the prevailing economic settings.

Companies are affected as well. One of the greatest challenges that the modern paper industry has faced so far, irrespective of the abrupt liquidity in the capital market, is inscribed in digitalisation and information technology (IT). Although the production efficiency owes much to the IT in computerised machinery and robotic technology, modern millennials apply internet, the archetype of collaborative multiverse, so extremely effectively that printed media cannot possibly match with the speed, space or price that is required to move any piece of information from place to place. The bigger the amount of transferred information the greater is the advantage of IT over the printed media. It is difficult to imagine our digital age without the fast news feeds and headlines, written or recorded ones – and completely impossible to write a thesis without digital content. There is no need to call for editors and printing houses anymore to get something published. Wherever people are, the news and information will follow. Anyone can post a blog, letter, message or a tweet and everyone is capable of being a freelancer of the passing moment in decentralised byte space. All that is need is a smartphone and connection to the grid to receive up-to-date news, videos, books, magazines, dictionaries, maps, scientific articles, music and games also. Whether it is for fun or educational purposes does not matter, since everything is delivered with a fraction of price and time of what it used to take. And the real boom, the internet of things, is yet to emerge.

Not that everything related to IT should bring a rainy forecast with it, there are societal factors affecting positively the forest industry's downbeat pulp and board economy. While more and more people rise from poverty for a better life, the advancing technology necessitates the delivery of goods for customers around the world in a process that calls for better, more ecological and economical solutions as well as recyclable, lightweight and eco-friendly ways to replace the non-renewable counterparts. Forest industry and particularly the packaging sector is able to answer this demand. Tissue paper has a bright future as well, since the sanitary products become necessary due to urbanisation in developing countries that used to dwell in poverty. Diapers fall into that category too. Also, still in many cases the readers prefer printed books over the "kindle" versions, something that did not pull through in

masses, albeit newspapers and magazines have become gradually less lucrative. The external pressure from the society, but also from the competitors, serves as a motive power for the research. The search for cost effective, nontoxic and environmentally benign solutions without compromising the quality of the product is, however, a challenge.

The Finnish forest sector's business cycle review provided by the Forest Research Institute (METLA) – nowadays a part of The Natural Resources Institute of Finland (LUKE) – forecasted taunting 25% cutbacks in timber, plywood, and paper and board demand on average in 2009 [1]. That was just after the global downturn that took place in September 2008. The greatest losses were predicted for P&P sector. The production of bleached sulphate pulp was estimated to be reduced by 25% and export to be cut by 30%. The average selling price was assumed to receive similar trends (Figure 1.1). Paper and board prices were expected to rise by some 8% due to necessary drop in capacity. The outcome of the downturn that had actually started already in 2007, and in the pulp sector even earlier than that, was quite clear for everyone. The depth and the length of the distress were not.

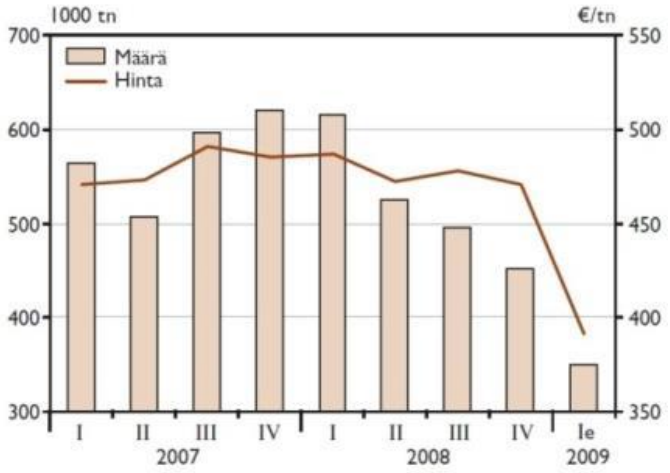

Figure 1.1 The gross export (bars) of bleached sulphate pulp in thousands of tons (left axis) and average price (right axis, red line) in yearly quadrants from 2007 to 2008 and its estimation (e) for 2009 in Euro per ton. Adopted from the Finnish forest sector business cycle review 2009 [1].

The LUKE report was hitting quite close with its predictions for 2009. Paper production has been forced to reduce its capacity in order to match the production costs with the demand (Figure 1.2). However, there has been an improvement in economic situation in the board manufacturing and pulping sector throughout the forest industry (Figure 1.3). For example, from the total sales in 2006 Stora Enso received 2/3 from the paper grades and 1/4 from packaging while in 2014 the same figures were approximately 1/3 and 1/3 respectively [2].

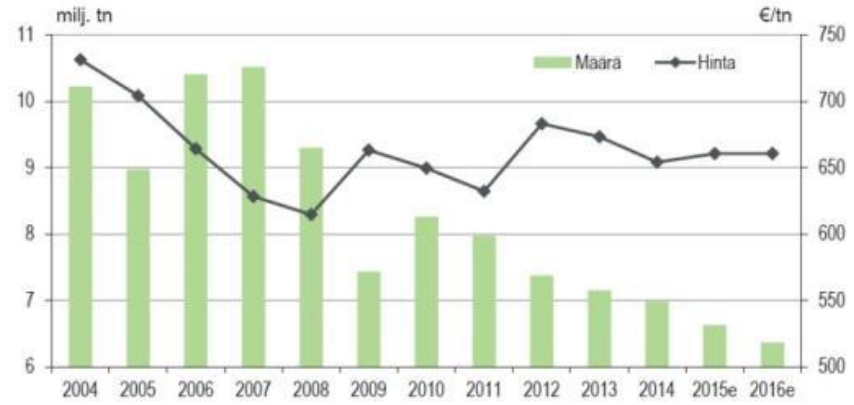

Figure 1.2 The gross export (green bars) of paper (bleached sulphate pulp) in millions of tons (left axis) and average price (right axis, blue line) between 2004 and 2014 and its estimation (e) for 2015 and 2016 in Euros per ton in Finland. Adopted from The Natural Resources Institute of Finland business cycle review [3].

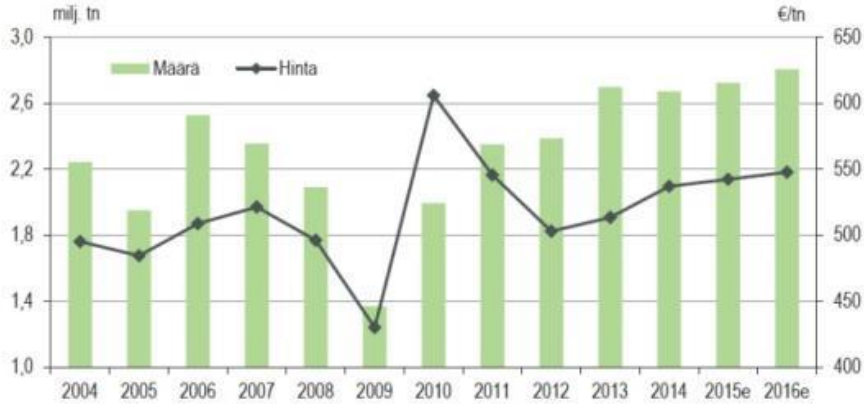

Figure 1.3 The gross export (green bars) of sulphate pulp in millions of tons (left axis) and average price (right axis, blue line) between 2004 and 2014 and its estimation (e) for 2015 and 2016 in Euros per ton in Finland. Adopted from The Natural Resources Institute of Finland business cycle review 2015-2016 [3].

1.1.3. Recent situation

Considering the main wood producers there are the Nordic countries, Russia and Canada, which hold the greatest resources for the softwood species (pine and spruce) and the tropical and subtropical areas in Latin America that produce large quantities of eucalyptus hardwood. The three most common wood species in Finland are spruce (*Picea abies*), pine (*Pinus sylvestris*) and two types of birch (*Betula pendula* and *B. pubescens*). Pine and spruce are softwoods, so-called cone bearing evergreens, while birch that flowers belongs to deciduous hardwood species. In the latest inventory that

was made in 2013, the amount of wood ripe for felling according to The Natural Resources Institute Finland was approx. 1200 million m^3 of pine, 650 million m^3 of spruce and 350 million m^3 of all deciduous trees [4]. The area covered by the forests in Finland is about 73%, while from the annual growth about 70% is used. Undoubtedly the widely-recognised knowledge in wood science and Finnish P&P manufacturing along with the sustainable forestry and good infrastructure are the keys for utilisation of the *green gold*.

New ventures in biomass fractionation will bring new chemical feedstocks to replace some of the global fuel capacity and fine chemicals demand. Although the news about large shale gas deposits, e.g. under the UK and the US seem to benefit fracking process – although regulations are yet to emerge. Besides, the low crude oil prices, currently slightly lifting its head, impart pressure on prices of renewables. A profitable future is, however, seen in disposables, tissue, hygiene, packaging and textile manufacturing, as already mentioned [2]. As a ripple effect, the packaging market affects the self-adhesive label production that went up as expected during 2015 [5].

The green gold gained considerable attention within EU politics that, as it were, forced forest industries to aggressively seek new revenues from their side streams and megatrends [2,6]. The focus in general has been on bio-based polymers, bio-composites, packaging materials and biofuels, which cover nicely the important societal sectors, namely the feedstock for fine chemicals, construction and transportation. The situation in the forest sector does not look all that bad, especially, since we now know that during 2015 the forest sectors invested over 650 million euros in Finland alone [7]. Also, the Chinese-owned Kaidi announced a billion-euro bio-refinery investment in a small northern town, Kemi. Other areas in which business is developing include carbon fibres and nano-crystalline cellulose production [8,9].

The bio-based polymers production is not meeting the global demand, but for the current situation, from 5.2 million tonnes we are, according to the Nova institute survey, in a good path to triple the production by 2020 [10]. The share for bio-plastics in 2012 was about 15% of the global market [11]. The so-called wood plastic composites (WPC) have caught consumers' attention as well. Typical WPC applications include decking, technical parts, automobiles, siding and fencing and furniture. For example, UPM's ProFi deck board takes advantage of label production waste and has been in consumer markets already for a decade. The plastic components in the mentioned products are often poly vinyl chloride (PVC), polyethylene (PE) or polypropylene (PP). These three matrix polymers take the greatest share by volume in global plastic manufacturing.

In the fuel sector Inventia in Sweden is actively involved in research and developments of jet fuels from wood-based materials, particularly from lignin, and UPM has invested into bio-diesel production with some 120 million litre annual capacity – a small drop in a big bucket. Currently at EU level within the horizon 2020 framework, there are approximately 2800 projects dealing at least with some parts of bio-economy. In this regard, the life of a Northern chemical engineer in the biomass sector is looking reasonably bright.

1.2. Wood and pulp

The focus in this chapter is on physical and chemical characteristics of pulp fibres. Functionalisation methods are discussed briefly.

1.2.1. The physical and chemical characteristics of wood pulp fibres

There are two different industrially important pulps in focus. The properties of the fibres and tracheids of those pulps are governed ultimately by the separation process and subsequent chemical treatments. Therefore, the wood microstructure and the common disintegration processes are explained as the discussion is funnelled towards the fibre's composition and properties.

The word fibre is often used to indicate the wood fibres as well as tracheids. Tracheids, as the name implies, conduct water and nutrients in wood, but at the same time they serve the purpose of supporting the structure of softwood just as fibres do in hardwood. It is also important to understand that wood pulp is composed out of different types of fibre-like structures. There are ray cells, parenchyma cells, early wood and late wood fibres as well as vessel elements that can only be found in hard wood (Figure 1.4). The pulping process also creates flakes, ribbons, threads and particle-like fine structures especially in mechanical pulping.

Wood is a natural composite. The main characteristics common to all fibres in sap wood are the intercellular middle lamella (I) that glue all the fibres together, the mesh or cage-like primary layer (P), two or three structurally important secondary layers (S1-S3) and the possible gelatinous layer (G) that is different in hardwoods and softwoods and occurs in fibres that are subjected to tension during the growth season (Figure 1.5). A thin wart layer (w) on the lumen side is also depicted in the schematic illustrations, but it cannot be found in spruce wood [12,13,14,15]. Ray cells, vessels and parenchyma cells are structurally different from the fibres.

The dimensions of fibres and the thickness and structure of cell walls and their chemical composition differ from species to species and vary within the wood according to the location in the stem, growth seasons, environment, geographical location and the possible interruptions in normal growth [16,17]. Greater differences are observed in the two broad categories, i.e. whether hardwoods or softwoods are being studied, than within the genetic order. Averaged dimensions and fractional compositions within the cell wall are presented in table I.1.

The two disintegration processes that produce pulp from wood are broadly categorised into mechanical and chemical pulping. Mechanical pulping is used for cheap products such as newspapers and card board. Chemically separated fibres are applied in magazines, labels and products that benefit from high base paper brightness.

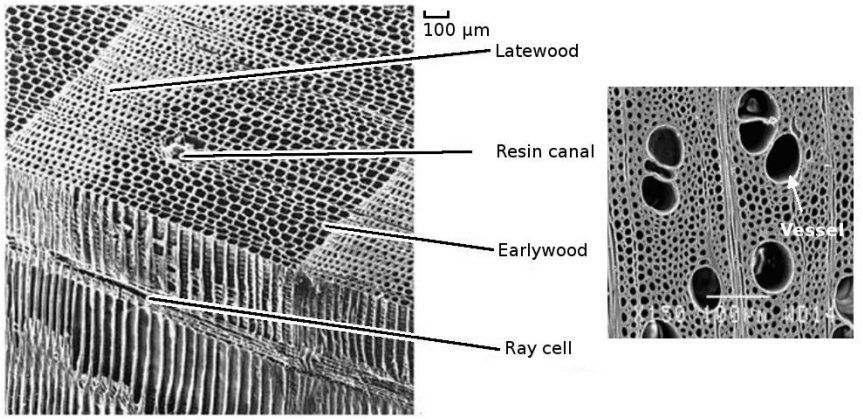

Figure 1.4 SEM micrograph from a pine wood sap showing some of the cell types and their distribution within a wood. Adopted from [18]. The SEM image on the right shows an example of sugar maple (a hardwood) and the size of the vessels. Adopted from http://theses.ulaval.ca/archimede/fichiers/23336/ch03.html.

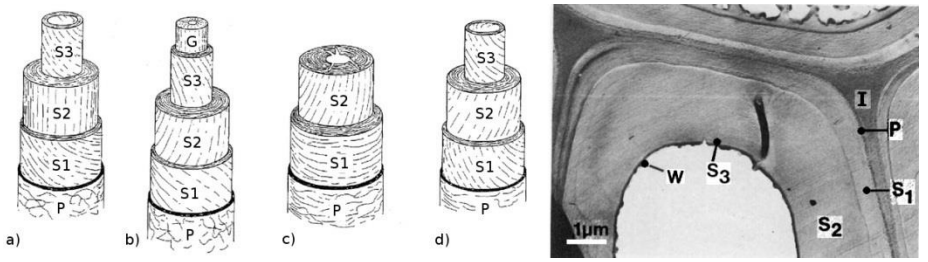

Figure 1.5 Schematic illustrations of normal hardwood (a), tension hardwood (b), normal softwood (c) and tension softwood (d) fibres. The lines indicate cellulose microfibrillar angles in each layer. Adopted from [19]. A TEM image of ultrathin transverse section from a hardwood fibre (Fagus crenata) is shown on the right. Intercellular layer, i.e. middle lamella (I), primary layer (P), secondary layers (S1-S3) and wart layer (w) are marked. Adopted from [20].

Table I.1 Selected physical dimensions and characteristics of mature wood fibres. Layer thickness and fibre width range (d), fractional composition (ϕ), fibrillary angle relative to the fibre axis (α), fibre length range (l) and the aspect ratio (r) calculated from the average length and width (r = l/d). Values adopted from [15,21].

Source	d (µm)	ϕ (%)	α (°)	l (mm)	r
P	0.23 - 0.34	7.0 - 14.2	-	-	-
S1	0.12 - 0.35	5.2 - 10.8	50 – 90	-	-
S2	1.77 - 3.68	73 – 84	10 – 30	-	-
S3	0.10 - 0.15	2.7 - 4.2	50 – 90	-	-
Picea abies	21-40	-	-	1.1-6.0	~135
Pinus sylvestris	14-46	-	-	1.8-4.5	~105
Betula pendula	18-36	-	-	0.8-1.8	~50

Fibres that are mechanically separated contain most of the constituting polymers, especially lignin, and heteropolysaccharides, but also pectin as well as some extractives and inorganic material [12,22] (c.f. table I.1). The two most common mechanical defibration processes are the grinding of logs against a ceramic stone and the disc refining of prefabricated chips in between the metallic discs of a defibrator. A process in which water steam is applied to plasticise the wood under pressurised conditions during the defibration is called a thermomechanical pulping process (TMP) [23]. The fibre damage is deliberate (Figure 1.6). For example, fibrillation is beneficial for the fibre to fibre interactions that lead to stronger paper due to increased surface area that will be available for mechanical interlocking and hydrogen bonding. Fibres become more flexible as well. In comparison to chemical pulping, the mechanical process is generally characterised by higher yield (approx. 98%), lower fibre web strength and higher consumption of electrical energy running the large stones and refining discs [24,25]. The benefit of mechanical pulp is the high volume to mass ratio that is advantageous for board and packaging manufacturing especially in the case of chemi-thermomechanical pulp (CTMP) production. High opacity that allows for production of cheaper and thinner paper is also beneficial. Fines that are generated in high numbers and typically defined as small fragments below 20 microns in all dimensions, provide scattering of light that makes the paper look brighter. Fines also densify the fibre web [26].

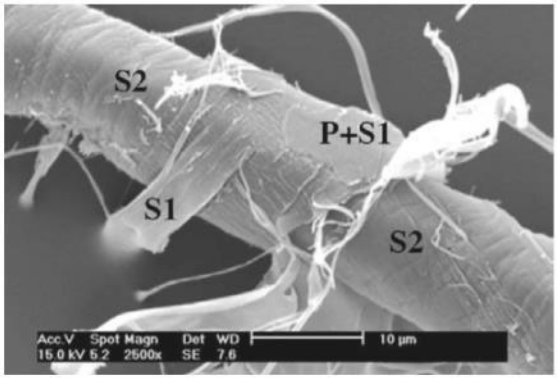

Figure 1.6 Different exposed layers in thermomechanical pulp fibre from spruce wood. Adopted from [27].

Kraft cooking is by far the most common chemical separation process in pulp production. It is characterised by a loss of the intercellular layer and primary layer. The process will also affect partially the S1 and S2 layers that reserve most the fibre cell wall volume.

The raw material in Kraft cooking is loaded into a digester that contains the reactive chemicals of NaOH and Na_2S. Fibres become impregnated by the chemicals with the help of steam. The cooking process is carried out at a relatively high temperature, around 140–170 °C for 2 hours [28]. Chemical pulping aims to remove the lignin from the pulp without damaging the cell wall structure physically. Although majority of the lignin is removed in the Kraft cooking, some 2–5% will

remain as quinone structures that have conjugated double bonds and very high absorption coefficients. Quinones are responsible for the reddish-brown colour of pulp fibres prior to bleaching [29,30]. During the subsequent bleaching reactions, the unwanted double bonds will be oxidised. The Kraft process in general produces pulp that has low yield (approx. 50%), low opacity (i.e. it allows light to pass through) and low volume to mass ratio (i.e. it has rather high density) [31,32]. However, the fibres have a strong inter-fibre hydrogen bonding ability.

The three major components in wood fibres, namely, lignin, cellulose and hemicelluloses are distributed throughout the cell wall structure in different proportions (Table I.2). Middle lamella (i.e. intercellular layer) is composed of lignin, pectin and hemicelluloses giving elasticity to the wood structure. The primary layer is also made from lignin and pectin, but some hemicelluloses and small amounts of cellulose (~ 5% w/w) that are distributed in a mesh-like fashion within it can be found as well (c.f. Figure 1.5). Going towards the lumen side the hemicelluloses and cellulose content increase in relation to the lignin (Figure 1.7).

Table I.2 Average compositional fractions of the five major constituting compound classes in wood are listed. Cellulose (C), hemicelluloses (HC), lignin (L), extractives (E) and inorganic residue (R) [21].

Source	C (%)	HC (%)	L (%)	E (%)	R (%)
Picea abies	41.7	28.3	27.4	1.7	0.9
Pinus sylvestris	40.0	28.5	27.7	3.5	0.3
Betula pendula	41.0	32.4	22.0	3.2	1.4

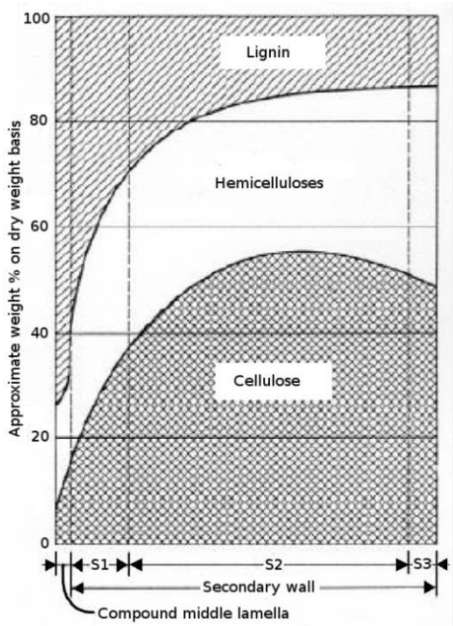

Figure 1.7 The approximate fractional composition of three main components in wood fibres according to [33].

Cellulose serves the wood by being responsible for the microstructural features of different cell wall layers and it is the major contributor to the overall physical characteristics as well. For example, the cellulose microfibrils govern the fibre's elastic modulus that increase as the microfibrillar angle tends towards fibre axis (i.e. gets smaller), although the relationship is not linear [34,35,36]. The upper boundary for elastic modulus in softwood holocellulose and bleached Kraft pulp has been found to lie between 20 and 80 GPa, while the lower boundary is approximately 20–35 GPa [35,37]. Holocellulose contains all the constituting hemicelluloses and cellulose, but lignin and extractives have been removed, whereas Kraft fibres still contain small amounts of lignin, but are missing some of the hemicelluloses. The two samples, according to the authors, were not markedly different from each other in a statistical sense, which suggests that the small amount of residual lignin or changes in hemicellulose content in the fibres do not significantly affect the elastic modulus. Furthermore, the microfibrillar angle of cellulose in laboratory prepared hand sheets is found to govern the tensile strength, stretch and stiffness [38]. The cellulose microfibrillar rotating orientations around the fibre axis are known to alter in the different cell wall layers. Some 2 - 6 fibrillary lamellae of the S1 layer, for example, are alternating between left and right-handed directions. The angle changes inward towards the fibre axis in transition from the primary layer to S2. In the S2 layer, the fibrils are right-handed and directionally the same throughout the layer thickness [15]. In the S3 layer the fibrils are again rotating in alternating fashion while the angle is directed more towards the fibre radius (c.f. Figures 1.5 and 1.6) The degree of polymerisation (DP) of cellulose polymer in a fibre is within 10 000 glucose units, which converts to approximately 5 μm in length [39]. The DP will drop during cooking and may be as low as 500.

Hemicelluloses are often grouped to include all heteropolysaccharides, but the main constituting ones in softwood Kraft pulps are arabinoxylan and galactoglucomannan, while in the case of hardwoods the reference is made to glucomannan and glucuronoxylan (Table I.3) [22]. Xylan is known to redeposit on Kraft pulp fibre surface during the cooking process and requires concentrated alkali in order to be removed afterwards [22]. Along with the cellulose microfibrillar angle, the Xylan has been found to influence the fibre's hygroexpansion, a property that dictates the fibre swelling at different humidity conditions [38,40]. The DP values for hemicelluloses are generally lower than for cellulose and may reach a length of 300 units [39]. Structurally, the hemicelluloses have been noted to increase tensile stiffness [41].

Table I.3 Average fractional compositions of the main polysaccharides and lignin in selected wood species, in hardwood and softwood in general, and, in the Kraft pulps. L = lignin, C = cellulose, M = mannans, X = xylans. Fully bleached, calculated as % from the initial weight prior to cooking. Values adopted from [22,32,42,43]

Source	Yield (%)	L (%)	C (%)	M (%)	X (%)
Picea abies	-	27.4	41.7	16.3	8.6
Pinus sylvestris	-	27.7	40.0	16.0	8.9
Betula pendula	-	22.0	41.0	2.3	27.5
Softwoods	-	21-31	32-49	11-26	6-8
Hardwoods	-	14-33	33-51	1-4	15-30
Kraft (softwood)	46-50	< 1	40-43	2-4	3-4
Kraft (hardwood)	46-50	< 1	36-42	< 1	7-12

The influence of lignin is accounted to its inherent properties but also to its distribution within the fibre walls. Since lignin is known to reside in between the cellulose microfibrils in the secondary cell wall, the removal of it will necessarily increase the flexibility of fibres as the stress transfer in transverse direction will subside. That will directly affect the fibre's compressing behaviour and to the response under micro level deformations during pulping [44,45]. Lignin is also known for its plasticising effect in wood matrix especially at higher temperatures and it is highly viscoelastic compared to cellulose and heteropolysaccharides [46,47,48]. For example, higher amount of lignin accounts for the higher amount of energy that is needed in refining to achieve optimum fibre web density [49]. Proofs exist that lignin is covalently bound to heteropolysaccharides at least to some degree via uronic acid esters in spruce wood fibre cell wall [50,51]. The higher the number of methoxy side groups in phenyl rings, the more the crosslinking ability of lignin will be hindered [52]. Regardless of the possible cross links, the glass transition temperature appears to be independent from other components in the fibre cell wall, wherefore the wood fibre can be modelled as a composite in which the lignin seems to act, at least in major part, as an individual component [53]. It is noteworthy that the glass transition temperature of lignin as well as hemicelluloses depends on the relative humidity, as depicted in figure 1.8.

Increased lignin content is found to reduce the tensile stiffness of anisotropic Kraft pulp fibre webs [40]. It should be noted, however, that the high stiffness of cellulose in direction of fibre axis – especially upon possible hornification – influences elasticity, and the level of refining leads to changes in paper density through the number of inter-fibre hydrogen bonds that also contribute significantly to elasticity [54]. It is also meaningful to consider the fibre’s orientation with respect to the direction of applied stress. In an anisotropic web, however, that is not a concern.

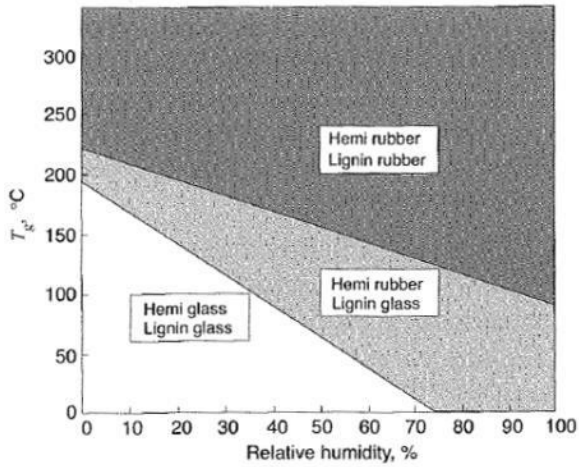

Figure 1.8 Simplified glass transition diagram of lignin and hemicelluloses. Adopted from [48].

Pulp fibres also contain non-diffusing charges that in the case of Kraft fibres originate from carboxylic functional groups present in heteropolysaccharides, lignin and in cellulosic back bone. In heteropolysaccharides the charged groups are 4-*O*-methylglucuronic acid (MeGluA) and hexenuronic acids (HexA) [55,56]. The HexA components are created from MeGluA during the several bleaching stages and contribute to the charge in final Kraft pulp to a greater degree because of prolonged Kraft cooking [57,58]. The residual guaiacyl and syringyl type lignin fragments contain carboxylic acids due to ring opening reactions that take place in the electrophilic bleaching process [59]. These acids, although low in quantity, may contribute significantly to Kraft fibres' overall charge [57]. Also, the reducing ends of polysaccharides may be oxidised to aldonic acids that induce surface charge on pulp fibres [56].

Non-diffusive ionic groups in untreated mechanical pulp fibres are mainly MeGluA and galacturonic acids (GalA) from hemicelluloses and pectin structures respectively. To a lesser degree e.g. in spruce wood, there are arabinogalactan linked glucuronic acids [58,60,61,62]. The theoretical ratio for glucuronic acids vs. galacturonic acids in untreated spruce TMP fibres is close to 3:1 [61]. The fines in mechanical pulp contribute to the overall charge significantly through their large surface area. For example, the effect of hemicelluloses on pulp fibres' surface charge is considerably smaller than the effect of fines when studied by polyelectrolyte adsorption [63].

Several methods have been devised to estimate the fibres' bulk charge but the most reliable ones appear to be the conductometric titration and methylene blue adsorption [64] (Table I.4). Other methods have been noted to either underestimate the content of anionic functional groups in fibres (e.g potentiometric titration) or overestimate them (e.g. polybrene adsorption) [65]. The anionic groups on the fibre surface have been investigated by labelling them with methylene blue and measuring the quantitative signal of nitrogen by means of x-ray photoelectron spectroscopy (XPS) [58]. Since the electrons originate only from the imminent surface ($d \leq 10$ nm),

it is possible to distinguish the surface-bound label molecules and, thus, quantify the charge from the bulk (Table I.4). Bulk charge in TMP and CTMP may vary between 150 and 200 µmol/g [66]. Surface charge at 10 nm depth remains below 3% from the total and over 60% of the charge resides within 1.0 µm depth.

Table I.4 Number of anionic groups by methylene blue adsorption expressed in concentration (C_{MB}) and by conductometric titration (C_{Cond}) from unbleached and total chlorine free bleached Kraft pulps and the specific amount of non-diffusive anionic groups at fibre surface (n_S) and in bulk (n_B). Values adopted from [58,64].

Source	C_{MB} (µmol/g)	C_{Cond} (µmol/g)	n_B (µmol/g)	n_S (µmol/g)
Pine Kraft	81 ± 3	79 ± 2	-	-
Pine Kraft, bleached	43 ± 6	45 ± 1	-	-
Birch Kraft	130 ± 6	124 ± 2	-	-
Birch Kraft, bleached	64 ± 5	66 ± 3	-	-
Spruce TMP	-	-	96 ± 5	1.0
Spruce TMP, bleached	-	-	183 ± 7	1.5

The carboxylic functional groups influence many important parameters in pulp and paper manufacturing such as ionic interactions, cell wall swelling, refining response, sheet and floc formation, water uptake of paper and its tensile strength [56,64,67,68,69,70].

It is well known that the refining and chemical treatments affect the fibres' porosity. The cell wall becomes semi-permeable, allowing diffusion of ions and small polymers into the cell wall due to removal of lignin and heteropolysaccharides and inclusion of physical defects [71,72,73,74,75]. There is some controversy in literature on how large the pores on the fibre's surface and in the cell wall exactly are, but the maximum seems to be within 80–100 nm (Figure 1.9) [76,77,78]. The variance in results may be attributed to different measurement techniques and the mechano-chemical history of the fibre material [79]. Generalisations can be made in that earlywood fibres appear to be more porous than latewood fibres and refining seems to open up the fibre structure through cell wall delamination even after possible hornification [80,73]. Swelling characteristics have a profound effect on pore volume and chemical reactivity [81,82]. Spruce wood fibres do not contain macro-pores, wherefore the formation of those is attributed to delignification [79]. In addition, within reasonable ionic concentration (μ) the cell wall structure remains relatively constant but the swelling begins to decrease, if $\mu > 100$ mM [83].

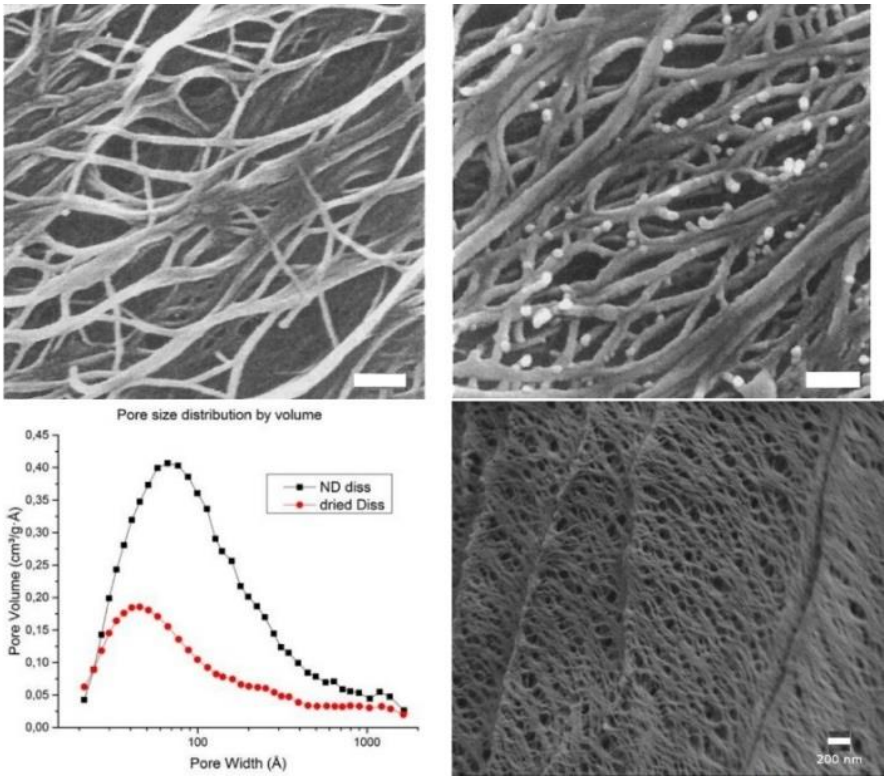

Figure 1.9 SEM micrographs from pores on unbeaten softwood Kraft pulp fibres after freeze drying (upper images). Scale bar equals to 100 nm. Adopted from [78]. The pore volume to pore width relationship in dissolving (diss) dried and non-dried (ND) hardwood pulp fibres and the corresponding SEM micrograph (scale bar = 200 nm) of ND is unpublished data provided by courtesy of Professor Thaddeus Maloney, Department of Forest Products Technology, Aalto University School of Chemical Technology, Espoo, Finland.

1.2.2. Functionalisation of pulp fibres

Functionalisation in chemistry may equally refer to a molecular level synthesis, specific material characteristics and to the usefulness and practicality of the material that is designed for a certain application. In the case of pulp fibres, the reference is often made to a molecular level surface modification. Common examples include grafting of co-polymers [84,85,86], polyelectrolyte adsorption [87,88], plasma gas treatment [89,90] and enzymatic treatments [71,91,92]. Apart from molecular level functionalisation, inorganic particles in different size range can be used for surface modification as well [93,94,95,96,97].

Inorganic particles in traditional P&P production are used as pigments. Minerals such as Kaolin ($Al_4Si_4O_{10}(OH)_8$), Talc ($Mg_3(Si_4O_{10})(OH)_8$), $CaCO_3$, $CaSO_4$ and TiO_2 are frequently used in coated papers. The rationale for using these inorganic materials stems from gained improvements in paper quality in terms of gloss, brightness, opacity, porosity, bulk, ink absorption and printability [98]. The shape and size

distribution of the particles are different from mineral to mineral as are their physical characteristics such as hardness, refractive index and density.

Because wood fibres are naturally acidic and the pigment particles either neutral (e.g. $CaSO_4$, TiO_2) or cation exchangers (silicates), there is a requirement to use binders to fix the inorganic minerals onto the fibre surface. In P&P the binders are usually starch or latex, especially styrene-butadiene based polymers [99]. It is noteworthy that the pigments and retention aids or binders are applied in a form of paste onto the ready-made fibre web and, thus, changes (e.g. stiffness, porosity, hydrophobicity) are anticipated on the fibre web level instead of individual fibre level [100]. In a way, the final product comprising the fibre network (i.e. the base paper) and surface coating resembles a laminated composite.

There have been attempts to fill the pulp fibres with minerals already in 1950's and some patents have appeared describing different methods of achieving high mineral loading [101,102,103,104,105]. The patents are all related to precipitation of $CaCO_3$ while the strategies vary. Pulp fibres have been loaded e.g. by transferring gaseous CO_2 into an alkaline Ca^{2+} ions containing solution and by allowing the fibres to swell in $CaCl_2$ solution that is followed by dissolution of Na_2CO_3. Patented methods also included utilisation of reactive CaO in alkaline CO_3^{2-} solution and dissolution of different Ca^{2+} salts in a pulp suspension that was made alkaline with ammonium carbonate. The method that involved *in situ* impregnation of fibres with a soluble $CaCl_2$ following precipitation with Na_2CO_3 gained some acceptance [106] and a similar strategy was recently applied in mineralisation of wood blocks to improve their flame-retardant ability [107]. Flame retardant wood was treated for 24 hours in a vacuum impregnation system in order to fill the lumens and cell wall pores with $CaCl_2$ and dimethyl carbonate (DMC). Subsequently, an excess of 1M NaOH was added to demethylate DMC leading to precipitation of $CaCO_3$ and generation of methanol and sodium chloride. The method seems to offer an alternative to mineralisation of entire wood structures as long as the size allows vacuum impregnation.

There have been discussions about nanoparticles (NPs) and their applications already for a few decades, but harnessing them for research and development involving wood-derived fibres is still in its early phase, although many interesting applications are emerging rapidly. Research is, however, concentrating more heavily on textile fibres and reeds. Patents that describe applications for nanoparticle containing wood fibres take advantage of materials such as ZnO for coatings [108], silica for laminates and boards [109,110] and various oil repellent clays [111]. Academic research covers catalytic TiO_2 and noble metals [95,112,113], antimicrobial copper [96] and magnetic Fe_3O_4 [114]. Nanoparticle suspensions are often stabilised by anionic ligands, wherefore the substrate must be converted to cationic prior to NP synthesis or the loading is achieved by the aid of cationic polymer such as polyethyleneimine [95,112,113,115,116]. In some cases, the substrate porosity is exploited as well [114].

1.3. Layered Double Hydroxides

This section covers the historical background of layered double hydroxides (LDHs) and reviews the mineral more closely, presenting the principles for the stacking sequence, thermodynamics and decomposition phenomena. Some applications are also given that exploit LDH in industrial scale.

1.3.1. Historical background

Several authors agree on the first encounter with the mineral that became known as hydrotalcite as described by German scientist Carl Hochstetter in the *Journal of Practical Chemistry* in 1842 [117,118,119,120]. It appears that Hochstetter received the mineral from a mineralogist, and it was said to accompany the steatite from Snarum, Norway [117]. The name steatite (στέαρ, *fat*) arose from the palpable feeling as if the mineral had a greasy surface. While C. Hochstetter was undoubtedly first in reporting about the new mineral, the exact origin has different accounts in literature. Whether the mineral originated from Zlatoust in the Urals or from Snarum in Norway, we can assume that there were two separate minerals traveling under the names völknerite and steatite. Albeit they shared identical chemical composition, one of them was named *hydrotalkite* (i.e. hydrotalcite) because it physically resembled talc and contained considerable amounts of water. Talc is a typical silicate (SiO_4), comprising significant amounts of magnesium oxide (MgO) in its structure.

1.3.2. Structural features of LDH

At the beginning, particular interest in the research was placed on the quantitative composition, which was true to all new minerals found at the time. Hochstetter apparently thought that the mineral under study was an aluminate, but Frondel laid out several examples for the dispute that prevailed during the first few decades after the discovery [120]. Some researchers, however, held the view that the steatite of Snarum as well as the völknerite and hydrotalcite were all identical minerals as first claimed by R. Hermann in 1849 [118,121]. Analogous minerals were found elsewhere. For example, the houghite, so named in honour of F.B Hough, an American scientist and pioneer in forestry, was found from Sommerville, New York shortly after Hochstetter's report and identified to belong to the hydrotalcite group [120,122]. Others insisted that the hydrotalcite is a hydrated oxide, just as Hochstetter suspected, arguing that the original mineral was a mixture of gibbsite, magnesite and brucite [120]. Gibbsite is an aluminium hydroxide ($Al(OH)_3$) that contains water of crystallisation, magnesite is magnesium carbonate ($MgCO_3$). Brucite is pure magnesium hydroxide ($Mg(OH)_2$) that also contains water of crystallisation. Yet others, such as J. D. Dana and R. Hermann maintained that the mineral is an alteration of brucite structure. They assumed that some of the mineral's magnesium atoms had been replaced by aluminium. It is worthwhile to note that the CO_2 that was constantly found to be present in the samples was overlooked for a long time as a constitutive part of the mineral.

It was allegedly the work of an Italian professor Ernesto Manasse that clarified the composition of hydrotalcite in 1915 [120,123]. He was also correct in assuming that the hydrotalcite was comparable to pyroaurite, a ferric (Fe^{3+}) analogue of the

hydrotalcite. Foshag concurred that the described hydrotalcite was a basic, viz. metal hydroxide containing carbonate [119,124]. Although the analysis unequivocally established that the original mineral was not talc-like metal oxide, the name hydrotalcite persisted and has been preserved for a particular type of LDH due to historical reasons. The chemical formula for any LDH can be written as shown below, in the chemical formula 1 (f1). In that formula, the M represents the metal atom and A is the counter ion. The hydrotalcite, the one that E. Manasse reported in 1915, is represented with the same notation in chemical formula 2 (f2).

$$\left[M^{II}_{1-x}M^{III}_{x}(OH)_2\right]^{x+}\left(A^{z-}_{x/z}\right)\cdot yH_2O \qquad (f1)$$

$$[Mg_{0.75}Al_{0.25}(OH)_2]^{0.25+}(CO_3^{2-})_{0.125}\cdot 0.5H_2O \qquad (f2)$$

A great deal of structural analysis has been put together from 1920 onwards, thanks to the development of X-ray crystallography. It took some time, however, before the intricacies of hydrotalcite and some of its analogues were fully elucidated [120,125,126,127]. Nowadays there are over 40 naturally occurring minerals identified under the hydrotalcite super group and many more, even ternary and quaternary LDH structures have been synthesised [128,129,130,131]. Moreover, there are the so-called non-charged hydroxy double salts that are structurally analogous with LDHs [132].

X-ray analysis has revealed that the hydrotalcite-like minerals' solid layers diffract the incoming radiation by appearing similar to the brucite that is solely built from hexagonally arranged hydroxides around a magnesium cation (Figure 1.10). While the hydroxide ligands define the shape of the complex, the unit cell of the brucite crystal is framed by the metal atoms that occupy the octahedral holes in the complex. The two white arrows in Figure 1.10 denote the two different edges of a unit cell parallelogram observed by looking directly along the c-axis that is orthogonal to *111* (*hkl)* surface of a face centred cube. The triangle that is drawn on top of each hexagon marks the vertices of those hydroxyls that are on the same plane with each other. Because all of the hydroxyls are hexagonally close packed around the cationic centres, each one of them shares its molecular orbitals with three metal ions, so that the net chemical formula becomes $Mg(OH)_2$.

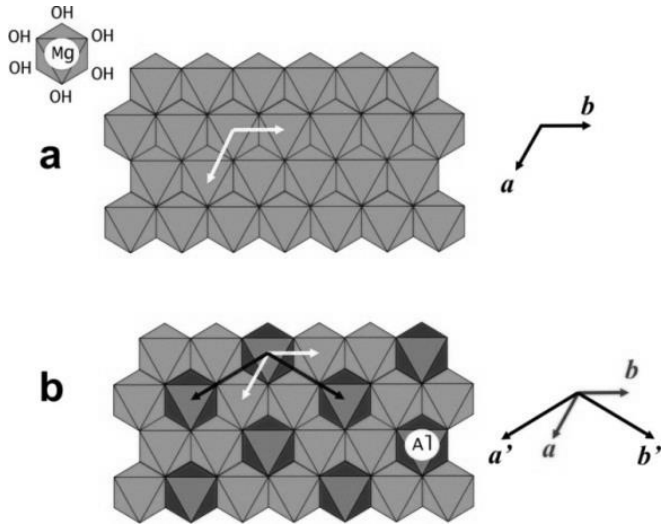

Figure 1.10 Octahedral brucite layer presented in z direction a) and the Al^{3+} doped layer b). Adopted from [133].

Some of the Mg^{2+} cations in LDH crystal layer are substituted with trivalent cations that grant extra positive charge for the two-dimensional (2D) sheet (Figure 1.10). Thus, the LDH incorporates anionic molecules that are said to intercalate into the crystalline structure and fix them in place to balance the charge. With the anions, water is often included. Substituting the Mg^{2+} with other divalent metals creates a lattice that is called a *hydroxy double salt*. These comprise a group of non-charged LDH that are outside the scope of this thesis. The LDH abbreviation is preserved for charged layered structure alone.

Structural anions in LDH are electrostatically bound as outer sphere complexes that are exchangeable. Another brucite type layer is therefore able to form next to the first 2D sheet and share its molecular orbitals with the intercalated anions creating a three-dimensional (3D) structure for LDH. The anionic species and water molecules are sandwiched almost as if a confined film between the doped brucite layers. Theoretically calculated diffraction pattern for the rhombohedral (R-3m) and the synthesised Mg-Al LDH $(Mg_4Al_2(OH)_{12}NO_3(H_2O)_3)_{0.5}$ are shown as an example in figure 1.11. The magnesium to aluminium ratio (R_{MgAl}) is 2.0.

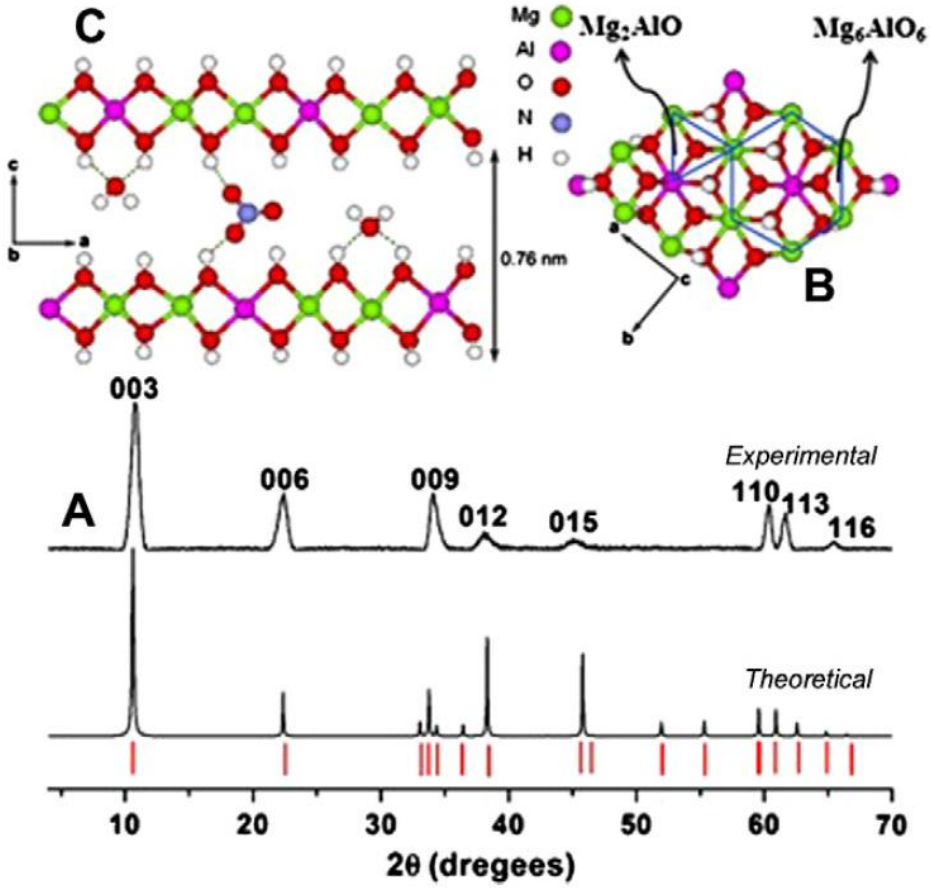

Figure 1.11 (A) Theoretical and experimental XRD patterns of NO_3-LDHs, $R_{MgAl} = 2$. (B) Top views of a simulated hydroxide layers with Mg/Al repartition and (C) Computational model of layered double hydroxides (LDHs) formulated as $(Mg_4Al_2(OH)_{12}NO_3(H_2O)_3)_{0.5}$. Adopted from [134].

The work of Bookin, Drits and Cherkshin established the notation for the polytypes observed in LDH structure [135,136]. They concluded that the X-ray diffraction intensity was highly dependent on stacking sequence and arrangement of cations, while the interlayer anions dictated over the unit cell parameters. Different layer stacking sequences were divided into 2 and 3-layered hexagonal (H) as well as to 3 and 6-layered rhombohedral (R) polytypes in *111* direction, i.e. in the c-axis (Figure 1.12) [135]. It is interesting that the two chemically identical naturally occurring manasseite and hydrotalcite minerals have adopted the two layers hexagonal (2H) stacking sequence and the three-layer rhombohedral (3R) sequence respectively [127].

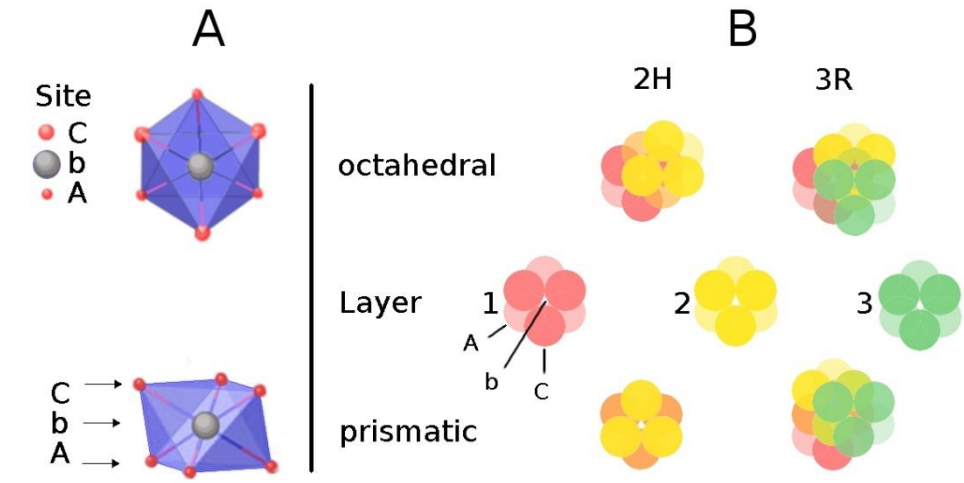

Figure 1.12. Representation of $M^{II/III}(OH)_6$ crystals, the site labels and examples of 2H and 3R stacking sequences. (A) Two orientations for the same crystal are illustrated, showing the oxygen atoms in red and the metal cation in grey. The site labels A and C correspond to the locations of the oxygen atoms while b is for the metal centre. (B) Stacking sequence is illustrated with semi-transparent discs. The lighter shade appears further from the viewer (site A) while the darker shade is closer (site C). Metal cation occupies the octahedral hole (site b). Overlaid brucite layers are shown with additive colours.

Some controversy appears in literature as to whether the inorganic cations are homogeneously distributed within the layers or not. Chemically the cation avoidance rule, i.e. the repulsion of similar charges dictates that the M^{III} ions cannot occupy the neighbouring octahedral holes. By doing so, sever lattice strain is introduced to the mineral [137,138,139]. To satisfy the cationic repulsion rule the minimum value for M^{II}/M^{III} ratio in the chemical formula is 2 and the maximum is 4. Therefore, the x in the same formula (f1) is between $0.20 \leq x \leq 0.33$. However, both high (0.50) and low (0.07) ratios have been reported in the literature [140,141]. It is noteworthy that there are several difficulties in determining the exact value for x since the crystalline phase may easily become contaminated with ternary components during the synthesis [138,139]. In the case of the two most common and well known LDH cations, Mg^{2+} and Al^{3+}, the proportional factor x tends to 0.25 ($R_{MgAl} = 3$) at least in hydrothermal synthesis [139]. If the proportional factor differs strongly from the optimal 0.25, the mineral phase includes $Mg(OH)_2$ ($x = 0.18$) or $Al(OH)_3$ ($x = 0.4$) [142].

The brucite layers may adopt different stacking sequences based on the intercalated anion. For example, carbonate containing synthetic LDH structures are often reported to stack according to the 3R sequence with prismatic orientation of hydroxyls, allowing efficient hydrogen bonding with the oxygen atoms in CO_3^{2-} [127,139,143]. If the interlayer anion is hydroxyl, the stacking may adopt octahedral symmetry of the same sequence [144]. In that case, both the cations as well as the hydroxyls are placed in staggered position in each successive layer. Newman et al. showed that the solvothermal synthesis route at relatively high temperatures favoured

the staggered positions, but noted also that the mineral contained CO_3^{2-} and OH^- anions. In addition, the proportionality constant *x* is assumed to have an effect in stacking sequence [139]. For example, if the cations are far from each other as in the prismatic 3R structure, the crystal is expected to have lower energy according to the cation exclusion rule. Therefore, it has less strain in the layers. In comparison, the prismatic 2H has all the cations on the same axis.

The stacking order may become inhomogeneous for many reasons. Quite often the contribution for the shift in *00l* diffraction pattern is associated with the interstratification, in which several different layers and stacking orders may be intergrown to form a single crystal. The turbostraticity that refers to extent of randomness in oriented layers is yet another type of structural anomaly [145,146,147,148,149,150]. Co-precipitation synthesis of metal hydroxides may lead to tailing of *01l* and *10l* peaks that are identified as intergrown rhombohedral and hexagonal polytypes [137] (Figure 1.13). The reason for the tailing peak shape is apparently in interactions between the intercalated anions and the adjacent brucite-type layers [139].

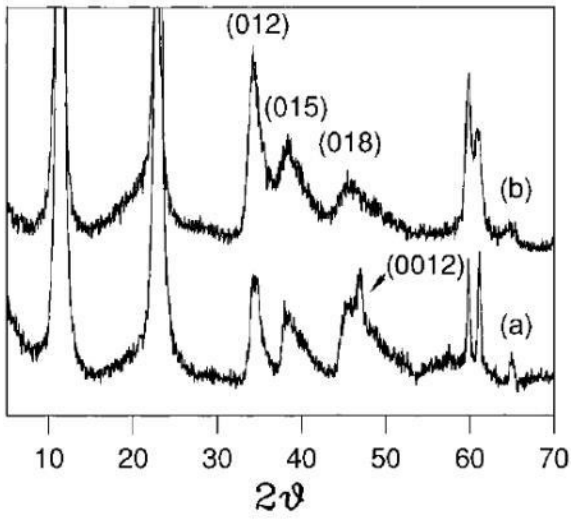

Figure 1.13 XRD peak broadening by disorder in stacking arrangement. Adopted from [137].

1.3.3. Chemistry of LDH

To understand how the LDH behaves, it is also important to understand the fundamental thermodynamics of them. The solubility of the LDH in aqueous solutions in different pH is reviewed. The effect of the interlayer anions and cations on the calculated enthalpy and Gibbs free energy is discussed also. Thermal decomposition phenomenon is briefly explained.

It had been proven already in the 1930's and again later in the 1960's by titration of an aqueous solution containing Al^{3+} or Fe^{3+} nitrates and Mg^{2+} in a form of alkaline MgO that the buffering effect of $Mg(OH)_2$ formation appears at lower pH than expect, i.e. below pH = 9.7 [151,152]. In the case of Al^{3+}, the buffering plateau appeared at pH 8.8, while with Fe^{3+} the precipitate pH was 9.2. The X-ray diffraction analysis

revealed that the precipitate at the titration plateau was LDH. Buffered solution contained amorphous particles indicating that the LDH structuring had taken place. The formation of LDH was thermodynamically favoured over the brucite crystal. Solubility products obtained at different μ also concurred that stability of the LDH was higher than the corresponding divalent hydroxide, i.e. $M^{II}(OH)_2$. The solution pH for stable LDH containing Ni^{2+}, Co^{2+}, Zn^{2+} or Mg^{2+} were 8, 9, 10 and 12 respectively [153]. The trivalent cation in the study was Al^{3+}. Also, in pH titration with NaOH, the thermodynamic stability of LDH with $M^{II}Al$ and $M^{II}Fe$ cation pairs with Cl^- as a compensating ion, has been found to increase in the order: Mg < Mn < Co ~ Ni < Zn [154]. The order follows the solubility equilibrium (pK_{sp}) values for hydroxo- ligand formation [155,156]. It was noted, however, that in alkaline titration the trivalent hydroxide formation appears before the LDH. The formation of LDH is not a single step process.

The stability of different mono- and divalent anions was first established by Miyata [157]. He studied the monovalent series of nitrate intercalated LDH and found the stability to degrease in the order: $OH^- > F^- > Cl^- > Br^- > NO_3^- > I^-$. Two divalent anions were tested and the carbonate was found to be more stable than the sulphate. Adsorption capacity experiments on calcified Mg/Al-CO_3^{2-} LDH proposed a sequence for anion stability to decrease in order: $SO_4^{2-} > F^- > HPO_4^{2-} > Cl^- > B(OH)_4^- > NO_3^-$ (Figure 1.14) [158]. Experiments were performed in 50 mmol concentrations. In aqueous SO_4^{2-} containing solution the adsorption of chloride ions has been found to be inhibited, and the affinity of CrO_4^{2-} over the sulphate is attributed to its lower solubility [159]. In the case of uncalcified Mg/Al- CO_3^{2-} LDH, the anion exchange has been proven to be impractical [158,159,160].

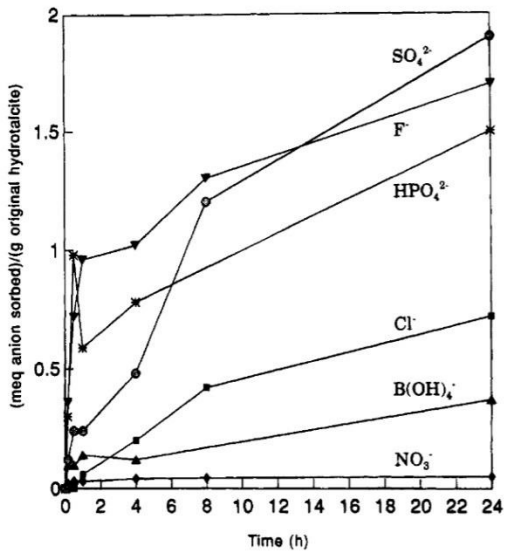

Figure 1.14. Adsorption of ions on calcified Mg/Al-CO_3^{2-}. Adopted from [158].

In a recent experiment with the Mg/Al-NO_3^- LDH, Prasad et al. demonstrated through a fairly simple electrochemical system that singly charged anions are

thermodynamically favoured over divalent ones [161]. The anion exchange was examined with respect to the intercalated NO_3^- on Pt electrode between 1 mM and 100 mM range. Anions were exchanged in the order: $F^- > Cl^- > Br^- > NO_2^- > SO_4^{2-} > NO_3^- > CO_3^{2-}$. The incorporation of carbonate ions that appeared thermodynamically unfavourable with respect to nitrate and sulphate was explained by lability of other ions in terms of hydration enthalpies associated with the outgoing ion. Proof exists that the greater the hydration energy is for the outgoing ion the more labile it is [162,163].

The LDH exhibits variable swelling properties that can be divided roughly into three types [164]. Type 1 is expandable, type 2 is slightly expandable and type 3 is practically non-expandable with little or no water within the interlayer structure. Examples for each of these are $Mg_3Al - SO_4$, $Mg_3Al - ClO_4$ and $Mg_3Al - Cl$ respectively. Some anions allow considerable swelling. For example, the citrate in the LDH gallery is expandable causing the basal spacing to change from 8.9 Å up to 18.9 Å with relative humidity [165]. In practice, contraction of the basal spacing is observed if the anion exchange involves carbonate, while nitrate brings about swelling of basal spacing due to incorporation of water and the change in molecular orientation [166]. Some studies claim that the Cl^- induce basal expansion as well [150]. Affecting factors are related to the shape and size of the anion, and the probability for sharing its HOMO electrons.

Computational molecular dynamic studies of the LDH structures verified the experimentally observed results that the lowest energy level is achieved when Mg/Al molar ratio is 3 (i.e. $x = 0.25$) [167]. The simulation also proved that the band gap energy was at the lowest with intercalated hydroxyl anions. The unit cell volume was found to be largest at the same ratio in the studied 1H and 2H stacking sequences. These calculations were performed assuming non-hydrated layers. Cautli and Ireta concurred recently with the findings, showing that the number of hydrogen bonds between the brucite type layers and the intercalated anions dictated over the energy barrier needed for anion exchange [168]. The lowest energy barrier was found for intercalated hydroxyl with $R_{MgAl} = 3$. Their study included the 3R stacking sequence.

There are few attempts to calculate the standard heats of formation ($\Delta_m H_f^\circ$) and Gibbs energies of formation ($\Delta_f G_m^\circ$) for different LDH structures. This is probably due to laborious experimentation, variety of the LDH in terms of chemical and structural composition, number of available methodologies and the extensive amount of predetermined thermodynamic data required for calculating those values from the chosen starting materials.

The current view is that the thermodynamic trends can be evaluated reasonably well by using simple constituting hydroxides, also referred to as single cation components (SCC) approach. These starting materials include the $M^{2+}(OH)_2$, $M^{3+}(OH)_3$ and $M^{2+}(A^{n-})_{2/n}$. The related enthalpy is referred to as $\Delta_m H_f^{SCC}$. The enthalpy is interpreted as a change in internal energy of the LDH mineral with respect to the single cation components. Usually, for the $Mg(OH)_2$, the tabulated values are chosen from brucite structure, while in the case of Al the reference is made to gibbsite and α-Al_2O_3. For metal carbonates (MCO_3), the enthalpy of calcite mineral is used.

An extensive work by Bravo-Suárez et al. indicated that the best thermodynamic approximations are achieved via the SCC [169,170]. The results from different

models that were proposed did not differ markedly from each other. Nevertheless, the SCC method was chosen for the $\Delta_m G_f^\circ$. The equation is shown here.

$$\Delta_{f,M1} G_m^{SCC}\{\mathrm{T}, LDH\} = \left(1 - \frac{3x}{2}\right)\Delta_f G_m^o\{\mathrm{T}, \mathrm{M^{2+}(OH)_2}\} + (x)\Delta_f G_m^o\{\mathrm{T}, \mathrm{M^{3+}(OH)_3}\} + \left(\frac{x}{2}\right)\Delta_f G_m^o\{\mathrm{T}, \mathrm{M^{2+}(A^{n-})_{2/n}}\}$$

In the equation, the standard molar Gibbs formation enthalpy ($\Delta_f G_m{}^0$) values in predetermined temperature T requires, as shown, the stoichiometric constants to adjust the salt composition of divalent cation M^{2+} with the intercalated anion A^{n-}. Proportionality factor x has its usual meaning (cf. p. 22). Enthalpies are calculated similarly.

Mazeina et al. studied $\Delta_m H_f^\circ$, $\Delta_m H_f^{SCC}$ and $\Delta_m G_f^{SCC}$ of green rust, an important mineral in soil and corrosion chemistry with four different Fe^{2+}/Fe^{3+} compositions, each containing sulphate as counter ion and variable stoichiometric amounts of water [171]. The $\Delta_m H_f^\circ$ values were found to be -1040 and -1080 kJ/mol regardless of the stoichiometric composition. Entropy related term was under -7 kJ/mol. Since there are two different ferrosulphates, the calculations were based on $FeSO_4$ and its hydrated form, the $FeSO_4 \cdot 7H_2O$ that is commonly found in soils. Although the absolute values differed, the trend remained similar.

Using a drop solution experiment, in which the LDH is dissolved into the molten salt of lead borate, leading eventually to the oxides of the constituting LDH cations, Allada et al. established that in the case of Co/Al-CO_3^{2-} LDH the $\Delta_m H_f^\circ$ could be estimated from the SCC approach [172]. The $\Delta_m H_f^{SCC}$ was found to lie between -970 and -1040 kJ/mol depending on the mineral composition (Table I.5). Later they used a similar approach to calculate the thermodynamic values for Mg/Al LDH with CO_3^{2-}, NO_3^-, Cl^- and I^- counter ions [173]. According to the authors, the experimented and modelled thermodynamic parameters were close enough to validate the SCC approach. Importantly, intercalated anions apparently have a remarkable effect on the solubility and, therefore, on the thermodynamic stability. Cation disorder in the brucite type layers did not contribute markedly to solubility. The nature of the cations seemed to be more important than their molar ratio [172,173,174]. Entropy was expected to remain within -3 kJ/mol. However, in the SCC approach the halides appeared more stable than carbonate, which the authors assumed to be related to the hydration enthalpies of the halide series and sulphates. For Mg/Al-CO_3^{2-} crystal the $\Delta_m H_f^\circ$ were in the range of -1200 kJ/mol (Table I.5).

It is well established that the decomposition process of the hydrotalcite begins with dehydrations and possibly, depending on the LDH synthesis route, with a partial loss of interlayer water that occurs at 250 °C [175,176] (Figure 1.15). The accompanying loss of chemically bound water from the LDH galleries takes place between 275 and 350 °C. Subsequently, the crystalline phase transformation with loss of carbonate and hydroxyls begins to take place. The final endotherm starts at approximately 377 °C. It is characterised by significant loss of CO_2 and OH and the formation of a rocksalt-type structure as the layered structure collapses creating strongly basic O^{2-} sites [177,178]. Further oxidation above 600 °C will form a spinel-type oxide that precludes recovery of the LDH structure.

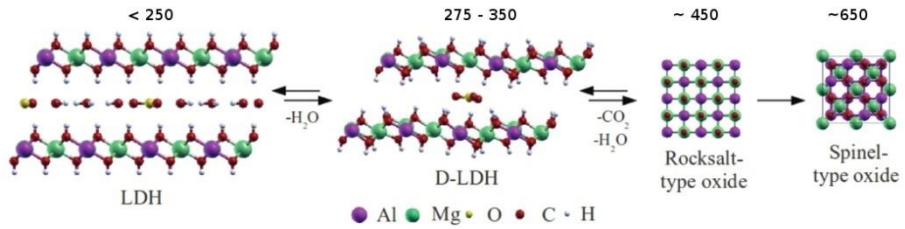

Figure 1.15 Simplified representation of an LDH crystal transformation under different calcination temperatures (°C). Adapted from [178].

1.3.4. Synthesis and preparation

The process that involves stabilisation of crystal formation by a metal cation is known as co-precipitation. It is a broadly exploited method in the LDH preparation. During the co-precipitation sequence, not only inorganic anions but also pre-polymers [179], graphene [180] and biologically active molecules [181] may be incorporated in LDH gallery.

Precipitation strategy depends on the preferred hybrid structure. The precursors should be chosen in order to promote affinity towards the intercalated anion. Usually nitrates are applied in this respect as noted earlier. Also, the intercalated anion is often dissolved in excess from the calculated fraction of trivalent cations in the crystalline lattice.

The co-precipitation is achieved either at high super saturated (*hss*) or at low super saturated (*lss*) conditions [182]. The *lss* system is preferred if charge density ratio needs careful control. The *hss* synthesis route may be chosen if the material is allowed to age hydrothermally. The problem in the *hss* method is the continuous pH change during the particle nucleation. Buffers, however, can be applied. Neither one of these synthesis routes are able to produce particles with narrow size range distribution, wherefore, a rapid nucleation procedure was developed [183,184].

Subsequent treatment after the LDH formation involves a calcification process. This is especially so, if the material is to be used as a catalyst or the intercalated anion exchange is required. Catalysts may be produced in any temperatures above approx. 350 °C, while in the case of ion exchange the temperature should be kept below 525 °C. The limit is set in the latter case by the LDH's rehydration ability. The so-called memory effect was first explained by Miyata [175]. The crystallographic data revealed that, once calcified, the mineral acquired its original structure upon hydration in an aqueous environment. Applying the memory effect procedure allows the LDH to incorporate many different anions without using high ionic concentrations or elevated pH.

Table I.5 Tabulated enthalpies for selected LDH structures and intercalated anions. The cation ratio (R) and the molar amount of water ($n(H_2O)$) is also given. $\Delta_f H^{SCC}$ = calculated enthalpy based on single cation composition, $\Delta_f H°$= calculated enthalpy based on elemental composition. Values are expressed in kJ/mol. The anion in parentheses indicates the contaminant. Values adopted from [150,171,172,173].

LDH	Zn/Al	Co/Al			Mg/Al						Fe/Fe			
A^{n-}	CO_3^{2-}	CO_3^{2-}		CO_3^{2-} (NO_3^-)	CO_3^{2-}	CO_3^{2-} (OH^-)	CO_3^{2-} (OH^-)	NO_3^- (OH^-)	I^- (OH^-)	Cl^- (OH^-)	SO_4^{2-}			
$R_{M2+/M3+}$	-	3.1	3.1	3.1	-	2.85	2.70	2.85	2.85	2.70	1.33	1.22	0.89	0.49
$n(H_2O)$	-	0.805	0.810	0.810	-	0.39	0.83	0.39	0.39	0.83	0.91	0.90	0.82	0.59
$\Delta_f H^{SCC}$	-22.65	-5.05	-9.78	-13.64	-19.72	-10.49	-7.2	-1.58	-12.26	-7.74	-6.6	-2.3	-2.5	-3.8
$\Delta_f H°$	-	-1044	-992	-968	-	-1166	-1297	-1119	-1079	-1252	-1079	-1084	-1069	-1037

1.3.5. Applications for LDH

The launch of the utilisation of LDH on an industrial scale was probably due to the work of Miyata and co-workers in the mid-1970's and early 1980's. Miyata found that HT and its calcified form was a useful halogen scavenger for the polyolefin produced by Ziegler-Natta catalyst or Fridel-Craft reaction, and a good heat stabiliser in PVC plastics [157].

The LDH is built from hydroxides, so it can act as an alkaline catalyst by sharing the electrons from the first brucite type layer. Intercalated ions may also undergo alkaline catalysed reactions when LDH is functioning as a host structure. Since the organic anions are usually oriented within the galleries, the LDH can direct the reaction pathways and protect intercalated molecules. For example, LDH has been proven to improve heat and photo stability of pigments [185]. We have already seen that the band gap energy in $R_{MgAl} = 3$ in the LDH crystal with intercalated OH^- is at the minimum. It is also highly basic in character, being able to catalyse alkaline reactions, especially those with anionic intermediates [167].

Since its early discoveries, the science around HT has boomed and numerous applications ranging from drug development to automobile industry, composites, semiconductors, water purifications and so on, have been addressed. According to SciFinder© the LDH has appeared in some 5500 scientific papers since 1985.

Other than the minerals that are listed in section 1.2.2 are rarely explored in context of pulp fibres. However, LDH seems to appear as a recently discovered mineral in this regard. For example, paper making drainage is used for producing colloidal LDH and the resulting cationic particles are exploited in stickies' control and capturing the anionic trash [186,187]. The thermal properties of LDH in flame retardant paper have been studied as well [188] and incorporation of LDH into polylactic acid and cellulose acetate films have received some attention [189,190]. The function that was carried with the LDH into the films was related to oxygen diffusion and thermal stability that are important in food package applications.

Several patents have been filed in the past 10 years or so that are related to LDH mineral and P&P and board manufacturing. For example, LDH appears as a component in filler and fluorescent whitening agent formulations [191,192,193,194], in the filter paper for biological samples [195,196], in pitch control additive [197] and fluoride scavenging agent in aqueous media [198]. An interesting function was achieved with fluorescence whitening agent (FWA) filled LDH that expressed pressure sensitive properties [199]. The emission wave length maximum was observed to change as the orientation of the FWA and therefore the chemical environment of exited functional group within the LDH crystal altered under applied pressure. LDH have been utilised also as a flame retardant in paper [200] and as a catalyst in lignin depolymerisation [201].

Considering the possibilities to apply LDH synthesis in pulp and paper production, the locations were envisaged as in figure 1.16. Based on the existing knowledge, the LDH synthesis could be exploited already at the refining stage or in the mixing chest.

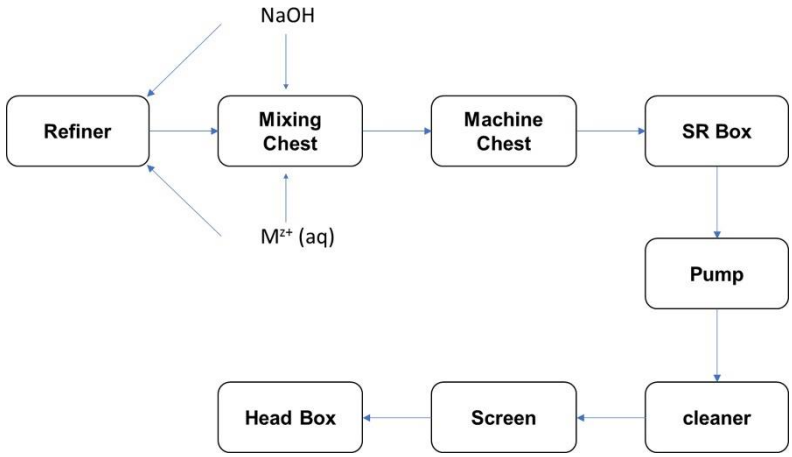

Figure 1.16 Example for LDH precursor application positions in a paper machine

2. Positioning of the scientific work

In this thesis, the *in situ* synthesis of LDH by using three different applicable approaches is being considered for large scale pulp production. The fundamental properties of hybridised pulp fibres are being studied in the context of a fibre filled polymer composite and lightweight pulp fibre foam.

To test the hypothesis for *in situ* synthesis and ability to apply LDH as a functionalisation platform for pulp fibres, co-precipitation of LDH onto BTMP fibre surface was used as a proof of concept. The experimental set-up is laid out in chapter 3.1 and the results presented in chapter 4.1.

The scientific experiments to clarify the physical and chemical properties of LDH modified fibres in terms of fibre compliance, the amount of non-diffusive charge, combustion behaviour and polymer degradation are presented in chapters 3.2 and 4.2.

The hypothesis arising from the lower surface energy to enhance the coupling of fibres is discussed in experimental chapter 3.3 and results in chapter 4.3.

Finally, to combine the combustion behaviour and *in situ* synthesis procedure the hypothesis was made to take advantage of the platform in a pilot to produce light weight fibrous foam out of the modified BTMP fibres. The experiments and results are presented in chapters 3.4 and 4.4 respectively.

3. Experimental

Thermomechanical (TMP) spruce (*picea abies*) and sulphate cooked (Kraft) pine (*pinus sylvestris*) pulps were used throughout the experimental work. Hydrogen peroxide bleached TMP (BTMP) pulp was provided by UPM (Rauma mill, Finland) in 2009, while the Kraft pulp with unknown bleaching sequence (BKraft) was provided by Metsä Fiber in 2011 (Rauma mill, Finland). The collection site in the mill was located after the bleaching tower at the dryer section.

The pulp, once collected, was transported to ÅAU in a polypropylene container and subsequently sampled into 1000 g aliquots within 48 hours and stored in 2000 ml polyethylene bags at a freezing temperature of -20 ± 2 °C. Each time a new sample was needed for experimentation, the pulp aliquot was thawed overnight at 10 °C before use. After thawing the samples, the pulp fibres were separated avoiding excessive damage by applying standard disintegration procedure according to ISO 5263:1995(E). Prior to disintegration, approximately 30 g of BKraft pulp or 40 g of BTMP was soaked for 30 min in a beaker that was filled with 2000 ml of distilled water. The pulp fibres were characterised with Kajaani FiberLab instrument. The arithmetic average length of BKraft fibres was 2.09 ± 0.1 mm with 2 ± 1% of fines determined as a number average of smaller than 0.20 mm fragments. For the BTMP fibres the values were 1.50 ± 0.1 mm and 22 ± 1% respectively.

From here onwards, whenever the weight of pulp is being mentioned in this thesis, we refer to the so-called oven dry (o.d.) weight unless otherwise stated. The oven dry content of pulp was determined by weighing approx. 2 g of sample onto an aluminium tray and placing it into an oven at 105 ± 5 °C for approx. one hour. Three replicate samples were prepared and the arithmetic average was used in subsequent calculations. The modification and functionalisation concepts appear frequently in the articles. Whenever modification (or hybridisation) is used we refer to pulp fibres that contain LDH particles. Functionalisation refers to the modified (or hybridised) fibres that are further treated with a sodium dodecyl sulphate surfactant.

3.1. *In* situ synthesis and functionalisation of BTMP fibres

The fibre functionalisation concept was explored by applying urea hydrolysis and *in situ* co-precipitation via the *lss* synthesis route of Mg-Al LDH particles. The pulp that was used for this work was spruce BTMP. Chlorides and nitrates were used as counter balancing ions in LDH synthesis. The stress was put on achieving high hydrophobicity with a common surfactant in a process that would be readily applicable for large scales. Pulp fibres were not pre-treated in any other way than already explained at the beginning of the Experimental section.

3.1.1. Fibre modification with Mg-Al LDH

Fibres were modified in a 500 ml three-neck round-bottom flask that was equipped with a reflux, mixing and urea dispensing system, and, via the *lss* titration method in a 1500 ml reaction vessel as described in article #1 (Figure 3.1). The concentrations and synthesis parameter are listed in table III.1.

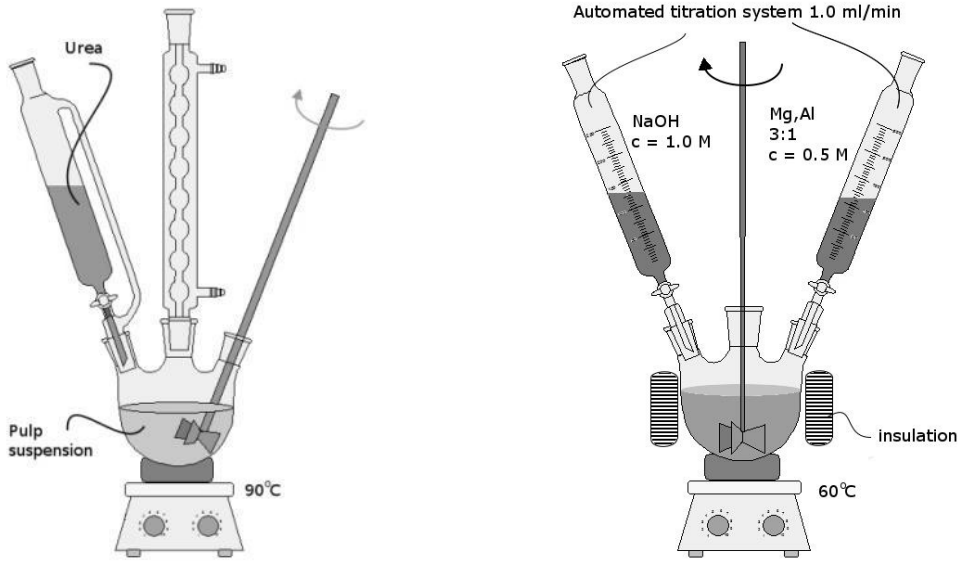

Figure 3.1 The system set-up for in situ particle synthesis on pulp fibres via urea hydrolysis and the lss titration method.

Table III.1 Parameters used in the modification of BTMP via urea hydrolysis and lss synthesis routes. The total metal ion concentration of LDH ($c(M_{tot}^{z+})$) was calculated from the final reaction volume. Parameters: Mg to Al cation ratio (R_{MgAl}), possible counter ion(s) (A^{n-}) with the most probable one in bold, synthesis and ageing temperature (T_s, T_a), and, synthesis and ageing time (t_s, t_a)

Synthesis	R_{MgAl}	$c(M_{tot}^{z+})$ (mmol/dm³)	A^{n-}	T_s (°C)	t_s (h)	T_a (°C)	t_a (h)
Uhyd	3:1	5	Cl^-, **CO_3^{2-}**	90	24	-	-
lss	3:1	10 / 100	**NO_3^-**, OH^-, CO_3^{2-}	60	0.5 / 6	135	24

Synthesised particles were analysed with XRD (Bruker D8 Discovery) that was equipped with a HI-STAR 2D detector and running with the GADDS software suite. Powder samples were gently pressed onto amorphous silica substrate with the aid of ethanol. A diffractogram was collected with 2θ range of 2.1–95.5° with CuK_α (λ = 1.54184 Å) radiation. Instrument resolution was 0.02° and the scanning speed was set to 0.1 °·s^{-1}. Operation voltage in X-ray tube was 40 kV and the current 40 mA.

Calibration was performed with a Bruker AXS certified corund (Al_2O_3) standard. Phase identification was carried out with a PDF-2 database (2010) supplied by the International Centre for Diffraction Data (ICDD).

The modification of pulp fibres via *lss* synthesis route was followed by a post-synthetic ageing in order to facilitate LDH crystallisation [182,202]. Modified fibres were transferred into a 1000 ml Teflon® linen autoclave and treated hydrothermally for 24 h at 135 °C (Table III.1). After the hydrothermal ageing the pulp fibres were thoroughly washed repetitiously at 1-2% consistency for 10 times.

Particle shape was examined with a Leo Gemini 1530 field emission scanning electron microscope (SEM) that was equipped with in-lens detector (LEO-Electron Microscopy Ltd., Oberkochen, Germany). Optimum working distance was 13 mm with 2.70 kV accelerating voltage. Samples were coated with carbon using Temcarb TB500 sputter coater (Emscope Laboratories, Ashford, UK)

Fibre morphology was examined with an analytical field emission SEM, (JEOL JSM 6335-F NT, Japan) coupled with an energy dispersive x-ray analyser (EDS). The optimum working distance varied with the chosen magnification. Accelerating voltages were 15 kV for SEM and EDS and 10 kV for SEM images containing large amounts of LDH particles.

The content of Mg^{2+} and Al^{3+} on pulp fibres after modification was examined with EDS and an inductively coupled plasma mass spectrometer (ICP-MS) (Perkin Elmer Sciex, Elan 6100 DRC Plus, Framingham, MA, USA). The energy spectrum was calibrated with cobalt. The EDS signal generated from a soft material such as fibres with a density around 1.5 $g \cdot cm^{-3}$ develops at depths of approximately 5 microns whereas the ICP-MS is a bulk analysis technique in which the sample is dissolved in a hot (200 °C) nitric acid and a small amount of hydrogen peroxide.

Laboratory hand sheets (Figure 3.2) were prepared from the modified fibres according to ISO 5269/1. Hand sheets were mechanically tested according to the ISO 5270, 1998 standard procedure.

Contact angle measurements were performed on functionalised fibres with CAM 200 (KSV Instruments Ltd, Finland). The applied sessile water droplet size on a 1 x 5 cm paper strip surface was 1.6 ± 0.2 µl. A total of five spots were analysed for each contact angle data point. The droplet was dispensed by slowly lowering the needle in order to allow the water droplet to gain contact with the paper surface. If the sample surface was hydrophilic, the needle was drawn back as fast as possible, and the measurement commenced immediately after the droplet had detached from the needle. From hydrophobic surfaces the needle was drawn back slowly in order to avoid the detachment of the droplet from the paper surface.

Images were collected in the beginning by 200 ms intervals and after a couple of seconds the frequency was reduced to 1/s until static conditions. Results were analysed on iterative bases with Young-Laplace function provided by Theta software (Biolin Scientific, Sweden). Standard deviations were approx. 10% on hydrophilic surfaces and 7% on hydrophobic surfaces. All experiments were performed on ambient conditions.

Figure 3.2 Examples of functionalised, i.e. hydrophobic, laboratory hand sheets.

Contact angles were corrected by applying a Wenzel model that considers the true contact area of a sessile drop on a solid surface. Solving the equation dictates that the surface roughness is estimated. A confocal microscope was applied to evaluate surface roughness. The microscopes lateral resolution was 1.56 µm.

3.2. Hybridisation and the properties of fibres

Physical and chemical changes that take place on BKraft fibres after treatment by *lss*, *hss*, or urea hydrolysis synthesis routes were explored in more detail. Mg-Al LDH particles with hydroxide, carbonate or nitrate counter ions were precipitated on pulp fibres surface. The fibre stiffness, thermal degradation and the capacity of non-diffusing charges are being addressed. BKraft fibres were not fractionated or refined.

3.2.1. Hybridisation and mineralisation of BKraft fibres

The fibre hybridisation was carried out in two stages. For the *lss* synthesis route, two automatic titrators were applied for dispensing the reagents into fibre sludge (5.0 g in 500 ml). The pH was kept close to 9.5 by dispensing 1.0 M NaOH from one of the titrators, while the acidic (pH = 3.7) aqueous solution of $Al(NO_3)_3$ and $Mg(NO_3)_2$ with $c(M_{tot}^{z+})$ equal to 0.50 M at molar ratio 1 : 2 was dispensed from the other. Dispensing rate was set to 0.33 $mL \cdot min^{-1}$ for both reagents. The fibre sludge was stirred vigorously during the synthesis.

In the case of the *hss* synthesis and urea hydrolysis, the fibres were soaked in the metal nitrate salt solution for 90 min before LDH nucleation was commenced. The $c(M_{tot}^{z+})$ in the final reaction volume (500 mL) in all experiments was 25 mM. The amount of carbonate in a form of Na_2CO_3 in *hss* and as urea in urea hydrolysis synthesis routes was set to $3.3 \cdot c(M_{tot}^{z+})$.

To advance the crystallisation processes in the second stage, the precipitates were transferred into 1000 mL reaction vessels and treated under hydrothermal conditions with autogenous pressure built up at 120 ± 10 °C for 48 h. Urea was assumed to hydrolyse completely in the given conditions.

Hybridised fibres were washed repetitiously at a maximum of 2% consistency and filtered through a filter paper (pore size 7–12 microns) until the filtrate showed less than 0.01 units change in absorbance at the dispersion edge of a non-sediment aliquot (240–250 nm) (Figure 3.3). The final pH of all filtrates was between 7.0 and 7.5. Finally, the pulp fibres were dried in an oven at 60 °C until constant weight. The synthesis of the neat LDH particles in absence of BKraft fibres was identical.

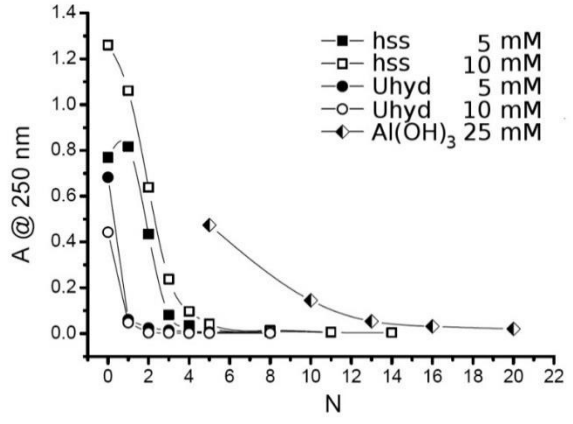

Figure 3.3 The washing efficiency on anionic LDH and colloidal non-charged aluminium hydroxide.

3.2.2. Setting up thermogravimetric analysis

Thermogravimetric analysis from an organic material that has a low density is challenging from the instrumental point of view. Several factors that are rarely discussed in scientific articles must be considered, including density, applicable sample weight, temperature ramping rate and the gas flow rate in the furnace. The effects of sample density and weight on thermogravimetric signal are presented in Figure 3.4. For example, the density causes problems if it is too low. On the other hand, if the weight is too high the thermal pressure exerted on the arm that holds the reference cup grows too high and appears as if the sample would be cooling off. This cooling effect appears as a delta signal or as a loop in T/dT plot making the energy calculations difficult. Higher density enables slower burning but also takes off some of the thermal pressure at pseudo equilibrium and causes the first depolymerisation to advance less, thus with the deeper curvature at around 340–425 °C. The effect of density and weight appears to be insignificant to onset temperature (T_{onset}) and residual weight.

Thermogravimetric analysis (TG) (TA Instruments SDT Q600, New Castle, DE. USA) of the LDH particles and hybridised fibres was carried out with a TA Instruments (SDT 2960, New Castle, DE, USA) apparatus. Thermographs were recorded by applying a linear 3 °C·min^{-1} sweep rate up to 600 °C under a constant air flow (100 ml·min^{-1}). The amount of LDH in each experiment was close to 20 mg in a 60 µL alumina cup. Hybridised fibres (w = 10 mg) were pelletised to a cylindrical shape of 5.0 ± 0.1 mm in diameter and 0.85 ± 0.05 mm in thickness. Sample density was optimised, as previously discussed, prior to analysis and set to 600 ± 50 kg·m^{-3}. The thermal history of the hybridised samples, was controlled with 10 min isothermal conditioning at 200 °C. Baselines were recorded with empty alumina cups. Since the results may differ based on the thermal history of the sample the baseline was recorded twice in a row using the same cup to affirm any changes imposed by the instrumentation itself. For energy calculations, the calibration was carried out with Pb and Zn standards. Calibration results are presented in table III.2.

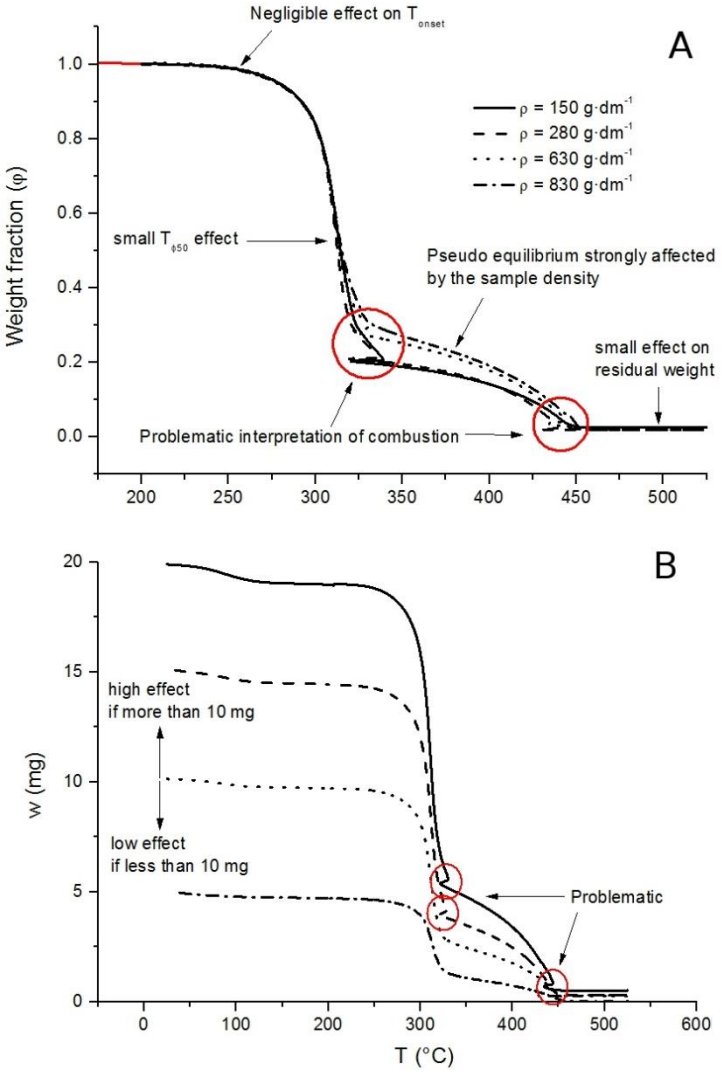

Figure 3.4 The effects of sample density (A) and weight (B) to thermogravimetric analysis. The sample weight in A was approx. 20 mg and the density in B was around 600 mg/ml.

Table III.2 Experimental and literature values for the calibration standards are presented. The fusion enthalpies ($\Delta_{fus}H_m$) and melting points (mp) were acquired from literature [203,204,205].

Standard	M $g \cdot mol^{-1}$	$\Delta_{fus}H_m$ $mmol \cdot dm^{-3}$	mp (lit.) K	n µmol	E_{tot} J	$\Delta_{fus}H_m$ $mmol \cdot dm^{-3}$
Pb	207.20	4765 ± 11	600.13 (600.61)	243	1.158	0.2699
Zn	65.39	7103 ± 31	692.25 (692.25)	275	1.951	0.3054

3.2.3. Setting up structural analysis for single fibres

A micro-robotic platform was used in evaluating the fibre compliance after and before hybridisation. The platform and its application in pulp fibre research are explained elsewhere [206]. The platform is presented in figures 3.5 and 3.6. The equations required for compliance analysis are shown in equations 3.1 and 3.2.

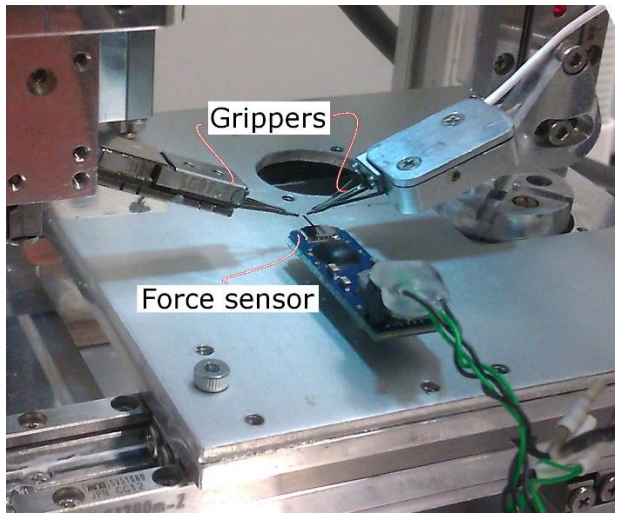

Figure 3.5 A digital photograph of the microrobotic test bench.

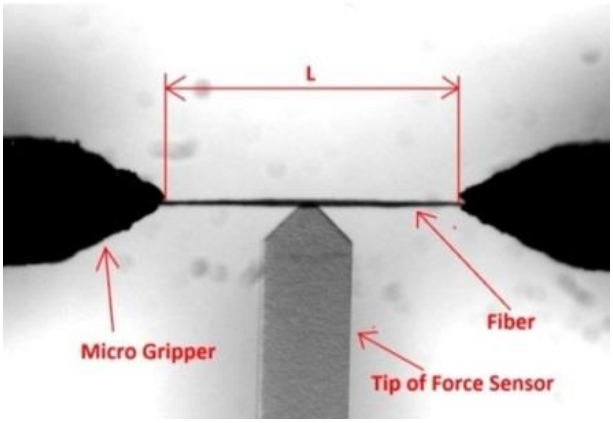

Figure 3.6 The microrobotic force sensor and gripper system setup.

$$Y_{max} = \frac{F \cdot l^3}{192 \cdot E \cdot I} \quad \text{(Eq 3.1.)}$$

$$\frac{1}{k} = \frac{1}{E \cdot I} \quad \text{(Eq 3.2.)}$$

In the equations, the deflection limit (Y_{max}) is related to the applied force (F) and to the length (l) of the fibre that has a Young's modulus of E. Fibre is assumed to be a rectangular beam that is fixed from both ends and having a moment of inertia of I. To verify the results significance between the samples, a t-test analysis was applied.

The effect of alkaline *in situ* LDH synthesis was studied by dissolving the fibres into a 0.5 M cupriethylene diamine (CED) solution. The apparatus and the method followed the ISO/FDIS 5351:2009(E) standard. In short: the dissolved fibre solution is allowed to pass through a 0.8 ± 0.05 mm capillary tube at 25 °C. Calibration of the tube and calculating the capillary constant was done with the aid of 65% glycerol solution that has known viscosity values (10 mPa·s at 25 °C). The capillary constant was calculated from equation 3.3. The diluted 0.5 M CED solution was tested against water to assure its freshness. The correlation value was found to be 1.284, tolerance being between 1.27 and 1.29. Limiting viscosity numbers (η_s) for the samples were calculated from the equation 3.4 by using the empirically tabulated viscosity ratios (η_R) [207]. All measurements were repeated as many times as needed to achieve 2% relative standard deviation.

$$h = \frac{t_c}{t_v t_s} \quad \text{(Eq. 3.3.)}$$

$$\eta_s = \frac{\eta_R}{\varrho} \quad \text{(Eq. 3.4.)}$$

In the equations, the viscometer constant (h) is directly proportional to the efflux time of 65% glycerol passing through the tube used for calibration (t_c) (d = 0.58 ±

0.02 mm), and inversely proportional to the efflux times of 65% glycerol (t_v) and 0.5 M CED (t_S) in the tube to be calibrated (t_v) (d = 0.8 ± 0.05 mm).

Non-diffusive charge was evaluated by using methylene blue (MB) and metanil yellow (MY) adsorption isotherms at 25 °C. The procedure for methylene blue adsorption on pulp fibres is explained elsewhere [64]. A short description is given here. A small amount of fibres (102 ± 2 mg) is disintegrated in 3 mL of deionised water for 30 min. Different amounts of buffered (pH = 8.2) MB solution (c = 400 μM) are then allowed to absorb on fibres for 15 min under gentle shaking. The suspensions are filtered through glass fibre filters and the filtrate is diluted to 20-fold in a volumetric flask prior to the UV-Vis analysis that is recorded at 664 nm wavelength. For MY adsorption 30 ± 2 mg of pulp was weighed while the initial concentration of MY was 49 ± 1 μM and the analysis wavelength 436 nm.

Adsorption isotherms were fitted with the Langmuir model defined in equation 3.5. The surface coverage of adsorbate (θ) on adsorbent at equilibrium (i_{eq}) has equilibrium constant (K). The fraction of adsorbed substances at equilibrium (a_{eq}) is proportional to the surface coverage and maximum adsorption (n) wherefore the Langmuir model may be rewritten according to equation 3.6.

$$\theta = \frac{K \cdot [i]_{eq}}{1 + K \cdot [i]_{eq}} \qquad \text{(Eq. 3.5.)}$$

$$\theta = \frac{a_{eq}}{n} \Leftrightarrow \frac{[i]_{eq}}{a_{eq}} = \frac{1}{n \cdot K} + \frac{[i]_{eq}}{n} \qquad \text{(Eq. 3.6.)}$$

3.3. Functionalisation and its effect on a thermoplastic composite

Taking advantage of the LDH functionalisation concept with a common surfactant to lower the fibres' surface energy, the BTMP and BKraft fibres' compatibility in injection moulded atactic polypropylene (aPP) matrix was explored. Shear dissipation in the composite and water absorption was studied to determine the compatibility and industrial applicability. In this work, both pulps were fractionated and the BKraft fibres were also refined prior to composite moulding.

3.3.1. Composite preparation

Prior to functionalisation, the fibres were fractioned with the Bauer-McNett fractionator (Lorentzen & Wettres, Kista, Sweden). Fibres that were retained by a wire with a nominal rectangular mesh opening of 1.19 mm were used in further process steps. BKraft fibres were also refined to Schoppler-Riegler (SR) value of 30.

The fibre functionalisation process followed the one described as *lss* synthesis route in article #1 (Figure 3.7). The c(M_{tot}^{z+}) was set to 100 mM. The surfactant was applied in 6% (w/w) on BKraft and BTMP fibres. In the washing sequence, the fibres were repetitiously dispersed into distilled water at 1% consistency and filtrated in a Büchner funnel under reduced pressure. Functionalised and modified fibres were dried in an oven at 60 °C for 24 hours and dry disintegrated.

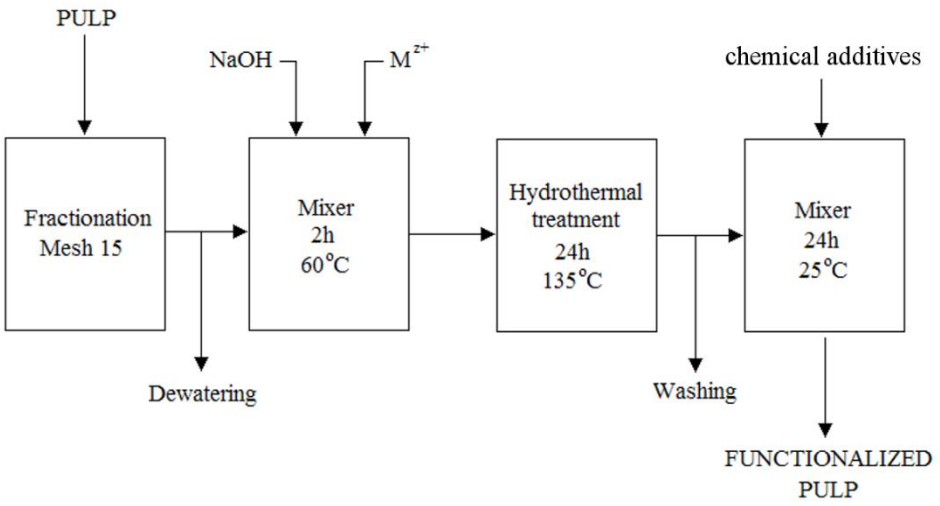

Figure 3.7 Schematic illustration for the modification and functionalisation sequence.

Composites were prepared with a DSM Xplore (DSM Xplore, Netherlands) micro injection moulding machine (5.5 ml sample chamber). The speed of conical twin screws was set to 200 rpm and the mixing chamber temperature was set to 190 °C. Matrix polymer was fed into the machine prior to the fibres that were conditioned on site in an oven at 60 °C for one hour. Injection moulded samples matched the ISO 527-2 1BA standard with intended 20% (w/w) fibre content (Figure 3.8). Mould temperature was kept at 40 °C, while the injection and holding pressures were 4 bars. Processing time was set to 1.0 seconds. Prior to any analysis, the samples were conditioned in 52 ± 2% relative humidity at 23 ± 1 °C for 60 days.

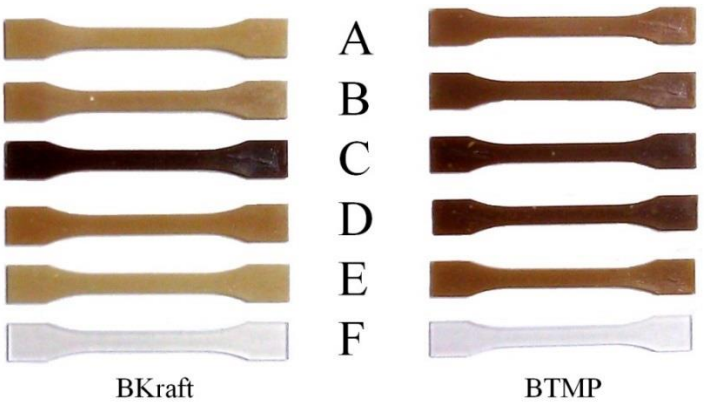

Figure 3.8 The injection moulded ISO 527-2 1BA samples from BKraft and BTMP pulp fibres. Atactic PP (F), aPP + 20% fibres (E), aPP + 20% modified (10 mM) fibres (D), aPP + 20% modified (100 mM) fibres (C), aPP + 20% functionalised (100 mM + 3% SDS) fibres (B), aPP + 20% functionalised (100 mM + 6% SDS) fibres (A).

3.3.2. The concept for fibre-matrix interactions

Uniaxial tensile stress behaviour was studied with Instron 8872 machine (Instron, England) in an ambient environment. Viscoelastic behaviour depends on the strain rate, wherefore two was applied (5.0 and 50 mm·min^{-1}). Young's and resilience moduli, ultimate strength and yield and elongation at break were recorded (Figure 3.9)

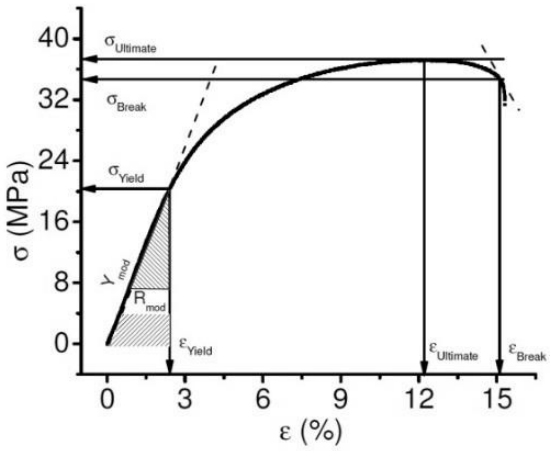

Figure 3.9 Extracting the parameters from the stress (σ) as a function of strain (ε).

Water adsorption was followed up to a reasonable level of quasi static kinetics (1600 h) and evaluated with generalised Langmuir's adsorption isotherm (Eq 3.7.)

$$S = S_{max}\left[\frac{(bx)^n}{1+(bx)^n}\right]^{m/n} \qquad \text{(Eq. 3.7.)}$$

In the equation, S is the adsorbed amount, Smax is the maximum adsorption, b is the binding energy term and x is the function against which the adsorption is measured. In this work the change in weight was recorded with respect to time. Equation reduces to Langmuir's adsorption isotherm when m = n = 1. The immersion depth maximum was set to 10 cm. The hydrostatic pressure and solvent temperature were kept constant throughout the experimentation. Samples were conditioned in an oven at 105 °C for 12 ± 1 s prior to weighing. Water desorption kinetics were studied under dynamic air flow at 60 °C.

3.4. The effect of hybridisation on the combustion of foamed light weight structures

The inherent property of LDH being flame retardant was exploited in the investigation of their applicability in foam formed panels. The foamed fibrous structures were produced from BTMP fibres that were modified with carbonate counter ion intercalated Mg-Al LDH particles. At the same time a semi-pilot scale particle synthesis route via urea hydrolysis was studied. The pulp fibres were used without additional pre-treatments beside freezing and thawing, as already mentioned.

3.4.1. Fibre hybridisation

A batch of 150 g of BTMP was soaked for 60 min in a 2000 ml solution of distilled water, urea (1.249 M) and metal nitrate salt with $c(M_{tot}^{z+}) = 0.375$ M and the Mg^{2+} to Al^{3+} ratio 2:1. The sludge was transferred into a pre-heated (93 °C) 3000 ml Teflon linen reactor that was equipped with a wing rotor sufficient to mix 7.5% fibre sludge. LDH synthesis was carried out at 90 °C. A mixing sequence of 20 rpm for 10 seconds in every 10 min was applied until the end of reaction (180 min). Sludge was then divided into two equal batches and treated hydrothermally in 1000 ml reaction vessels at 130 ± 10 °C for 12 hours. Pulp washing was carried out repetitiously in 1.5% consistency. A second step for *in situ* synthesis of nano-range LDH particles via the *lss* route was applied as before.

3.4.2. Foam formation

An in-house built sheet former was used in preparation of foamed structures with average grammage of 100 $g \cdot m^{-2}$. Sodium dodecyl sulphate (SDS) was used as a foaming agent. The aqueous fibre sludge was vigorously mixed with prefabricated foam. The amount of SDS was optimised to 0.15-0.2 $g \cdot L^{-1}$ leading to 60–70% air content in the foam. Stabilised foam was decanted into the sheet mould. The system is designed to allow fibres to be oriented with the suspension flow. The settling of foam is followed by vacuum suction. The detached sheet is dried on a separate suction table that is equipped with a 5 mm wide slit enabling for air to pass through the foam-laid sheet.

3.4.3. Flammability test bench

Thermal properties were evaluated with a TG by applying a linear heating rate of 5 $°C \cdot min^{-1}$ between 25–525 °C. X-ray photoelectron spectroscopy (XPS) (Physical Electronics, PHI 5400 and Quantum 2000 ESCA, Eden Prairie, MN, USA) analysis was carried out for the hybridised fibres before and after a controlled oxidative combustion process at 350 °C (Phi 5400) and for the pristine samples including cone calorimeter combusted modified fibres (Quantum 2000). The samples were cut to approx. 0.8 x 0.5 mm pieces in such a way that a clean surface was revealed from the middle of the pellet. The clean surface was subjected to ambient air for no more than 5 min before they were loaded into the ultra-high vacuum (UHV) chamber (operated at $5 \cdot 10^{-9}$ Torr). Analysis was performed with monochromatic Al Kα X-ray source (E_{photon} = 1486.6 eV) together with an electron flood gun for photoelectric effect neutralisation. The anode was operated at 14.5 kV with 300 W power (PHI 5400) and

49.0 W (Quantum 2000). The take of angle for both instruments was 45°. The image area was set to 1.5 mm^2 (PHI 5400) and 0.2 mm^2 (Quantum 2000). The survey-mode photoelectron spectra were acquired with 89.54 eV (PHI 5400) and 117.40 eV (Quantum 2000) pass energy. Applied energy steps were 0.5 eV. Reference photoelectron was taken from a 100% cellulose filter paper before and after the sample measurements in order to control the UHV environment and sample contamination.

Visual inspection for the flame spread in the foamed structure was carried out with the aid of a high-speed video recorder (HsVid) (Citius C 100 centurio, Citius Imaging Ltd, Finland). Small samples (approx. 8 mm in size) were detached from the foamed sample and burned on the top of a resistive wire (Alucrom I, Cr 20%, Al 5%, R = 42.200 $\Omega \cdot m^{-1}$). A power supply of 30 W was used for heating the wire that ultimately burned the fibres. Aluminium mesh was put on top of the sample to maintain the focus for the HsVid.

The sample flammability tests according to ISO 5660 and ASTEM E 1354 standards were carried out with a cone calorimeter (CC) (Fire Testing Technology, West Sussex, UK). The installation included a 3-term (PID) temperature controller and three K-type thermocouples. Instrument accuracy was 0.01 g. A 10 kV spark ignition system was applied in all experiments. Heat flux was set to 25 $kW \cdot m^{-2}$. Nominal duct flow rate was set to 24 $L \cdot min^{-1}$. The foamed panels were cut to 94 ± 2 mm squares. Sample thickness was 7.5 ± 0.5 mm. The calculated flat surface area of all samples was 89 ± 3 cm^2 and the density 35 ± 3 $kg \cdot m^{-3}$. An aluminium tray was used as a sample support and the sample was placed horizontally 60 mm below the heating element. The heater element and the sample were separated by a split shutter mechanism. Ambient conditions during all of the experiments were: T = 25 °C, RH = 55% and p = 102.6 kPa. Five replicate tests were carried out.

4. Results

4.1. *In situ* synthesis and functionalisation of BTMP fibres

In section 4.1, the *in situ* synthesis of LDH particles in the presence of pulp fibres and the functionalisation of the LDH containing fibres with sodium dodecyl sulphate are explained.

4.1.1. Composition of the LDH particles and fibres morphology

According to the energy dispersive spectrum (EDS), the relative molar composition of Mg^{2+} to Al^{3+} ($R_{Mg\text{-}Al}$) was 1.6 after the *Uhyd* synthesis route (Table IV.1). Titration of NaOH gave 2.8-3.0 instead. The composition of LDH after the *lss* synthesis route as indicated by EDS matched relatively well with the ICP-MS only if LDH precursors were used in large excess (100 mM). Since the sample weight used in ICP-MS instrumentation is extremely low, the statistical reasons are expected to explain the observed differences in between hybridised and functionalised pulp fibres. Also, EDS gives only semi-quantitative results especially at low concentrations.

Table IV.1 The atomic composition of Mg^{2+} and Al^{3+} in the modified BTMP pulp fibres by EDS and the weight composition according to ICP-MS instrumentation are presented. The calculated molar fraction of aluminium $\phi(Al^{3+})$ and the relative molar composition of Mg^{2+} and Al^{3+} ($R_{Mg\text{-}Al}$) are also listed taking into account the amount of the metals in reference pulp.

Sample	Mg^{2+} %	Al^{3+} %	$\phi(Al^{3+})$ %	$R_{Mg\text{-}Al}$
EDS (atomic %)				
Uhyd	5.7 ± 0.1	3.7 ± 0.1	39 ± 1	1.6
lss 10 mM	0.9 ± 0.1	0.3 ± 0.1	25 ± 1	3.0
lss 100 mM	3.2 ± 0.1	1.1 ± 0.1	26 ± 1	2.8
ICP-MS (weight %)				
Reference pulp	0.05 ± 0.01	0.01 ± 0.01		
lss 10 mM	0.96 ± 0.03	0.26 ± 0.01	19.8 ± 0.1	4.1
lss 100 mM	3.28 ± 0.06	1.18 ± 0.02	24.6 ± 0.1	3.1
lss 100 mM + 3% SDS	2.79 ± 0.06	1.07 ± 0.02	25.8 ± 0.1	2.9

The nano-sized LDH particles were densely packed on the fibres' surface and the topology of the functionalised fibres differed greatly from the reference (Figure 4.1). A clear distinction between individual LDH particles was difficult to make. In the freeze-dried pulp fibres, the particles appear to be coarse, growing as if facing the brucite layers in right angles with respect to the fibre's surface. It has been proposed that the orientation of LDH particles may be influenced by the substrate and especially by the hydroxyl groups that it contains [208]. The surfactant itself did not induce any additional topological changes in the applied range (6% w/w).

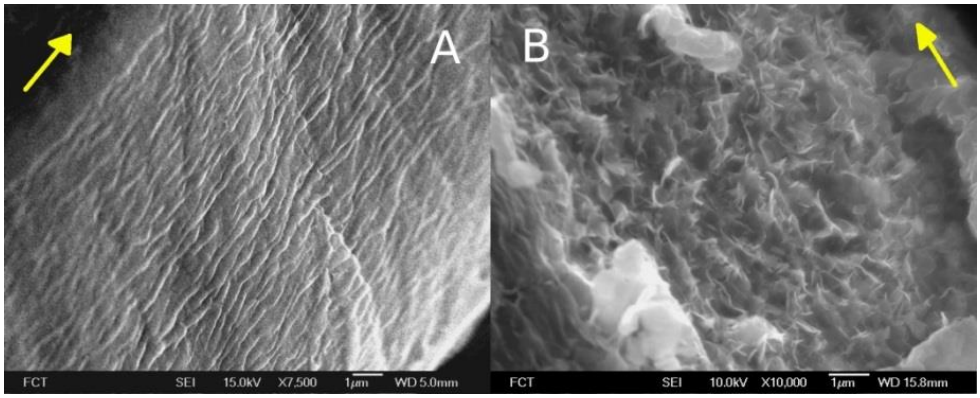

Figure 4.1 BTMP fibre's morphology upon modification via the lss route using chloride salts. The reference fibre (A) show a clearly visible S2 layer. The spruce fibre's surface topology changes greatly at submicron level after modification with high number of LDH (100 mM) (B). Arrows are pointing towards the fibre axis.

To confirm the presence of Mg and Al elements on the fibre's waxy surface, an energy dispersive analysis was carried out and an example of the results is shown in figure 4.2. As an example, three separate analytic areas from a functionalised fibre surface studied at magnification of 5000 are shown with the corresponding SEM image. Visually the bleached TMP fibre surface resembled one that had not been extracted [209]. A small amount of sulphur that belonged to SDS was also found.

4.1.2. Formation of fibre web and the inter-fibre bond strength

It is well known that fibres fibrillate externally and internally upon mechanical agitation that carries sufficient shear forces. External fibrillation provides greater number for inter-fibre bonds while the internal fibrillation provides fibres with greater flexibility. Both of these will affect positively the fibre web tensile strength.

Samples subjected to the tensile strength tests were the bleached reference TMP, modified TMP fibres from the *lss* and *Uhyd* synthesis routes and the fibres that were treated as if in reaction solution but without reactive agents, i.e. the metal precursors (Table IV.2). These are found in the table under Ref.

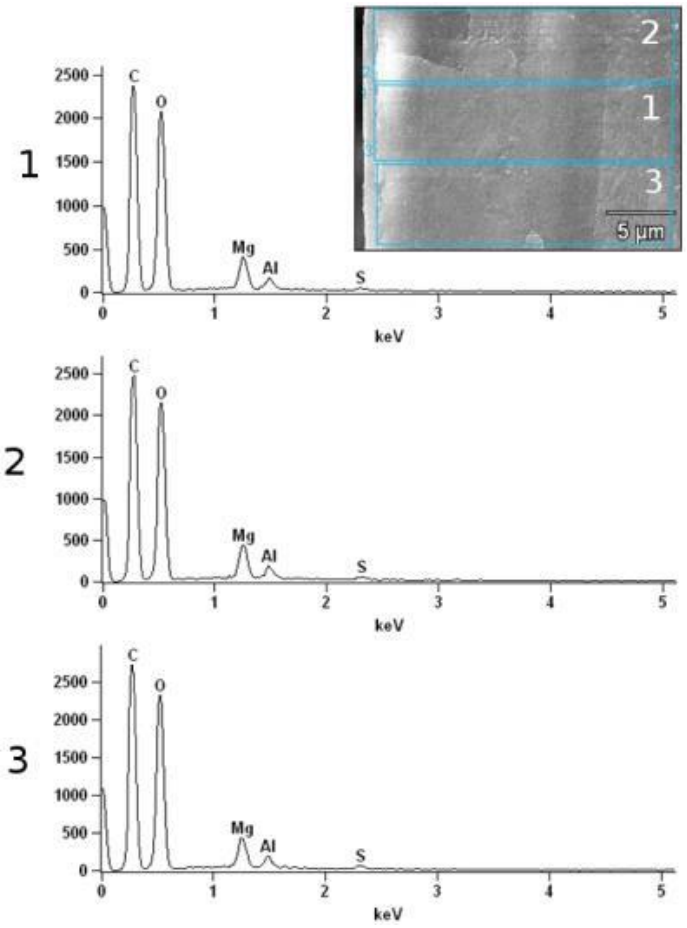

Figure 4.2 The EDS analysis from a functionalised fibre surface and the corresponding SEM image. SDS was applied in 6% w/w load. Previously unpublished.

Table IV.2 The tensile strength (σ), stretch (ε), stiffness (E) and the fibre fraction contents of a laboratory hand sheet.

Sample	σ Nm·g^{-1}	ε %	E kNm·g^{-1}	fraction (mm) and content %			
				≤0.2	0.2-0.6	0.6-3.0	>3.0
Ref.	35±1	2.5±0.2	3.4±0.1	2.3	17.3	68.8	12.3
H_2O	46±2	2.0±0.2	4.8±0.2	-	-	-	-
urea	45±3	2.1±0.1	4.8±0.2	-	-	-	-
NaOH	50±1	2.5±0.1	5.1±0.1	3.7	20.2	62.6	13.5
Uhyd 5 mM	32±2	1.8±0.2	3.9±0.2	-	-	-	-
lss 10 mM	42±3	1.8±0.3	5.6±0.2	4.8	27.2	62.6	6.5
lss 100 mM	8±1	0.7±0.1	1.7±0.2	3.6	21.7	66.5	8.1

Fibres' dimensions were not expected to significantly change during any of the treatments. However, where particle formation was present the increase of shorter fibres' fraction was clear. The particles themselves did not show up in Kajaani Fiberlab analyses, wherefore the fines and short fibres appeared to be generated from the longer fibre fraction. Increasing the particle concentration appears to diminish this effect, but we believe that LDH was accumulating on fine structures that carry higher surface area and greater non-diffusive charge to weight ratio. Thus, the number of longer fibres probably remained the same. It is known that the number of fibrillary and flake-like fines in a paper sheet affects beneficially in providing filling material into the voids that are created during a fibre web formation [210]. Extensive amounts, however, counter this phenomenon.

The results unequivocally suggest a lower hydrogen bonding ability for fibres with LDH particles on the surface. Although the relative content of shorter fibres and fines increased with the expense of the longer fibre fraction, these changes cannot alone explain the drastic changes in fibre web stiffness and tensile strength especially as the physical dimensions are not that much different between the two *lss* samples.

It is also important to note that urea did not change the fibre web characteristics in comparison to treatment in water. Therefore, contribution of urea was ruled out and the isocyanate intermediate in urea hydrolysis was proved not to influence fibre surface in the given experimental conditions, as the kinetics of ammonia and carbonate formation was clearly not the rate determining step (reactions 4.1 and 4.2).

$$CO(NH_2)_2 \rightarrow NH_4CNO \quad \text{(R. 4.1)}$$

$$NH_4CNO + 2H_2O \rightarrow (NH_4)_2CO_3 \quad \text{(R. 4.2)}$$

4.1.3. Functionalisation of the hybrid fibres

Applying sodium dodecyl sulphate on modified fibres altered the surface energy, as observed by a contact angle of a sessile water droplet on the surface of a laboratory prepared hand sheet. The BTMP fibres were not refined prior to hand sheet formation. In order to evaluate true contact angles, and therefore the hydrophobic character, the sample surface roughness was studied with a confocal microscope that is able to measure sample height variations in micron scale. Contact angle measurement is extremely surface sensitive and a paper represents one of the most difficult substrates to be studied due to the natural tendency of a fibre to absorb water that results in substrate swelling, and, due to the difficulty in addressing the chemical components on the fibres' surface precisely under the sessile droplet. In addition, micro roughness, grooves, asperities and geometry all influence the result outcome and are subject to sample preparation techniques and experimentation environment.

Reference fibres absorbed the water always in less than 5 s (figure 4.3). The hand sheets showed sidedness regardless of the used LDH amount. Contact angle (θ) at higher LDH content improved as SDS content increased. SDS had, therefore, adopted the inverted micelle configuration on LDH surface, aliphatic tail pointing out of the solid interphase. The hydrophobic character ($\theta > 90°$) was achieved already at 2% loading level, while the maximum attainable $\theta \sim 135°$ stabilised with 6–9% of SDS. Reorientation of the surfactant molecule on the LDH particle surface would influence the water penetration that was not observed in the given timeframe. Therefore, the

electrostatic forces governed the particle-surfactant interactions and ultimately the fibre's hydrophobic character. The effects of surface roughness as estimated with Wenzel's equation (equations 4.1 and 4.2) are presented in figure 4.4.

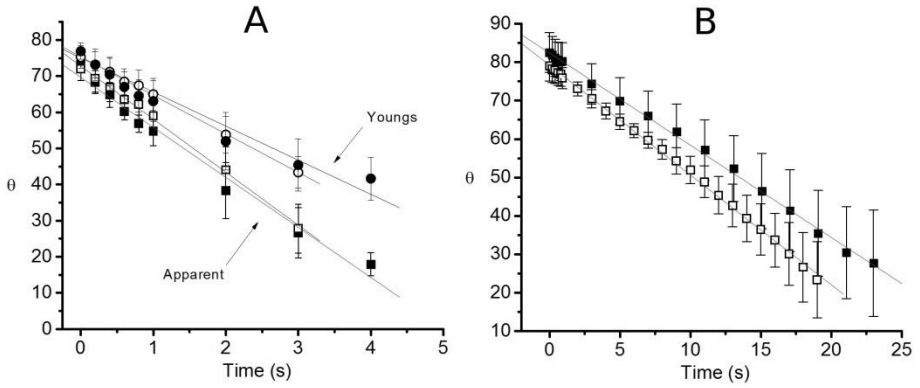

Figure 4.3 The apparent and roughness corrected contact angle of a sessile water droplet on a reference BTMP paper surface (A). The wire side (□) and the upper side (■) with corresponding Young's contact angles (○ and ●). An example for apparent contact angles of laboratory handsheet prepared form functionalised BTMP fibres. LDH were synthesised from a 10 mM solution and the hybrid fibres were functionalised with 6% of SDS. Previously unpublished.

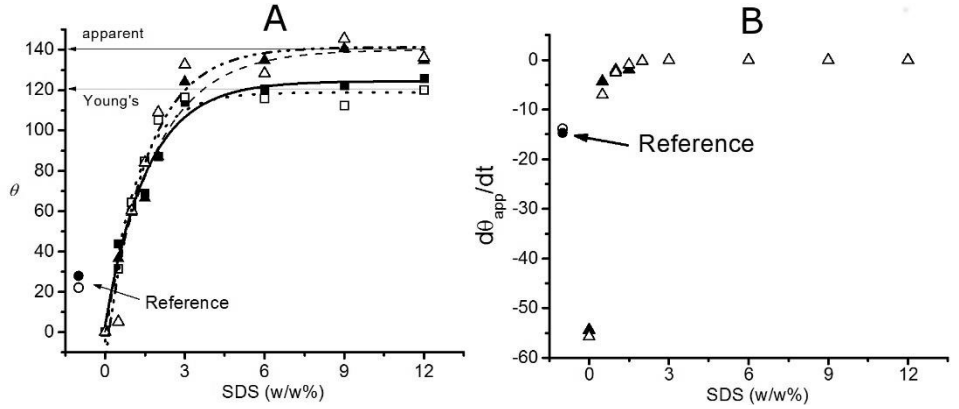

Figure 4.4. The relationship of the apparent and calculated Young's contact angle (A) and the kinetics (B) plotted against the extent of functionalisation. Legend: (◢) upper side, (△) wire side and the calculated Young's contact angles (■ and □) respectively.

$$cos\theta_{app} = rcos\theta_Y \quad \text{(Eq. 4.1)}$$

$$r = 1 + \frac{S_{dr}}{100} \quad \text{(Eq. 4.2)}$$

The Wenzel's model considers the fraction of the true contact area to the projected area (r). This relationship can be estimated from the surface roughness value (Sdr)

determined by a confocal microscope. The greater the Sdr the more apparent contact angle (θapp) deviates from the calculated Young's contact angle defined by the substrate surface energy.

4.2. Hybridisation and the properties of fibres

The chemical and physical changes that occur upon modification were examined. The BKraft pulp fibres were modified by *in situ* LDH synthesis either via urea hydrolysis, low super saturation or high super saturation route.

4.2.1. Crystalline structure of the neat LDH particles

The *in situ* synthesised LDH particles on fibres' surface were assumed to resemble those that were synthesised in the absence of pulp fibres. The diffractograms of neat particles are presented in figure 4.5.

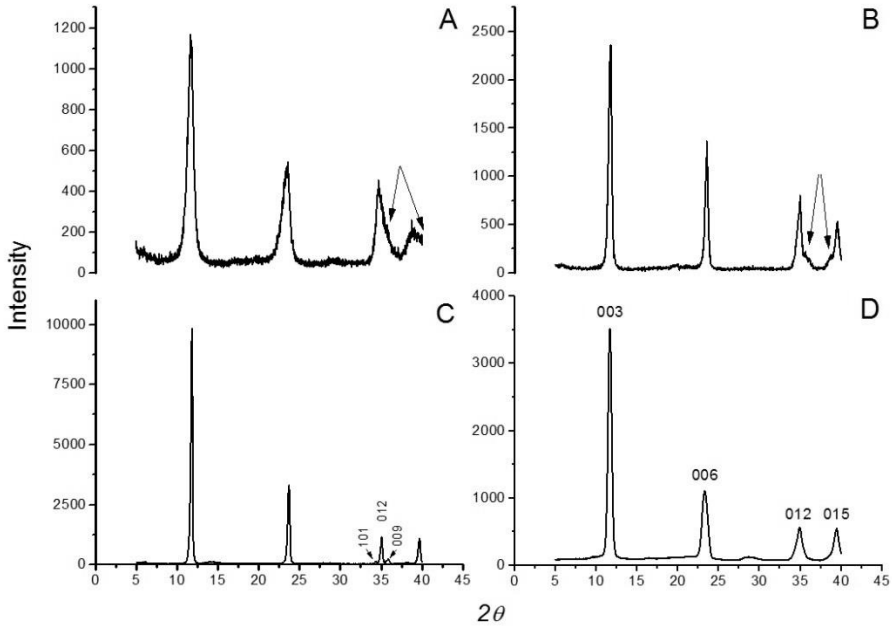

Figure 4.5 The XRD diffractograms for neat LDH particles from lss (A), hss (B), Uhyd (C) synthesis routes and commercial hydrotalcite (D). Asymmetric peak broadening suggesting octahedral $3R_2$ arrangement are indicated with arrows.

The FWHM values of all peaks increased in order *Uhyd* < *hss* < HT < *lss*. Therefore, the size of the LDH particles on fibres' surface was expected to follow the reverse order. The observed asymmetry in *lss* and *hss* samples may arise from interstratification, inclusion of hydroxyls and possibly nitrate due to statistical reasons but also if the crystal adopts octahedral arrangement in the brucite layers [139].

4.2.2. Coating and mineralisation of pulp fibres

SEM analysis confirmed the XRD results in that the hydrolytically synthesised LDH's size followed the FWHM values (Figure 4.6). Most of the particles appeared to reside in flat orientation on fibre surface and the hexagonal shape was especially clear from the clay sized LDH. The concentration of metal nitrate solution measured from the final suspension volume was 25 mM. The amount corresponds to approximately 2.0 g of ideally formed LDH crystals with nitrate anion excluding any crystalline water. The amount of pulp fibres in the suspension was 5.0 g.

TEM survey revealed mineralisation of Kraft pulp fibres after LDH synthesis via *Uhyd* route (Figure 4.7). Threshold analysis with ImageJ 1.48C program revealed that approx. 3% from the visible fibre wall area contained mineral species. The possibility for particles to be spread over the epoxy moulded specimen during the ultra-thin (200 nm) sectioning with a diamond blade was ruled out as there were no particles to be seen on the epoxy matrix. However, a small number of particles had been spread over the matrix in *hss* and *lss* samples.

The thickness of the particle layer on the fibre surface in the *hss* sample varied in between 200 and 500 nm while in the *lss* sample it was close to 100–200 nm. Particle size according to TEM was considerably smaller in the *lss* sample than in the *hss* and clearly in the nano range.

The reason for mineralisation in the case of *Uhyd* synthesis route is attributed to the presence of hexenuronic and 4-*O*-glucuronic acids in the fibre wall, fibres porosity and swelling characteristics in alkaline media. It is known that the fibre swelling occurs at pH 8–9 [211] while LDH particles' two-stage nucleation with Al^{3+} begins at pH 8.8. The slow pH change in *Uhyd* route allows the fibres to swell with the aid of increased temperature prior to particle nucleation. The non-diffusive charges that are fully deprotonated at the precipitation pH facilitates the ion exchange through the semipermeable fibre wall. In addition, urea that is used in excess may exchange some of the water molecules in the fibre wall, and, as hydrolysis increases, the pH internally in the fibre wall promotes hydroxyl formation of Al^{3+} and Mg^{2+} ions and presumably LDH. At this point, however, it is impossible to rule out that the particles inside the fibre wall are other than LDH, for example, metal hydroxyls.

4.2.3. Thermal behaviour of modified fibres

The onset temperature (T_{onset}) for the oxidative combustion was defined according to the level of noise and set to -0.025 K^{-1}. At that point approx. 0.3–0.5% of the sample had been degraded. The qualitative margin of error was accepted to stay within 3 K. the density of a sample pellet in the given range (250–700 $mg \cdot cm^{-3}$) did not affect the onset temperature. Thermal conditioning at 200 °C provided a standard point that excluded, in major parts, the water of crystallisation from LDH (approx. 14–15%) and hydration from the pulp fibres. The crystalline transformation processes of LDH at that temperature are subtle, while the water of crystallisation is effectively removed. Cellulosic material is expected to remain intact, provided that the isotherm is carried out in a relatively short amount of time.

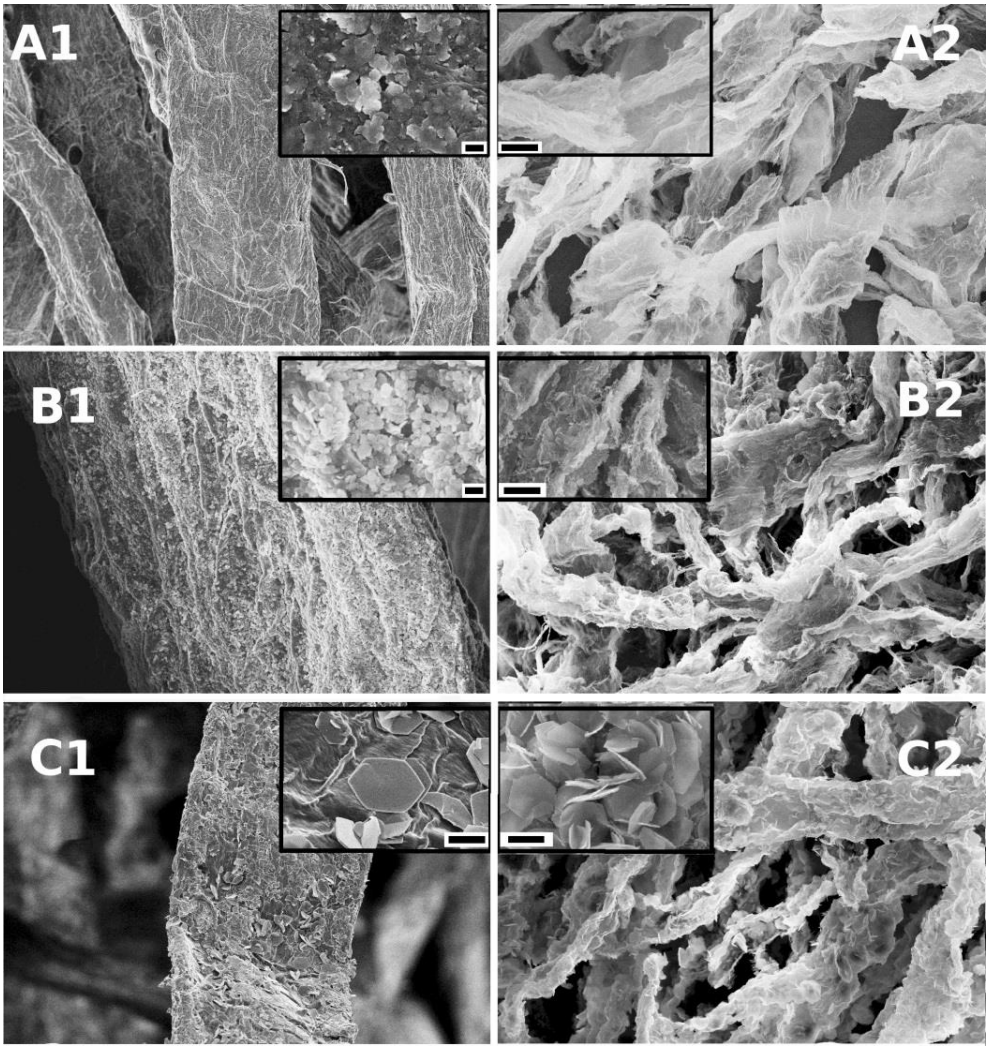

Figure 4.6 Modified BKraft pulp fibres (A1, B1, C1) and combusted ones respectively (A2, B2, C2). The lss (A) and hss (B) routes produced irregularly shaped nanoparticles while the Uhyd (C) synthesis route resulted in clay sized hexagonal particles on fibre surface. Magnifications: 1000x in A1, A2, B2, C1, C2 and 5000x in B1. Scale bars in the insets: 200 nm in A1 and B1, and, 2.0 µm in A2, B2, C1 and C2.

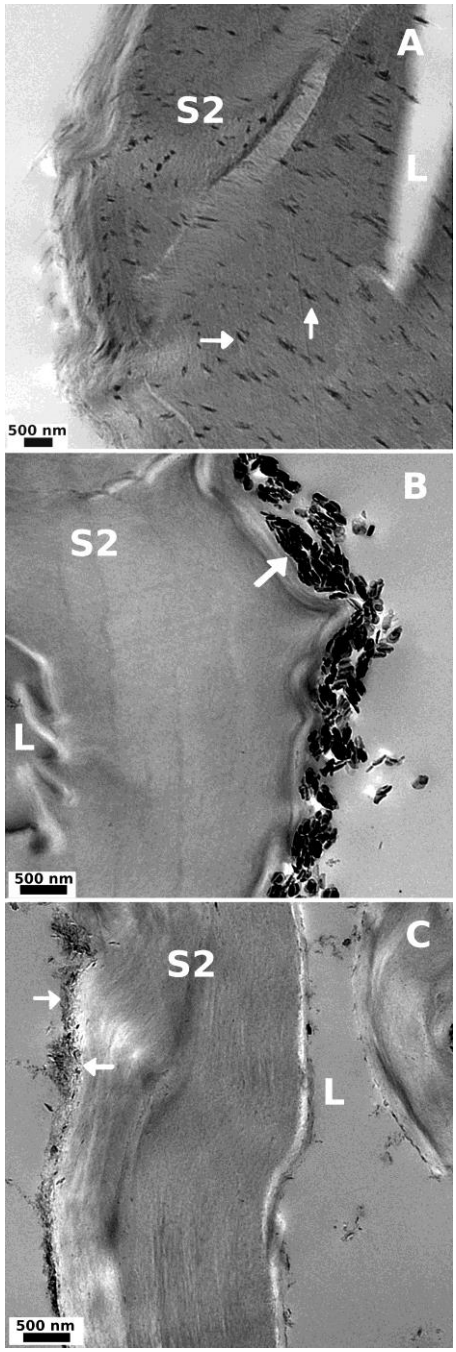

Figure 4.7 TEM images of BKraft fibres after Uhyd (A), hss (B) and lss (C) synthesis route. The lumen (L) and particles (arrows) are marked.

The reference fibres began to depolymerise at 224 ± 3 °C, while T_{onset} for the modified ones was between 234 and 239 °C. The first depolymerisation reactions

peaked at around 320 °C in all samples including reference fibres. The LDH particles appeared to increase the rate of depolymerisation at first. However, after treating the fibres with alkaline aqueous solution with pH corresponding to the LDH synthesis, the effect was similar with the exception that the second exothermic heat evolved around 460 °C that was 20 °C higher than the reference and 10 °C higher than the fibres modified by the *Uhyd* process. It is known that CO_2 from combustion of cellulose evolves in two phases at approx. 320 °C and 475 °C [212]. The literature values fit well within the experimental results (figure 4.8). Therefore, it is probable that during the LDH synthesis the alkaline conditions helped to remove residual hemicelluloses, mainly xylan, from the fibres, thus, pushing the initial depolymerisation to higher temperatures.

The alkali extracted sample appeared to degrade more (82%) than the rest of the samples (78–80%) during the first exothermic reaction. However, it is difficult to address the significance of the apparent difference in oxidation due to small density variations between the sample batches. For example, the pellet density of the *hss* samples gave an error of 2% in relative weight at the pseudo-equilibrium conditions and after complete combustion.

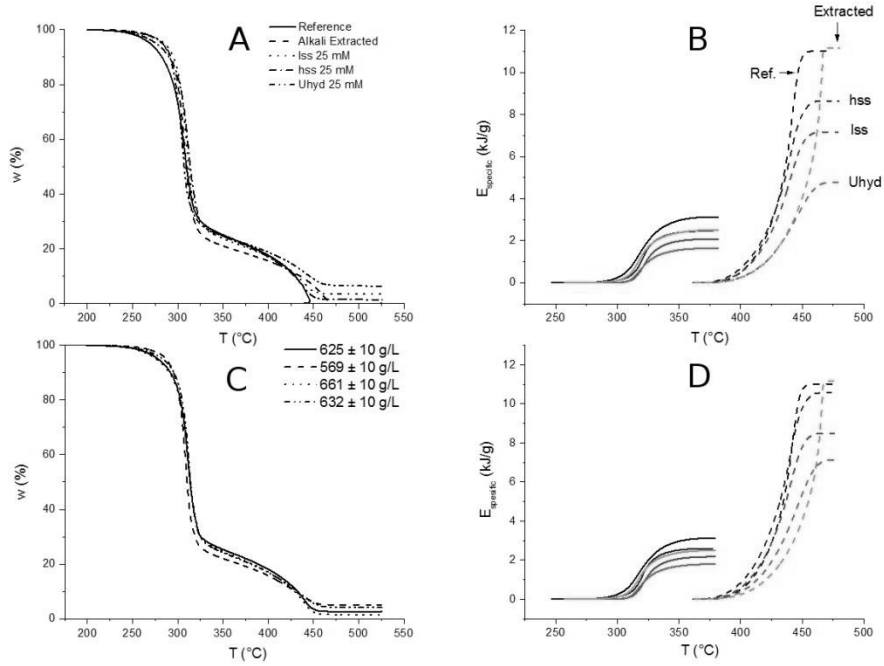

Fig. 4.8 The thermogram (A) and energy release profile (B) for modified BKraft fibres. The effect of density variation in the hss sample (C) and the organic material content corrected specific energy (D) are shown as well. Previously unpublished.

In order to evaluate the effect of LDH in the samples TG response, the initial LDH content as well as the relative amounts after both exothermic reactions must be established. Knowing the relative amount lost in the crystalline transformation and dehydration processes (41–44%) during the thermogravimetric analysis of the neat

LDH particles in the given temperature range, and, the amount of ash from pulp (0.8% ± 0.2%), the initial weight of LDH in each sample can be calculated. The same applies to the pseudo-equilibrium conditions at approx. 370 °C. Results are shown in table IV.3. In the calculations, we are assuming that the energy and weight are linearly related within the given temperature range and system configuration. Furthermore, care should be taken in the interpretation of the results due to factors explained in the experimental chapter.

It appears that the small amount of LDH in comparison to the organic substance cannot contribute to damping of the first or the second exothermic transformations of cellulosic fibres. Thus, the LDH is not capable to induce or limit the cellulose oxidation within the given test environment.

Table IV.3 The calculated weight fractions (ψ) of organic material (org) and LDH particles in modified BKraft fibres at 25 °C, 200 °C and 370 °C. Residual weight (w) and the total weight change in combustion of LDH (Δw_{LDH}) are also presented. In addition, material specific unit energies (E_p) for both exothermic signals, the LDH corrected exothermic energy (E^0_{p1}) and limiting viscosity numbers (η) are listed as well.

Sample	Ψ^{25}_{org}	Ψ^{25}_{LDH}	Ψ^{200}_{LDH}	Ψ^{370}_{LDH}	w	Δw_{LDH}	E_{p1}	E^0_{p1}	E_{p2}	E^0_{p2}	η
			%				kJ·g^{-1}				mL·g^{-1}
Ref.	100	0	0	0	~0	-	3.9	3.9	11.7	11.7	923
lss	95.0	5.0	4.2	15.5	3.6	43.8	2.6	3.1	7.3	8.6	813
hss	94.2	5.8	5.0	18.2	4.1	43.4	3.0	3.7	7.6	9.3	868
Uhyd	90.3	9.7	8.3	33.0	6.5	40.8	1.7	2.5	4.3	6.4	754

It is evident from the results that the limiting viscosity number (η) correlates linearly, within the experimental error, with the first and the second specific unit energies ($E_{p1}{}^0$ and $E_{p2}{}^0$).

Combustion kinetics was evaluated by treating the samples at 340 °C for pre-set time intervals. The results are presented in Figure 4.9. Signal evolution proceeded gradually in all LDH containing samples, while reference pulp fibres charred relatively slowly. However, after 240 s the combustion kinetics increased markedly. All LDH modified samples contained organic material even after 420 s of combustion, while reference pulp was practically incinerated. Deconvoluted spectra revealed the differences in combustion kinetics in each LDH containing samples. The signal at around 1585–1620 cm^{-1} arises from diones, presumably from 1,3-diketones, while the absorption at around 1775–1720 cm^{-1} is assigned as carboxylic acids, aldehydes, and 1,2-diketones [213,214]. In all LDH containing samples combustion produced partially oxidised cellulose in relatively high amounts. Pulp fibres without LDH were readily oxidised to carboxylic acids. We assume that the lower energy needed for aldehyde and dione formation drives the combustion in LDH containing samples due to loss of water and hydroxyls from LDH crystals. The carbonate in LDH particles contributed to the deconvoluted spectra of the *lss* and *Uhyd* samples (peak numbered as 4 and 5 respectively). Similar effect with the *hss* sample was observed after 300 s. Small contribution from water was also needed for the fitted curve in *Uhyd* to match the recorded absorption signals. The interference curve in *lss* and *Uhyd* deviates from the original below 1525 cm^{-1} due to additional signals

originating from complex absorption of cellulose and carbonate in LDH gallery. In *lss* the contribution from nitrates should, however, be born in mind. We cannot distinguish the fractional basis of CO_3^{2-} and NO_3^- .

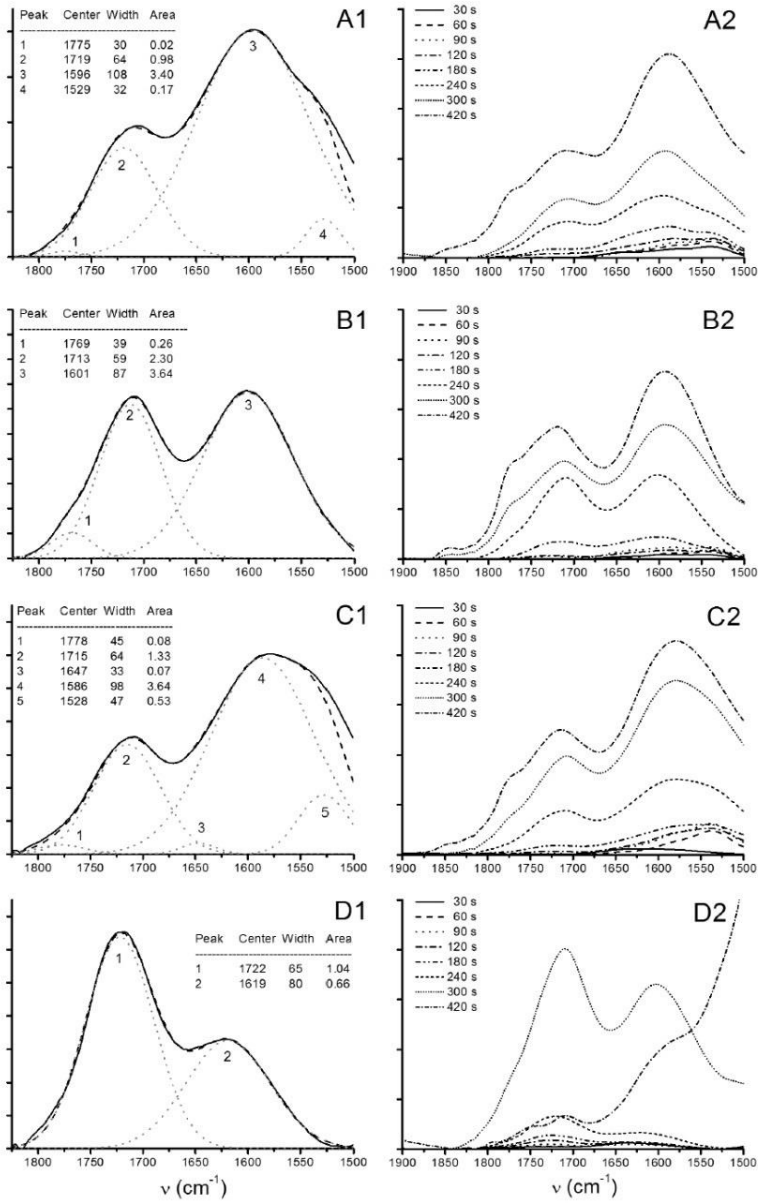

Figure 4.9 ATR-FTIR spectra from the thermal decomposition kinetics of lss (A), hss (B), Uhyd (C) and fully bleached Kraft pulp (D) at 340 °C. Deconvoluted FTIR spectra after 240 s in range of 1500–1850 cm^{-1} are presented in figures (A1–D1) and signal evolution within 420 s in figures (A2–D2).

4.3. Functionalisation and its effect on a thermoplastic composite

In our third article, we present the experiments related to composite preparation. The atactic polypropylene was chosen to serve as a matrix polymer and the functionalised BKraft and BTMP fibres were used to fill the matrix. Prepared composites were tested after conditioning at 52 ± 2% relative humidity at 23 ± 1 °C. The composites were subjected to uniaxial tension and immersed into water to evaluate the stress transfer behaviour and water absorption properties.

4.3.1. The effects of compounding on fibres' dimensions

The fibre length distribution was evaluated on a rough scale distinguishing the fibres' average length and the length averaged content of fines. Fines were assigned, in this case, to be smaller than 100 μm particulates (Table IV.4). One important characteristics of a filler element in a composite material is its aspect ratio (L) that determines the shear distribution within the material under stress. Reinforcing polymer matrix with fibres requires the L to be large enough so that the interfacial coupling constant remains in accessible levels. Typically, the average L in coniferous pine and spruce is less than 100 due to statistical reasons. Fractionation that separates fibres based on their dimensions is often time, energy and water intensive process, consuming unnecessary resources and, therefore, not preferred in industrial manufacturing. If fractionation is used, however, it is applied only to exclude the smallest particulates and fibrils from the intact fibres. In our case, we were looking for the changes in fibres' dimensions during the processing wherefore fractionation provided the frames for the interpretation of the results.

It appears that the fines content in BTMP is reduced in hybridisation, but increases again after functionalisation (column B in Table IV.4). The statistical increase in the fibre length is understandable in that the fines content is small. In the case of BKraft fibres the fines content increases in each step. Average fibre thickness (d_{av}) is reduced significantly in the BTMP sample but the BKraft fibres do not change markedly in this respect. Thus, the average L of BTMP increased but for BKraft it decreased.

Fibres suffered significant reduction in average length during the composite moulding (column C in Table IV.4). Shear dissipation from matrix to fibres was expected due to harsh conditions in micro injection moulding machine, but the surfactant was also expected to reduce this phenomenon. Functionalisation appeared to be able to protect the BKraft fibres to some extent while the BTMP fibres did not benefit in that regard. Since the *lss* synthesis route was chosen to precipitate LDH on fibre surface we must assume the fibre stiffness was not affected. However, small particles may have nucleated into BKraft fibres' cell wall.

The d_{av} was expected to reduce in all cases due to lumen collapse that is known to occur under an extensive load across the fibre axis. The functionalised BTMP deviated from anticipated results possibly due to the presence of matrix polymers that remained on the fibre surface after extraction. Therefore, d_{av} are to be considered indicative affecting also to values in L. The fibre loading levels did not reach the aimed 20% w/w, but 12–17% instead.

The weight fraction of fibres found through extraction was evaluated by immersion technique after equilibrating the injection moulded specimen at 40 °C for 10 days. The average sample volume was calculated from 10 to 12 samples that were immersed in water at 23 ± 1 °C. The density of injection moulded matrix polymer was found to be 0.91 ± 0.01 g·cm^{-3}, while for fibre containing samples it was 1.01 ± 0.01 g·cm^{-3} irrespective of the applied modification. The density of cellulose and lignin are close to 1.5 and 1.4 g·cm^{-3} respectively [215]. Sometimes the carbohydrate density used in calculations is 1.58 g·cm^{-3} [32]. Bleached Kraft fibres contain only residual lignin fragments. After the lumen collapses, the density should equal the fibre's cell wall structure. Therefore, the density of the injection moulded specimen that contain BKraft fibres should be between 1.50 and 1.58 g·cm^{-3}. Bleached thermomechanical pulp from spruce contain 28% of lignin on average that brings the density close to 1.47–1.53 g·cm^{-3}. By using the volume of a standard tensile test specimen (1.0 g·cm^{-3} for ISO 527-2 1BA) the w/w fibre loading in the BKraft samples was calculated to be 0.15–0.17. For the BTMP samples it was 0.16–0.18. Calculations fits relatively well to the experimental results.

Table IV.4 The length weighted averages of fibre length (l_{av}), width (d_{av}), fines content (fines) and aspect ratio (L) after fractionation (A), functionalisation (B) and compounding (C).

Sample	Parameter	A	B		C		
			0%	6%	Ref.	0%	6%
BKraft	l_{av} (mm)	2.28 ± 0.03	2.06 ± 0.06	1.95 ± 0.04	0.37 ± 0.01	0.19 ± 0.01	0.43 ± 0.02
	d_{av} (µm)	30.8 ± 0.2	30.9 ± 0.6	31.0 ± 0.4	22.6 ± 0.3	23.0 ± 0.5	22.9 ± 0.3
	fines (%)	0.4	1.0	1.1	76.3	93.8	69.6
	L	74	67	63	16	8	19
	Ψ (%)				15	12	14
BTMP	l_{av} (mm)	1.74 ± 0.03	2.06 ± 0.01	1.69 ± 0.02	0.25 ± 0.01	0.22 ± 0.01	0.27 ± 0.01
	d_{av} (µm)	36.8 ± 0.3	32.9 ± 0.2	29.4 ± 0.3	27.7 ± 0.4	24.8 ± 0.3	32.5 ± 0.2
	fines (%)	4.0	0.3	1.9	91.0	93.1	87.6
	L	47	63	57	9	9	8
	Ψ (%)				17	17	12

4.3.2. Tensile properties of fibre filled PP composites

The tensile test is typically the first step to evaluate elastic properties of the prepared composites. Specimens are subjected to uniform stress with predetermined strain rate. Viscoelastic properties of the matrix component are known to influence on the stress-strain curve derived values as strain rate changes [216]. Typically, strength (σ) and elastic modulus (Y) will increase, while elongation (ε) decreases. These changes were observed in our work as well (Table IV.5). Resilience (R) either increases or decreases depending on the σ/ε relationship.

The reference fibres improved the load bearing capacity (higher σ and Y) of PP as expected, while the modified and the functionalised fibres increased plasticity (lower Y and higher ε). The ductility of the BTMP fibre filled PP composites increased upon functionalisation indicated by ε in two different strain rates. Elasticity was lost as R became smaller upon modification and functionalisation. For the BKraft fibres the functional particles on the fibre surface affected only slightly to stiffness (Y) (<5%).

Material toughness in both fibre types at the level of yield became lower upon modification and functionalisation. The BKraft fibres were less affected in this regard. However, correcting the strength values with the material content found after extraction, and assuming other parameters to remain constant, the results show a change in σ in the elastic region due to functionalisation only. Toughness followed the same trend. The torque needed to knead the composite material in the conical chamber followed the fibre content reasonably well.

The deformation study with a SEM and optical microscope revealed the micro-crack formation, agglomeration and fibre pull-out effect upon modification and functionalisation (figures 4.10 and 4.11).

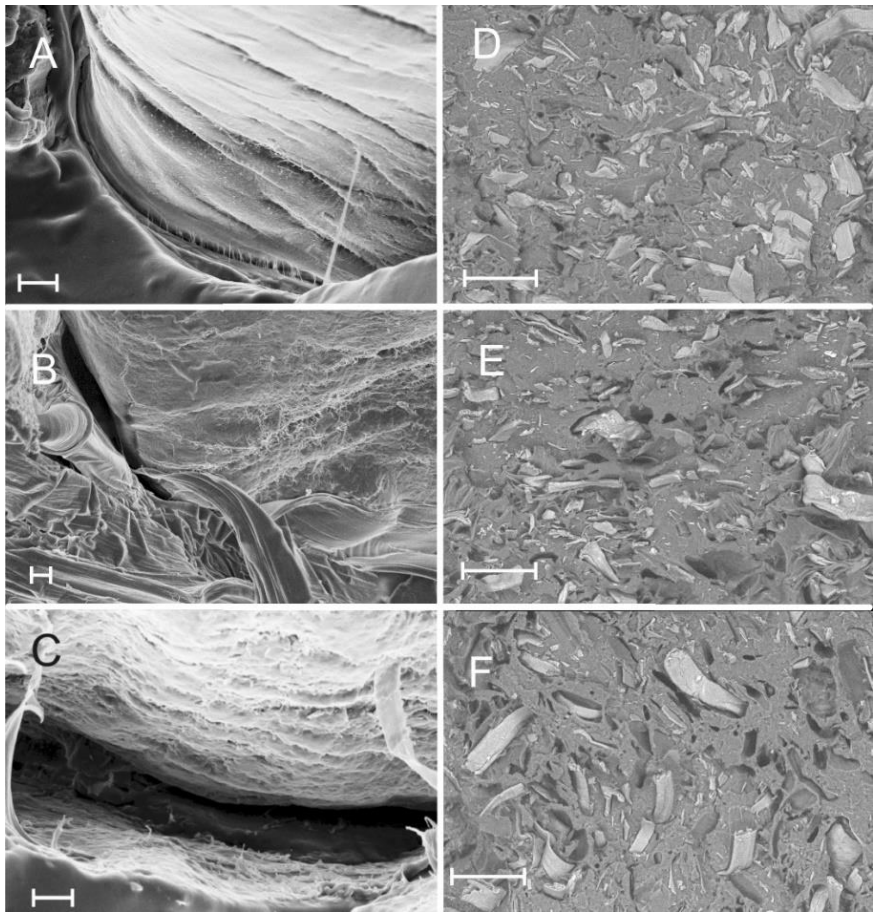

Fig. 4.10 SEM images of the BTMP fibre-matrix interphase. The reference fibres (A,D), the hybrid fibres (B,E) and the functionalised fibres (C,F). Images D-F are taken from the back scattered electrons for contrast enhancement. The length of the scale bars in figures A-C are 1 µm while in D-G they are 100 µm.

Table IV.5 The test parameters for the uniaxial stretch deformation at two different strain rates including yield strength (σ_{yield}), Young's modulus (Y), modulus of resilience (R), ultimate strength and elongation ($\sigma_{ultimate}$, $\varepsilon_{ultimate}$), strength and elongation at break (σ_{break}, ε_{break}). Compounding torque (T) is presented as well.

Parameter	PP	BKraft			BTMP					
	5 mm / min	5 mm / min			5 mm / min			50 mm / min		
		Ref.	0%	6%	Ref	0%	6%	Ref	0%	6%
σ_{yield} (MPa)	8 ± 1	17 ± 1	14 ± 2	14 ± 2	19 ± 2	18 ± 1	12 ± 1	22 ± 1	21 ± 2	13 ± 1
Y (GPa) *	0.50 ± 0.04	1.08 ± 0.05	0.96 ± 0.08	0.92 ± 0.04	0.98 ± 0.08	1.05 ± 0.04	0.94 ± 0.03	1.08 ± 0.08	1.14 ± 0.06	1.07 ± 0.08
R (kJ m^{-3}) **	61 ± 9	130 ± 20	110 ± 20	100 ± 20	180 ± 40	160 ± 20	70 ± 9	220 ± 30	200 ± 30	80 ± 10
$\sigma_{ultimate}$ (MPa)	27 ± 2	39 ± 3	31 ± 4	34 ± 3	36 ± 2	34 ± 1	29 ± 1	41 ± 1	35 ± 3	31 ± 3
$\varepsilon_{ultimate}$ (%)	22 ± 1	14 ± 1	13 ± 1	14 ± 1	11 ± 1	11 ± 1	12 ± 1	9 ± 1	7 ± 2	10 ± 1
σ_{break} (MPa) [a]	21 ± 2 [b]	37 ± 3	27 ± 4	31 ± 3	34 ± 2	32 ± 1	24 ± 2	40 ± 1	31 ± 3	29 ± 4
ε_{break} (%) [a]	39 ± 3 [b]	16 ± 1	21 ± 1	17 ± 1	14 ± 3	16 ± 1	24 ± 3	9 ± 1	14 ± 2	15 ± 2
T (N)	1.15 ± 0.03	1.30 ± 0.03	1.35 ± 0.03	1.50 ± 0.03	1.33 ± 0.03	1.33 ± 0.03	1.28 ± 0.03			

* Defined from a linear fraction at 0.1–1.1% strain.

** Calculated according to Eq. 3.3 from the secant at 0.1% offset.

[a] The values were defined as the point where the rate of change in stress exceeds -5 MPa.

[b] The values for PP matrix refers to the drop after $\sigma_{ultimate}$, which occurs due to extensive necking of the sample.

$$R = \frac{{\sigma_{yield}}^2}{2Y} \qquad \text{(Eq. 4.3)}$$

The BTMP fibres were slipping out of the matrix under uniaxial tensile stress as can be seen from figure 4.10. Studying the fibre-composite interphase, it seems that particles that contained SDS surfactant were adhering with the polymer while the cohesion of particles on fibre surface was failing under strain.

The optical examination shows the material to produce micro cracks throughout the sample under stress (figure 4.11). Necking, however, is barely noticeable. Functionalisation appears to aid in fibre dispersion within the melt as well as the stress dissipation.

Comparing the results from the tensile tests together with the SEM and optical images, it appears that the LDH particles are acting like the ball bearings on fibre surface. The SDS surfactant, although increasing the coupling with PP matrix, also enhances ductility, i.e. the flow properties of the material. Functionalised fibres will therefore resist agglomeration during the moulding process. Stiffness is barely affected but the resilience in the linear region degreases, mainly due to lower strength values.

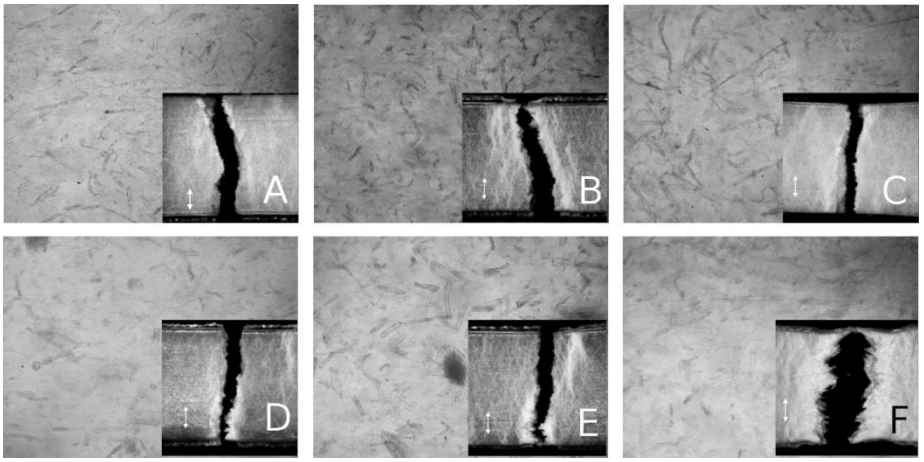

Figure 4.11 The optical micrographs from the composite skin layers and the fractured areas after tensile tests. the BKraft fibres are presented in figures A-C and the BTMP in figures D-F. The reference fibres (A and D), the hybridised fibres (B and E) and the functionalised fibres (C and F).

4.3.3. Water absorption of fibre filled PP composites

The Fick's diffusion predicts that an average mass flux of molecules (n_{spec}) at time t is linearly correlated with respect to $t^{1/2}$ according to equation 4.4. This is the case if the initial diffusion (D) occurs in a plane with thickness L [217,218]. In our experiment, the diffusion of water occurred from both sides of the composite sample L being half the sample thickness (L = 1 mm). The effects of sample edges were neglected thus D approximates to upper boundary value.

$$\left[\frac{n_{spec}}{n_{spec,\infty}}\right]^2 = \frac{16}{L^2}\left[\frac{D}{\pi}\right]^a t^a \qquad \text{(Eq. 4.4.)}$$

The equation reduces to Fick's diffusion when the exponent *a* is unity. As can be seen from figure 4.12, the curves begin to deviate from linearity at $t^{1/2} = 15$. However, the timespan up to 200 h gives possibility to evaluate initial diffusion coefficients using the maximum adsorption derived by Langmuir isotherm (Figure 4.13). Results are listed in table IV.6.

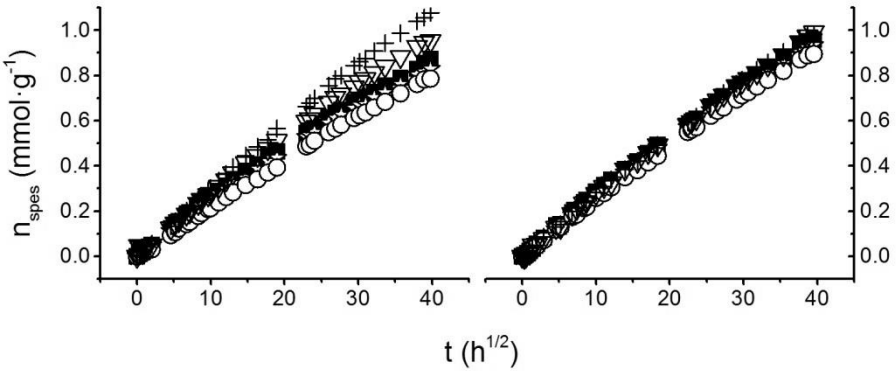

Figure 4.12 The adsorption and desorption kinetics of the BKraft (right curve) and BTMP (left curve) are plotted against the $t^{1/2}$. Reference pulp (■), hybridised pulp 10-0% (⭐), hybridised pulp 100-0% (○) and functionalised pulp 100-3% (▽) and 100-6% (+).

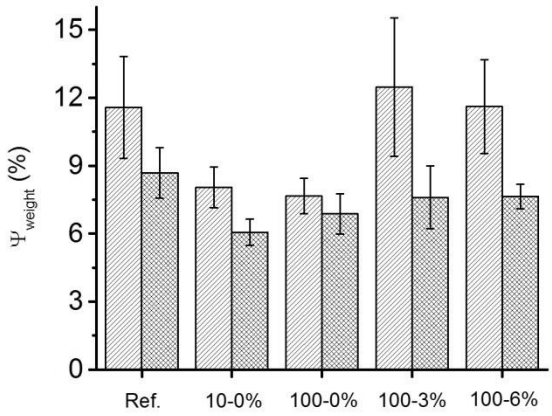

Figure 4.13 The relative mass increase (Ψ_{weight}) of the composites in different filler compositions at equilibrium in water as predicted by Langmuir's model. The lighter shade represents the BTMP fibres and the darker shade the BKraft fibres. Previously unpublished.

The Langmuir adsorption most likely overestimates the maximum weight increase in the composites. Surprisingly, the composites filled with functional fibres adsorbed almost as much water as reference fibres did, while particles without surfactant seemed to inhibit absorption.

Desorption of water did not change markedly upon modification and hybridisation of the pulp fibres. Some differences were observed in the beginning of the experiment

(inset in figure 4.14), as the BKraft fibre filled composites kept water more tightly within the material than the BTMP fibres did. At the end of the test, the trend was the opposite.

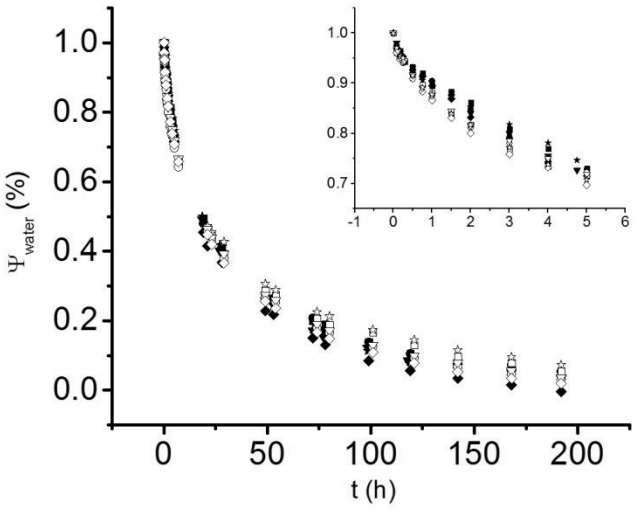

Figure 4.14 Desorption kinetics. The solid symbols represent the BKraft fibres and the open symbols represent the BTMP fibres. The reference (■), hybridised pulp: 10-0% (□) and 100-0% (●). The functionalised pulp: 100-3% (▼) and 100-6% (◆). The inset magnifies the beginning of the desorption process. Unpublished data.

Table IV.6 The maximum absorption (S_{max}) and the calculated initial diffusion co-efficient (D) are tabulated.

Parameter	BKraft					BTMP				
	Ref.	10	100	100-3	100-6	Ref.	10	100	100-3	100-6
S_{max} (%)	12 ± 2	8 ± 1	8 ± 1	12 ± 3	12 ± 2	9 ± 1	7 ± 1	7 ± 1	8 ± 2	8 ± 1
D ($m^2/s \cdot 10^{-15}$)	1.28	2.02	1.62	2.04	2.46	0.92	1.97	1.71	0.93	0.92

4.4. The effect of hybridisation on the combustion of foamed light weight structures

The purpose of chapter 4.4 is to address the flammability of the foam formed light weight material. The elemental composition, combustion kinetics and particle size was studied to link the information from the cone calorimeter to the LDH particle properties.

4.4.1. Topology and particle content on hybridised fibres

The fibres that were used in light-weight fibrous foam (lwFF) were characterised by TEM instrumentation. The LDH particles were found mainly on the fibres surface and lumen as well as on the fine structures (Figure 4.15). Interestingly, the fibre cell wall was void of particles. FTIR showed a strong carbonate peak at 1358 cm^{-1} (Figure 4.16).

It appeared that the sequential synthesis of LDH particles on BTMP fibres effectively fibrillated the fibres by forming thread-like structures (Figure 4.17). Energy dispersive spectra showed a small amount of sulphur on the surface of the foamed reference panel. The foaming agent must have been adsorbed onto the fibres during the dewatering of foam-laid fibre web. These webs, when prepared from the hybridised fibres, contained sulphur throughout the cross-section. Estimation for the effective absorption of SDS surfactant on LDH containing fibres can be made via aluminium to sulphur ratio. It was noted that the Mg^{2+} to Al^{3+} ratio ($R_{Mg\text{-}Al}$) in panel prepared from hybridised fibres did not change markedly while Al^{3+} to S^{6+} ($R_{Al\text{-}S}$) was slightly higher in the middle layer (Table IV.7). The surfactant was prone to adsorb onto the panel surface. The listed values are the average of five analyses.

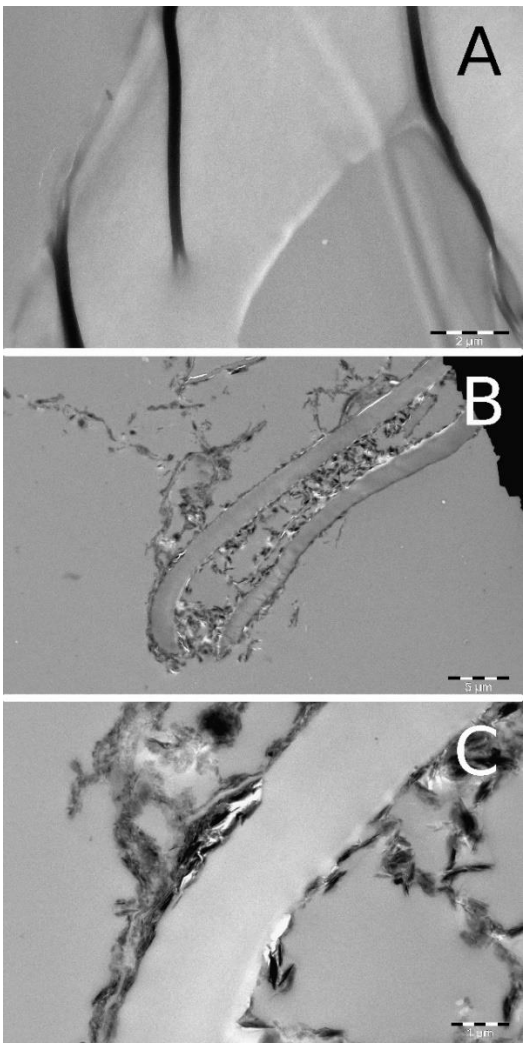

Figure 4.15 TEM images of the reference BTMP fibres (A) and the hybridised fibres (B, C). LDH particles appear to have nucleated mainly on fibre surface and lumen as well as to fine structures.

Table IV.7 The element ratio in the foamed panel according to EDS.

Ratio	Surface	Middle layer
R_{Mg-Al}	1.5	1.4
R_{Al-S}	7.9	9.0

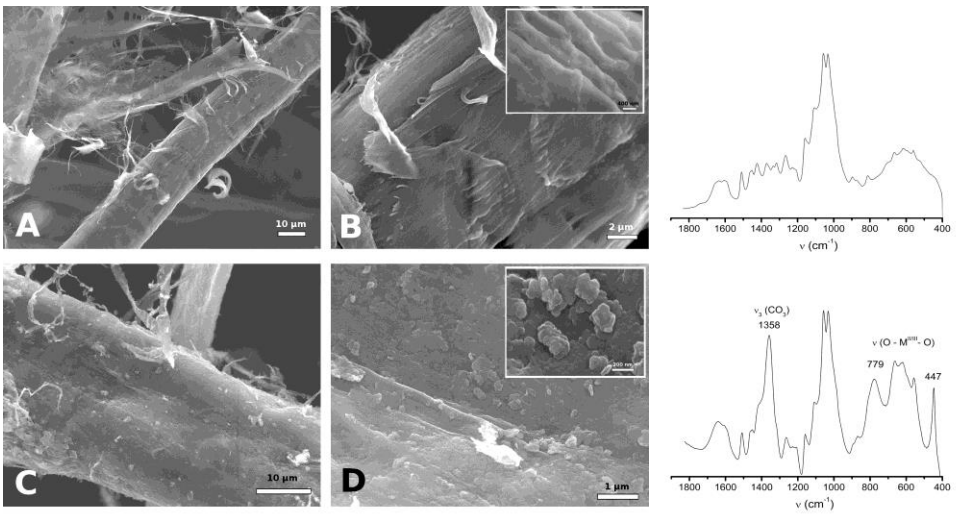

Figure 4.16 The SEM images from a single fibre of foamed reference panel (A,B) and the panel prepared from the hybridised fibres (C,D). Corresponding FTIR spectra are shown next to the images.

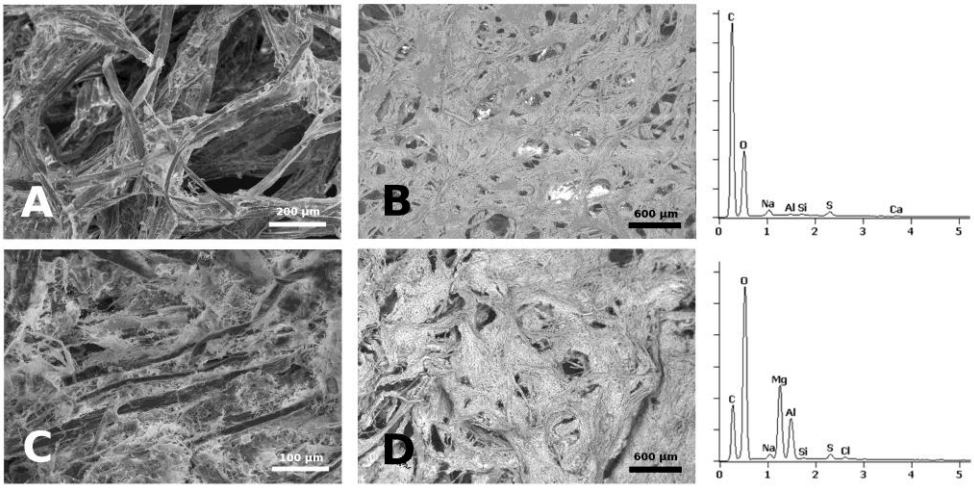

Figure 4.17 The SEI images from the surface of reference (A) and hybridised (C) lwFF with the corresponding BSE images (B,D) and ED spectra are shown next to them.

4.4.2. Combustion behaviour of foamed materials

The outcome of the combustion experiment in a CC is influenced by the vertical distance of the sample from the external heat source, applied heat flux, the sample holder system and the physical dimensions of the specimen. Applicability of CC in prediction of hazardous fires has been discussed by others [219,220]. In our experiment, the distance of the sample surface from the external heat source was 60 mm. This distance is relatively long and may cause the centre of the sample to absorb higher relative irradiance per unit time than the sample edges [219]. However, the tested *lwFF* were dimensionally unstable under forced burning. The relatively low irradiance (25 $kW \cdot m^{-2}$) was targeted to address the ignition phenomenon. Sample thickness is also a key factor in CC experiments. Foam-laid fibre panels are meant to be applied as a bulk material, wherefore the 7.5 mm sample thickness is within a practical limit. Typically, several such layers are combined to a lamellar structure that is eventually compressed to appropriate density in a suitable mould. Thin samples tend to show higher peak heat release rate (PHRR) values, while thick samples burn longer allowing better estimation of flame propagation within the structure. Furthermore, the cut samples were placed on a 20 μm thick aluminium tray. Aluminium transports irradiated heat away from the sample. The effect of thermal transport is assumed to be small, however, because the wood fibres are heat insulators and the contact interface area between the sample and aluminium tray was considerably smaller than the geometrically measured flat surface area of the specimen.

Although CC cannot mimic real fire due to measurement restrictions, its importance is in data related to the material behaviour after heat radiation impinges the sample surface. In cone calorimeter, the HRR is the crucial factor and it is calculated from the flue gas oxygen consumption. Anything that limits oxygen usage upon flaming, such as generation of soot, decarbonation, temperature drop within the material, water evaporation, etc., will affect the observed HRR [221]. The *in situ* synthesised LDH particles on the fibres' surface provided reduction in PHRR, CO_2 production rate and smoke yield (Figure 4.18 and Table IV.8). Tailing in HRR signal predicts that both systems are charring to some extent. The mass loss rate is reduced in the LDH-lwFF sample indicating slower material volatilisation. Narrow HRR profile – rapid combustion – was expected due to the sample thickness. The carbon monoxide yield and production rate increased relative to the lwFF reference. Partial oxidation that appeared before the advancing heat release in both samples, also related to CO production and material pyrolysis at the reaction zone front, appeared similar in rate and yield. The production rate of the CO in material glowing phase, i.e. after the combustible volatiles have been released to allow the temperature to remain sufficiently high for material pyrolysis, however, was three times faster in the case of the LDH-lwFF. The combustion efficiency is defined as the ratio of the total heat evolved (THE) to the mass loss change until flame out. This parameter was reduced by LDH.

Table IV.8 Combustion parameters from CC experiments of five replicate samples. t_{ig} = time to ignition, t_{fo} = time to flame out, PHRR = peak heat release rate, ψ_{CO} and ψ_{CO_2} = CO and CO_2 production yields, v_{CO} and v_{CO_2} = maximum CO and CO_2 emission rates, E = total energy release, τ = total smoke release.

Sample	t_{ig} (s)	t_{fo} (s)	PHRR (kW/m²) [Δ_{ig} / s]	ψ_{CO} (kg/kg) [ψ / %]	ψ_{CO_2} (kg/kg) [ψ / %]	v_{CO} (mg/s)		v_{CO_2} (mg/s)		E (MJ/m²)	τ (m²)
						1.	2.	1.	2.		
lwFF	8±1	24±2	177±6 [14]	0.058±0.004 [2.1]	2.7±0.3 [97.9]	1.8±0.2	2.10.2	127±7	133±7	3.7±0.2	0.17±0.02
LDH-*lwFF*	12±1	34±3	68±10 [20]	0.18±0.03 [6.5]	2.6±0.2 [93.5]	2±1	4.60.3	40±20	51±7	2.1±0.1	0.04±0.03

[1] *Δ_{ig} in brackets refers to the average elapsed time in seconds from the material ignition to the peak value.*
[2] *The fraction (ψ) of the volatile gas from the total gas production is presented in brackets.*

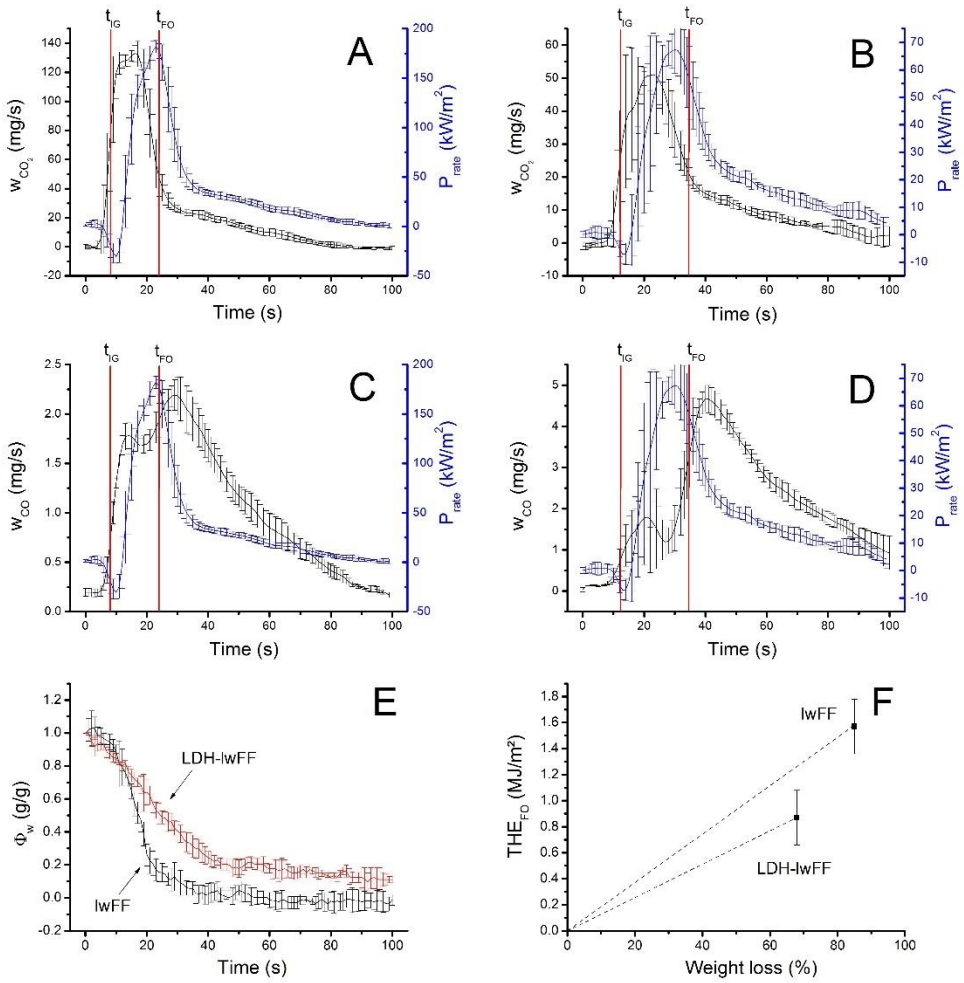

Figure 4.18 The mass release rate of CO_2 (A,B) and CO (C,D) (black lines) during the oxidative pyrolysis is compared against HRR (blue line) in the lwFF reference (A,C) and the LDH-lwFF (B,D). Data from the mass fraction extent (E) and combustion efficiency (F) are presented as well. The time to ignition (t_{IG}) and the time to flame out (t_{FO}) are marked with red vertical lines.

Some researchers have suggested that materials safety, in case of fire, can be evaluated and characterised indicatively from CC results by simple calculations based on PHRR, t_{ig}, and from the total energy release [222]. For example, in our case, the so-called flash over propensity that is defined as the ratio of the PHRR to t_{ig}, reduces from the initial 22 (high risk) to 6 (moderate risk). Total energy release fell to low risk assessment in both samples. In addition, the smoke production of the LDH-lwFF sample subsided within 15 s after ignition, while for the reference foam, it took nearly 22 s. Also, the amount of soot was about four times greater in reference lwFF sample (Table IV.9). The mineral containing foam will therefore produce less fine particulates upon fire. In comparison, the ammonium polyphosphate treated plywood releases significantly higher amounts of smoke, while the PHRR values and the

relative amounts of CO formation were similar to our experiments [223]. It was interesting to note that the flame subsided slowly in the LDH-lwFF sample, albeit it did not develop as it did in the reference lwFF. The LDH particles seem to act as a heat barrier and reduce the liberation of burning volatiles. An example of material morphology after combustion is given in Figure 4.19. Carbonised organic substances are seen in the lwFF while particles that resemble features of fibres are seen in the LDH-lwFF sample.

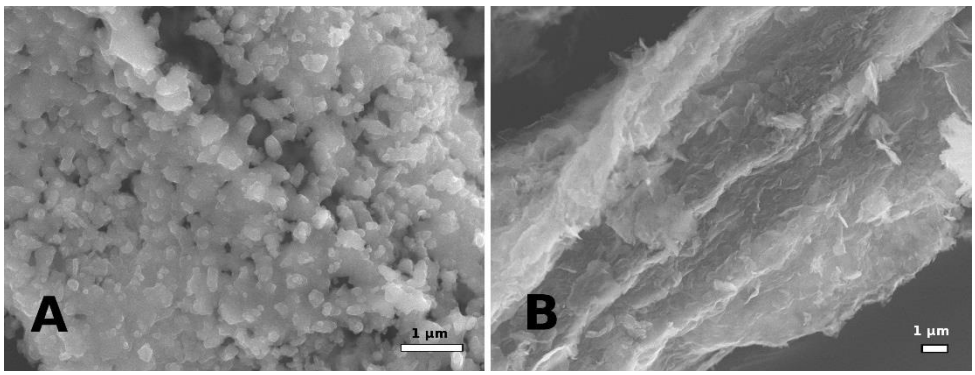

Figure 4.19 SEM close up images from the large residues of reference lwFF (A) and LDH-lwFF (B) after oxidative pyrolysis in cone calorimeter.

The combustion of the volatiles in CC was rapid and the glowing stage was also subsiding within 90 s after material ignition. It is known that heat transfer from the external heat flux and from the flame in CC is in the same order of magnitude. It is therefore assumed that the dehydroxylation and loss of carbonate in a form of water and CO_2, and volatisation of the free and crystalline water, comprising 15% from total weight of the LDH, occur during the combustion phase.

To find out how the ratio of C to O changed during the pyrolytic phase in CC, i.e. in the beginning of the combustion process, X-ray photoelectron spectroscopy was utilised before and after the process (Figure 4.20). Photoelectron spectroscopy is a highly surface sensitive analysis technique penetrating some tens of nanometres into the material, and it is widely used in investigation of elementary composition and chemical structure of material surfaces. In our study, the carbon content on material surface was found to be relatively high after the combustion (Table IV.9). The LDH contain carbon only in a form of inorganic carbonate. Considering the chemical formula for the LDH we can conclude that the relative amount of carbon from organic material has obscured the detection of photoelectrons originated from Mg^{2+} and Al^{3+}. This organic material includes possibly xylan and other hemicelluloses that are typically redeposited on pulp fibres during the alkaline processes at elevated temperatures, such as those in the LDH synthesis. Even though sample transferring via air has also caused some additional C and O concentration on the surface, the effect is assumed to be small and systematic for all samples. After oxidative pyrolysis, the precursor metals were detected in similar proportions by XPS compared to the EDS and ICP-MS results from the bulk material. The relative amount of carbon still remained high, which can be explained only by charred organic material on the surface of LDH.

Table IV.9 The elemental surface composition of C, O, Mg and Al from the pelletised lwFF and LDH-lwFF that was also oxidatively pyrolyzed in the cone calorimeter (LDH-lwFF^{CC}). The values are given in atomic weight per centile. The relative rate of change in % for C_{1s} and O_{1s} signals and C/O ratio after 2 min of controlled burning sequence is also given.

Sample	C_{1s}	O_{1s}	Mg_{2s}	Al_{2p}	C/O	$v(C_{1s})$ min^{-1}	$v(O_{1s})$ min^{-1}	$v(C/O)$ min^{-1}	w_{Mg} mg/g	w_{Al} mg/g	R_{MgAl}
lwFF	66±1	35±1	-	-	1.9±0.2	3	3	0.9	0.07	0.1	-
LDH-lwFF	33±1	51±1	10±2	5±2	0.65±0.07	7	-4.5	0.6	54±1	37.5±0.7	1.60±0.05
LDH-lwFF^{CC}	16±2	58±2	15±1	9±1	0.31±0.05						

In the case of the lwFF, an abrupt change in carbon and oxygen contents were detected depending on the duration of the controlled burning at 350 °C (Figure 4.20). The LDH-lwFF sample provided more gradual change for both elements. The rate of change of C to O ratio after initiation at 2 min was 0.9 min^{-1} for the lwFF and 0.6 min^{-1} for the LDH-lwFF sample (Table IV.9). However, comparing the C_{1s} and O_{1s} values detected in both samples, the relative amount of carbon is seen to increase faster on the particle surface. Mineral content alone cannot explain these changes. It appears therefore that the heat transfer is restricted in the presence of LDH due to the known transformation processes taking place in the mineral. Temperature drop is expected across the mineral layer on the fibre surface that leads to inefficient oxidation of organic material. However, the pyrolysis on particle surface appears relatively rapid. The effects of controlled burning at 280 °C and 340 °C in a confined space in a muffle oven that allow only convection of gaseous products are shown in figure 4.21. The unconjugated stretch vibration of carboxylic acids at 1715 cm^{-1} increases significantly in the lwFF sample at 340 °C. In the LDH-lwFF, however, the oxidation to acids is almost non-existent. It is worth noting that the skeletal vibration from phenolic units of lignin at 1510 cm^{-1} does not show major changes in relative strength at these temperatures in the given time frame. Changes in the regions that arise primarily from vibrations of carbohydrates, viz. 950 - 1150 cm^{-1} and 1300 - 1425 cm^{-1} are, due to thermodynamic considerations, relatively intense in comparison to those that arise from the aromatic units. Furthermore, the lwFF reference does not have absorption band at 1540 cm^{-1}. This band arises from the splitting of carbonate vibration during the pyrolysis [224]. Partial oxidation contributes to the formation of the diones and ketones that are observed in 1592 - 1597 cm^{-1} in both samples. It was interesting to note that the absorption bands arising from the ring vibration of guaiacyl lignin at 1268 cm^{-1} had relatively low absorption intensity in LDH-lwFF sample. Similar reduction in absorption has been observed e.g. during the Kraft cooking of the softwood pulp fibres [225]. The *in situ* synthesis of LDH with thermomechanical softwood pulp fibres must therefore affect similarly the lignin structure as does the conventional Kraft cooking process. The common nominator here is the alkalinity of the medium.

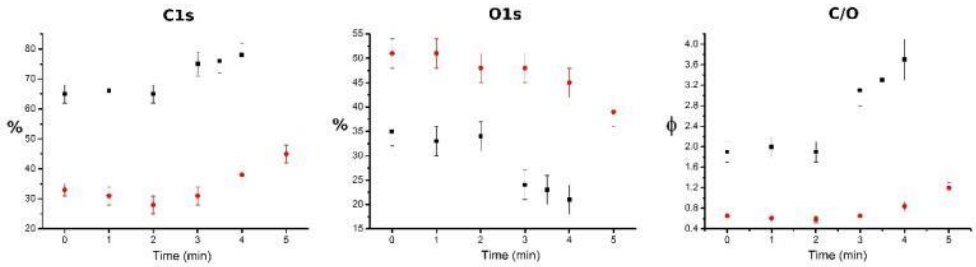

Figure 4.20 XPS results for C1s and O1s contents in % from pelletised lwFF reference (■) and LDH-lwFF (●) after oxidative pyrolysis at 350 °C.

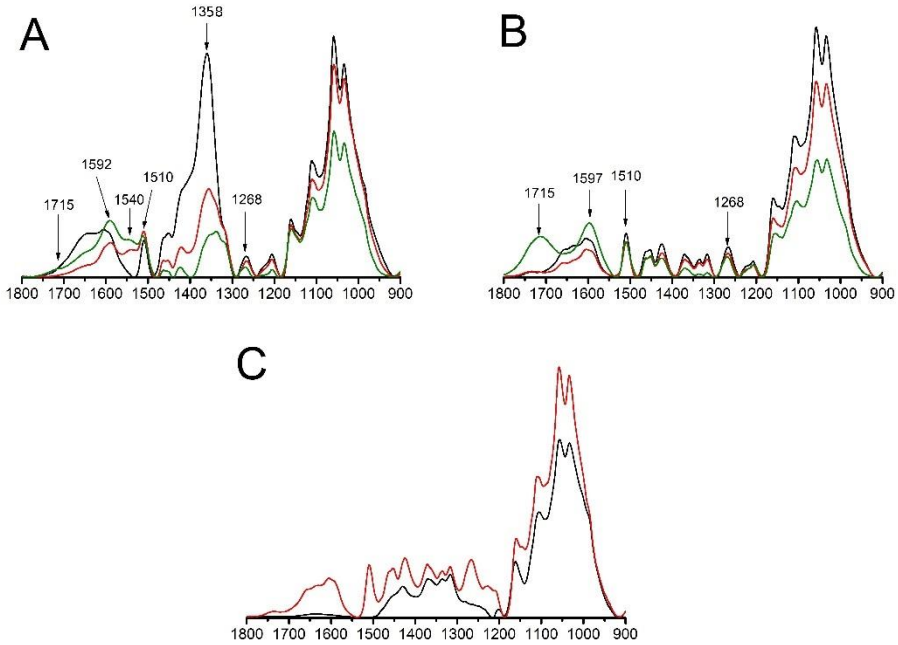

Figure 4.21 FTIR spectra from LDH-lwFF (A) and lwFF (B). The spectra were acquired from the pristine sample (black) after 120 s pyrolysis at 280 °C (red) and after 120 s pyrolysis at 340 °C (green). The spectra from the Kraft pulp (black line) and BTMP (red line) are shown for comparison (C).

Examples from the ignition, flame spread and incineration of foam-laid samples by HsVid observations are shown in figure 4.22. The advancing flame front is preceded by materials dimensional changes that were attributed to loss of easily volatised compounds, such as water, and the fibre collapse. Dimensional changes in the lwFF seemed to occur everywhere in the area of imaging approximately at the same time. In the LDH-lwFF sample the dimensional changes were subtle. The flame spread and incineration, however, were conducted from fibre to fibre.

Once the flame was initiated by the heated resistive wire, the material incinerated from that point onward. It was noted above that majority of CO_2 is released after ignition. During the oxidative pyrolysis of the LDH-lwFF the flame spread was observed as an advancing glow, yet the incineration was practically completely dampened by the particles on the fibre surface. Since the exothermic reactions observed in TG suggest that both samples carry similar energies, provided the temperature ramp is reasonably slow, the rapid pyrolytic temperature change due to material volatilisation in the flaming zone front must be used up by the LDH.

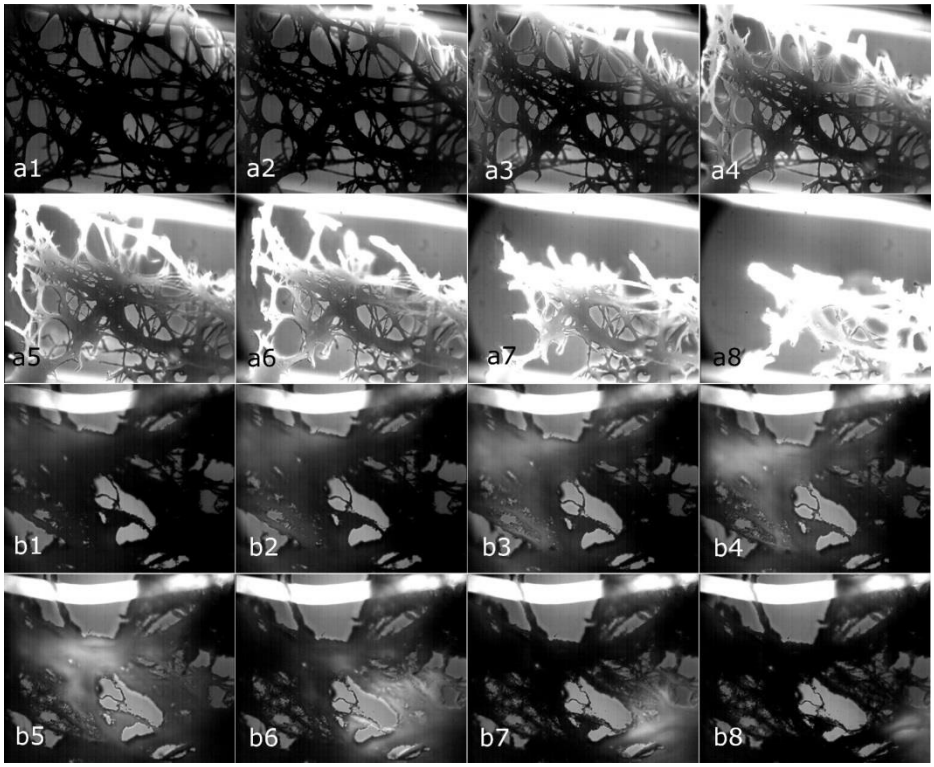

Figure 4.22 HsVid images from the combustion of reference fibres (a1-a8) and hybridised fibres (b1-b8). Each image was acquired in 50 ms intervals. The resistive wire is 250 µm in diameter and the exposure settings were ISO 400 with 1.4 ms exposure time.

5. Conclusions

The surface modification of the BTMP fibres with the *in situ* synthesised layered double hydroxides via the low super saturation route in the system that applies Mg^{2+} and Al^{3+} nitrates and slow titration of NaOH, changes the fibre's surface morphology in sub-micron scale. The generated LDH particles are intergrown and active to adsorb sulphate containing aliphatic surfactant, thus, dramatically increasing the pulp fibres hydrophobic character. The pulp fibres can be functionalised with small organic molecules in an aqueous solvent, providing an alternative method to bind anionic substances on the fibres' surface.

The LDH particle nucleation on the fibres' surface was successfully conducted in aqueous medium by the low super saturated (*lss*), high super saturated (*hss*) and the slow urea hydrolysis (*Uhyd*) synthesis methods. In these synthesis procedures, the applied pulp fibres were acting as templates for nano- (70 nm), sub-micron (200 nm) and micron (>2 μm) size LDH particles, respectively. The i*n situ* nucleation of the LDH from the *hss* system with fully bleached Kraft pulp fibres in an autoclave, does not induce particle synthesis or migration into the fibre wall, even if the fibres are fully saturated and swollen in alkaline medium (pH = 10) at elevated temperature T = 120 °C. The synthesis via the *lss* route results in some particle migration into the fibre wall. Considerable particle nucleation inside the fibre wall was discovered with TEM after hydrothermally induced urea hydrolysis (*Uhyd*) that results in 50% reduction in bending compliance. The LDH that was bound to the fibres' external surface had a marginal effect on the fibres' flexibility.

Synthesis conditions were found to induce cellulose depolymerisation reactions. The LDH acts as a catalyst. The cellulose polymerisation degree followed each synthesis in the order: *hss* > *lss* > *Uhyd*. Utilizing a sequenced *in situ* particle synthesis via the urea hydrolysis and homogeneous co-precipitation, resulted in high mineral content (34 ± 2)% on the fibres' surface. The fines are prone to act as a substrate for the LDH nucleation and are favoured over fibres. The LDH provides a relatively dense structure that envelopes the fibres's outer cell wall. Synthesis of LDH at alkaline conditions liberates organic substances from the TMP fibres. Some of the compounds are re-deposited on the LDH surface.

Significant reduction in specific exothermic heat was observed after each synthesis route. The reduction in the cellulose polymer length influenced to the measured heat of combustion during the first exothermic reaction at around 320 °C. Influence of the LDH in enthalpy reduction was weight related. Carboxylic acids are created in higher relative amounts during the slow combustion in comparison to rapid temperature increase that produces diones, most likely, due to simultaneous removal of water and hydroxyls from the LDH. The effect is amplified by the particles in the fibre wall.

The LDH particles that were synthesised via the *lss* method had the highest capacity for sulphate containing probe molecules, while the better crystallised particles from the *hss* and the *Uhyd* had the highest affinity. Most of the acidic groups in the cellulose pulp fibres were free after LDH synthesis. The fibres had, therefore, become ampholytic after the modification.

Functionalisation of the hybrid fibres with SDS surfactant enhanced material plasticity in polypropylene composite and allowed homogeneous dispersion of pulp fibres in the polymer matrix. Functional BKraft fibres endured the applied shear forces better during compounding than the BTMP fibres. The particle cohesion forces were identified as the bottleneck in the process, while addition of the SDS surfactant seemed to promote particle matrix adhesion to a limited extent.

The flammability, production of soot and CO_2 production rates during the oxidative pyrolysis were significantly reduced by carbonate containing nano- and micron sized LDH particles. The *in situ* synthesised LDH particles slowed down the fibres' pyrolysis rate. The LDH appears to restrict the liberation of volatiles after the ignition slowing down the flame propagation as well. Charring was initiated at the interphase of nano-sized LDH and organic material that, in turn, amplifies the flame retardant effect. However, partial oxidation of fibres appears relatively rapid.

6. References

[1] Hänninen, R. & Sevola, Y. (ed.) (2009) *Metsäsektorin suhdannetiedote.* Helsinki: Metsäntutkimuskeskus http://www.metla.fi/julkaisut/suhdannekatsaus/tiedotteet/suhdannetiedote-28-5-2009.pdf

[2] *Progress book* (2014) Stora Enso annual report 2014, 12–17.

[3] Viitanen J. & Mutanen A. (2015) (ed.) *Metsäsektorin suhdannekatsaus.* Helsinki: Luonnonvarakeskus, 2015.

[4] http://www.metla.fi/metinfo/kestavyys/pdf/finlands-forests-facts-2015-small.pdf

[5] *More with Biofore* (2015) UPM Interim report *Q3* 2015, 6–8. http://www.upm.com/Aboutus/Newsroom/Releases/Pages/Interim-Report-Q32015-Momentum-for-improvement-continues-UPM-shows-improved-Q3-e-001-Tue-27-Oct-2015-09-42.aspx.

[6] Niemelä M. (2014) *Value from renewable raw materials*. Forward, Valmet's customer magazine 2014:1, 36–41.

[7] Helsingin Sanomat, 22.1.2016, Anni Lassila, Talous: *Metsäteollisuus investoi ahkerasti.* http://www.hs.fi/talous/a1453354107035.

[8] Back S. (2015) *Europas första pilotanläggning för nanokristallin cellulosa*. Svensk Pappers Tidning 2015:5. 34–35.

[9] Lockner M. (2015) *Lignin blir lättviktsmaterial och flygbränsle.* Svensk Pappers Tidning 2015:6, 34–35.

[10] Nova institute (2015) *Bio-based building blocks and polymers in the world. Capacities, Production and Applications: Status Quo and trends towards 2020*. 2015:4. http://www.bio-based.eu/markets/.

[11] Nova institute (2014) *Wood-Plastic Composites (WPC) and Natural Fibre Composites (NFC): European and Global Markets 2012 and Future Trends*. 2014:10. http://www.bio-based.eu/markets/.

[12] Timell, T.E. (1967) Wood Science and Technology 1, 45.

[13] Bentum, A.L.K. & Coté W.A. & Day, A.C. & Timell, T.E. (1969) Wood Science and Technology 3(3), 218.

[14] Coté W.A. & Day, A.C. & Timell, E.T. (1969) Wood Science and Technology 3, 257.

[15] Ilvessalo-Pfäffli, M.-S. (1977) *Puu ja sen kemia*. In: Jensen, W. (ed.) Suomen Paperi-insinööriyhdistyksen oppi- ja käsikirja, 2nd. ed., Turku, Teknillisten Tieteiden Akatemia, I Puukemia, pp. 28–29.

[16] Sirviö J. (2008) *Fibres and bonds.* In: Niskanen K. (ed.) Paper Physics*,* 2nd edition, Porvoo, Paperi ja Puu Oy, Papermaking Science and Technology 16, 62.

[17] Varhimo, A. & Sirviö, J. & Tuovinen, O. (2009) *Wood raw materials.* In: Lönnberg, B. (ed.) Mechanical Pulping, 2nd edition, Porvoo, Paperi ja Puu Oy, Papermaking Science and Technology 5, 90.

[18] Core, H.A. & Coté, W.A. & Day, A.C. (1979) Wood Structure and Identification, 2nd ed., Syracuse: Syracuse University Press.

[19] Barefoot, A.C. and Hankins F.W. (1982) Identification of modern and tertiary woods, Oxford (UK), Oxford University Press.

[20] Harada, H. & Coté, W.A. (1985) *Structure of Wood*. In: Higuschi, T (ed.) Biosynthesis and Biodegradation of Wood Components, London, Academic Press Inc., 22.

[21] Hakkila P. & Verkasalo, E. (2009) *Structure and properties of wood and woody biomass.* In: Kellomäki, S. (ed.) Forest Resources and Sustainable Management, 2nd ed., Porvoo, Paperi ja Puu Oy: Papermaking Science and Technology 2, p. 147.

[22] Sjöström, E. (1993) Wood Chemistry: Fundamentals and Applications. 2nd edition, San Diego, Academic Press Inc., pp. 63-68, 154, 249.

[23] Sundholm, J. & Lönnberg, B. (2009) History of Mechanical Pulping, In: Lönnberg, B. (ed.), *Mechanical Pulping,* 2nd edition, Porvoo, Paperi ja Puu Oy, Papermaking Science and Technology 5, 24-34.

[24] Pitkänen, M. & Mannström, M. & Lumiainen, J. & Lundin, T. (2009) *Thickening, storage and post-refining*, In: Lönnberg, B. (ed.), Mechanical Pulping*,* 2nd ed., Porvoo, Paperi ja Puu Oy: Papermaking Science and Technology 5, 400–417.

[25] Salmén, L. & Lucander, M. & Härkönen, E. & Sundholm, J. (2009) *Fundamentals of mechanical pulping.* In: Lönnberg, B. (ed.), Mechanical Pulping*,* 2nd edition, Porvoo, Paperi ja Puu Oy, Papermaking Science and Technology 5, 36–61.

[26] Pauler, N. (2008) *Paper Optics.* In: Niskanen, K. (ed.) Paper Physics, 2nd ed., Porvoo, Paperi ja Puu Oy: Paper Making Science and Technology 16, 160.

[27] Fernando, D. & Daniel, G. (2004) Nordic Pulp and Paper Research Journal 19(3), 278.

[28] Gustafsson, J. (2011) *Pulping*, In: Fardim .P (ed.) Chemical Pulping Part 1, Fibre Chemistry and Technology, 2nd ed., Porvoo, Paperi ja Puu Oy: Papermaking Science and Technology 6, 203.

[29] Gierer, J. (1970) *The reactions of lignin during pulping,* Svensk Pappers Tidning, 18, 571-595.

[30] Lachenal, D. & Benattar, N. & Allix, M. & Marlin, N. & Chirat, C. (2005) Proceedings of 13th ISWEPC, Auckland, New Zealand, May 16-19, 2005 Proceedings Vol. 2, pp. 23-27.

[31] Ojala T. (1999) *Chemical bonds in papermaking*. In: Neimo L. (ed.) Papermaking Chemistry, Jyväskylä, Fapet Oy, Papermaking Science and Technology 4, 31.

[32] Sixta, H. & Potthast, A. & Krotschek, A.W. (2006) *Chemical Pulping Process*. In: Sixta, H. (ed.) Handbook of Pulp, Weinheim, WILEY-VCH Verlag GmbH & Co., pp. 110, 127.

[33] Panshin, A. J. & de Zeeuw, C. (1980) *Textbook of wood technology: structure, identification, properties and uses of the commercial woods of the United States and Canada*, New York: McGraw Hill Book Company.

[34] Cave, L.D. & Hutt, L. (1969) Wood Science and Technology 3, 40.

[35] Page, D.H. & El-Hosseiny, F. & Winkler, K. & Lancaster, A.P.S. (1977) Tappi Journal 60(4), 114.

[36] Ping, X. & Huawu, L. (2004) Wood Science and Technology 38, 363.

[37] Gassan, J. & Chate, A. & Bledzki, A.K. (2001) Journal of Materials Science 36, 3715.

[38] Courchene, C.E. & Peter, G.F. & Litvay, J. (2006) Wood and Fiber Science 38, 112.

[39] Willför, S. & Alén, R. & van Dam, J. & Liu, Z. & Tähtinen, M. (2011) *Raw materials.* In: Fardim, P. (ed.) Chemical Pulping Part 1, 2nd edition, Porvoo, Paperi ja Puu Oy, Papermaking Science and Technology 6, 50-51.

[40] Antonsson, S. & Henriksson, G. & Lindstöm, M.E. (2009) Nordic Pulp and Paper Research Journal 24(4), 403.

[41] Molin, U. & Teder, A. (2002) Nordic Pulp and Paper Research Journal 17(1), 14.

[42] Willför, S. & Sundberg, A., & Hemming, J. & Holmbom, B (2005) Wood Science and Technology 39, 245.

[43] Willför, S. & Sundberg, A., & Hemming, J. & Holmbom, B (2005) Wood Science and Technology 39, 601.

[44] De Grâce, J.H. & Page, D.H. (1976) Tappi Journal 59(7), 98.

[45] Page, D.H. & Seth, R.S. (1980) Tappi Journal 63(10), 99

[46] Mannström B. (1977) Mekaanisten massojen valmistus. In: Jensen W. (ed.) Suomen Paperi-insinööriyhdistyksen oppi- ja käsikirja, 2nd. ed., Turku, Teknillisten Tieteiden Akatemia, I Puukemia, p. 281.

[47] Åkerholm, M. & Salmén L. (2003) Holzforschung 57(5), 459.

[48] Ketoja, J. (2008) *Rheology*. In: Niskanen, K. (ed.) Paper Physics, 2nd ed., Porvoo, Paperi ja Puu Oy: Paper Making Science and Technology 16, 298.

[49] Norström, B. (2014) Nordic Pulp and Paper Research Journal 29(3), 462.

[50] Obst, J.R. (1982) Tappi Journal 64(4), 109.

[51] Lewoko, M. & Henriksson, G. & Gellerstedt, G. (2005) Biomacromolecules 6(6), 3467.

[52] Olsson, A.-M. & Salmén, L. (1997) Nordic Pulp and Paper Research Journal 12(3), 140.

[53] Salmén, L (2015), Annals of Forest Science 72, 679.

[54] Molin, U. & Teder, A. (2002) Nordic Pulp and Paper Research Journal 17(1), 14.

[55] Dahlman, O. & Jacobs, A. & Liljenberg, A. & Olsson, A.I. (2000) Journal of Chromatography A 891, 157.

[56] Sixta, H. (2006) *Pulp Properties and Applications*. In: Sixta, H. (ed.) Handbook of Pulp, Weinheim, WILEY-VCH Verlag GmbH & Co., pp. 1013, 1016.

[57] Buchert, J. & Tenkanen, M. & Tamminen, T. (2001) Tappi Journal 84(4), 70.

[58] Fardim, P. & Holmbom, B. (2005) Colloids and Surfaces A: Physicochemical and Engineering Aspects 252(2-3), 237.

[59] Chirat, C. & Hostachy, J.-C. & Paloniemi, J. & Pelin, K. & Pohjanvesi, S. & Nordén, S. & Vesala, R. & Wennerström, M. (2011) *Bleaching*. In: Fardim P. (ed.) Chemical Pulping Part 1: Fibre Chemistry and Technology, 2nd ed., Porvoo, Paperi ja Puu Oy: Papermaking Science and Technology 6, p. 461.

[60] Holmbom, B. & Pranovich, A.V. & Sundberg, A. & Buchert, J. (2000) *Charged groups in wood and mechanical pulps*. In: Kennedy, J.F. & Phillips, G.O. & Williams, P.A. (ed.) Cellulosic pulps, fibres and materials, Cambridge, Woodhead Publishing, Ltd., pp. 109-119.

[61] Pranovich, A.V. & Sundberg, K.E. & Holmbom, B. R. (2003) Journal of Wood Chemistry and Technology 23(1), 89.

[62] Koljonen, K. & Mustaranta, A. & Stenius, P. (2004) Nordic Pulp and Paper Research Journal 19(4), 495.

[63] Lyytikäinen, K. & Saukkonen, E. & Kajanto, I. & Käyhkö, J. (2011) BioResources 6(1), 219.

[64] Fardim, P. & Holmbom, B. (2003) TAPPI Journal 2(10), 28.

[65] Fardim, P. & Holmbom, B. & Ivaska, A. & Karhu, J. & Mortha, G. & Laine, J. (2002) Nordic Pulp & Paper Research Journal 17(3), 346.

[66] Fardim, P. & Moreno, T. & Holmbom, B. (2005) Journal of Colloid and Interface Science 290(2), 383.

[67] Barzyk, D. & Page, D. & Ragauskas, A. (1997) Journal of Pulp & Paper Science 23, J59.

[68] Laine, J. & Stenius, P. (1997) Paperi ja Puu 79(4), 257.

[69] Susilo, R. & Chandraghatgi, R. & Li, X.S. & Englezos, P. (2005) Canadian Journal of Chemical Engineering 83, 537.

[70] Sundman, O. & Öhman, L.O. (2006) Nordic Pulp & Paper Research Journal 21, 372.

[71] Suurnäkki, A. & Li, T.-Q. & Buchert, J. & Tenkanen, M. & Viikari, L. & Vuorinen, T. & Ödberg, L. (1997) Holzforschung 51(1), 27.

[72] Andreasson, B. & Forsström, J. & Wågberg, L. (2003) Cellulose 10, 111.

[73] Laine, C. & Wang, X. & Tenkanen, M. & Varhimo, A. (2005) Holzforschung 58(3), 233.

[74] Köpcke, V. & Ibarra, D. & Ek, M. (2008) Nordic Pulp and Paper Research Journal 23(4), 363.

[75] Hänninen, T. & Thygese, A. & Mahmood, S. & Madsen, B. & Hyghes, M. (2012) Industrial Crops and Products 39, 7.

[76] Stone, J.; Scallan, A. (1968) Pulp & Paper Magazine of Canada 69, T288.

[77] Stone, J.; Scallan, A. (1968) Cellulose Chemistry and Technology 2, 343.

[78] Alince, B. (2002) Nordic Pulp and Paper Research Journal 17(1), 71.

[79] Maloney, T.C. (2000) Acta Polytechnica Sandicavica, vol. 275, pp. 1-52.

[80] Maloney, T.C. & Paulapuro, H. (1999) Journal of Pulp and Paper Science 25, 430.

[81] Pönni, R. & Kontturi, E. & Vuoringn, T. (2014) Carbohydrate Polymers 93(2), 424.

[82] Grönqvist, S. & Hakala, T.K. & Kamppuri, T. & Vehviläinen, M. & Hänninen, T. & Liitiä, T. & Maloney, T. & Suurnäkki, A. (2014) Cellulose 21, 3667.

[83] Andreasson, B. & Forsström, J. & Wågberg, L. (2005) Cellulose 12, 253.

[84] Inushima, T. & Tanaka, K. & Yano, S. & Moriya, K. & Sato, Y. & Honda, K. (2003) Japanese patent: JP 2003119689.

[85] Sigworth, W.D. & Cheney, R.A. & Panzer, L.M. & Mei, H.L. (2004) US patent: US 20040072924

[86] Sigworth, W.D. (2005) Polyolefins, the International Conference on Polyolefins: The Challenges of Globalization, Houston, TX, United States, Feb. 27-Mar. 2, 2005, 052/1-052/11.

[87] Granberg, H. & Coppel, L.G. & Eita, M. & de Mayolo, E.A. & Arwin, H. & Wågberg, L. (2012) Nordic Pulp and Paper Research Journal 27(2), 496.

[88] Grigoray, O. & Wondraczek , H. & Heikkilä, E. & Fardim, P. & Heinze, T. (2014) Carbohydrate Polymers 111, 280.

[89] Pykönen, M. & Sundqvist, H. & Tuominen, M. & Lahti, J. & Prston, J. & Fardim, P. & Toivakka, M. (2008) Nordic Pulp and Paper Research Journal 23(2), 181.

[90] Pykönen, M. & Silvaani, H. & Preston, J. & Fardim, P. & Toivakka, M. (2010) Nordic Pulp and Paper Research Journal 25(1), 93.

[91] Henriksson, M. & Berglund, L.A. & Isaksson, P. & Lindström, T. & Nishino, T. (2008) European Polymer Journal 43, 3434.

[92] Yoo, S. & Hsieh, J.S. (2010) Industrial & Engineering Chemistry Research 49(5), 2161.

[93] He, J. & Kunitake, T. & Nakao, A. (2003) Chemistry of Materials 15(23), 4401.

[94] Bogana, M.P. & Bottani, C.E. & Dellasega, D. & Di Fonzo, F. & Facibeni, A. (2008) Italian patent: IT 2008MI0792 & United States patent: US 20110110999.

[95] Castellanos, L.J. & Blanco-Tirado, C. & Hinestroza, J.P. & Combariza, M.Y. (2012) Cellulose 19, 1933.

[96] Chowdhury, M.N.K. & Beg, M.D.H. & Khan, M.R. & Mina, M.F. (2013) Materials Letters 98, 26.

[97] Ovalle-Serrano, S.A. & Carrillo, V.S. & Blanco-Tirado, C. & Hinestroza, J.P. & Combariza, M. Y. (2015) Cellulose 22(3), 1841.

[98] Lehtinen, E. & Paltakari, J. (2009) *Coating materials–general*, In: Paltakari, J. (ed.) Pigment Coating and Surface Sizing of Paper, 2nd ed., Jyväskylä, Paper ja Puu Oy: Papermaking Science and Technology 11, 62.

[99] Bruun, S.-E. & Schmidt-Thümmes, J. & Lawrenz, D. & Kröner, H. (2009) *Pigments* In: Paltakari, J. (ed.) Pigment Coating and Surface Sizing of Paper, 2nd ed., Jyväskylä, Paper ja Puu Oy: Papermaking Science and Technology 11, pp. 192-223.

[100] Husband, J. & Gane, P.A.C. & Gantenbain, D. & Aarni, E. & Turkki, T. & Imppola, O. & Kermis, T.W. & Brown, J.T. & Healy, D.V. & Kramer, K. & Alatalo, M. & Haikkilä, K. (2009) *Pigments* In: Paltakari, J. (ed.) Pigment Coating and Surface Sizing of Paper, 2nd ed., Jyväskylä, Paper ja Puu Oy: Papermaking Science and Technology 11, pp. 93, 106, 145.

[101] Graig, W.L. (1952) *Production of pigmented cellulosic pulps*. US patent: 2583548

[102] Green, H.V. & Fox, T.J. & Scallan, A.M. (1985) *Lumen-loaded paper pulp, its production and use.* US patent: US4510020 A

[103] Klungness, J.H. & Caulifield, D.F. & Sachs, I.B. & Sykes, M.S. & Tan, F. & Shilts, R.W. (1993) *Method for fiber loading a chemical compound.* US patent: US 5223090 A.

[104] Joisson, D. & Richard, C. & Schohn, G. & Schu, C. (2004) Method for fixing a mineral filler on cellulosic fibers and method for making a sheet of paper. US patent: US6706148.

[105] Hess, H. & Katzenmeier, T. (2008) Method for loading fibres in a fibrous suspension with calcium carbonate formed from (hydrogen)carbonate compounds. World patent: WO2008131820 A1

[106] Allan, G.G. & Carrol, J.P. & Negri, A.R. & Raghuraman, M. & Ritsenthaler, P. & Yahiaoui, A. (1992) Tappi Journal 1, 175.

[107] Merk, V. & Chanana, M. & Keplinger, T. & Gaan, S. & Burgert, I. (2015) Green Chemistry 17, 1423.

[108] Koch, M. & Jonscher, G. & Renker, S. (2007) Prepared in situ nanoparticles ZnO, World patent WO 2007134712.

[109] Endesfelder, A. & Pereira, E. & Burger, M. & Binder, J. (2009) Wood or wood fiber laminate with top paper layer impregnated by aminoplast with surface-modified silica nanoparticles, World patent: WO2009133144.

[110] Braun, R. & Gier, A. & Hasch, J. (2012) Hybrid adhesive and use of same in wooden boards, World patent: WO2012055791.

[111] Johnston, J.W. & Townsend, D. F. & Hagiopol, C. & Talbert, L.D. & Ruffner, C.G. (2014) *Improved oil repellency paper prepared by treatment with aqueous dispersion of surface modified nanoparticles.* World patent: WO 2014059118.

[112] He, J. & Kunitake, T. & Nakao, A. (2003) Chemistry of Materials 15(23), 4401.

[113] Dong, H. & Hinestroza, J.P. (2009) ACS Applied Materials & Interfaces 1(4), 797.

[114] Small, A.C. & Johnston, J.H. (2009) Journal of Colloid and Interface Science 331(1), 122.

[115] Chia, C.H. & Zakaria, S. & Nguyen, K.L. & Abdullah, M. (2008) Industrial Crops and Products 28, 333.

[116] Wu, W.-B. & Jing, Y. & Gong, M.-R. & Zhou, X.-F. & Dai, H.-Q. (2011) BioResources 6(3), 3396.

[117] Phillips, W. (1844) An Elementary Treatise on Mineralogy, Boston, MA, William D. Ticknor & Co., 134.

[118] Rammelsberg C. (1856) Philosophical Magazine, Series 4 11:73, 405.

[119] Foshag, W.F (1920) Journal of the Chemical Society, Abstracts 118, ii765.

[120] Frondel, C. (1941) Journal of the Mineralogical Society of America 26:5, 295.

[121] Hermann, R. (1849) Journal of Practical Chemistry 46, 257.

[122] Dana, J.D. (1851) American Journal of Science 12, 365.

[123] Manasse, E. (1915) Atti della Società Toscana di Scienze Naturali, Processi Verbali 24, 92.

[124] Foshag, W.F. (1921) Proceedings of the United States National Museum 58, 147-153.

[125] Allmann, R. (1968) Acta Crystallographica B 24, 972.

[126] Taylor, H.F.W. (1969) Mineralogical Magazine 37, 338.

[127] Taylor, H.F.W. (1973) Mineralogical Magazine 39, 377.

[128] Marchi & Apesteguía (1998) Applied Clay Science 13(1), 35.

[129] Das, N.N. & Das, R. (2010) Reaction Kinetic, Mechanisms and Catalysis 99, 397.

[130] Mills, S.J. & Christy, A.G. & Génin, J.-M.R. & Kameda, T. & Colombo, F. (2012) Mineralogical Magazine 76:5, 1289.

[131] Williams, G.R. & Crowder, J. & Burley, J.C. & Fogg, A.M. (2012) Journal of Materials Chemistry 22, 13600.

[132] Meyn, M. & Beneke, K. & Lagaly, G. (1993) Inorganic Chemistry 32, 1209.

[133] Krivovichev, S.V. & Yakovenchuk, V.N. & Zhitova, E.S. & Zolotarev, A.A. & Pahkomovsky, Y.A. & Ivanyuk, G. Yu (2010) Mineralogical Magazine 74:5, 821.

[134] Wang, Y. & Wu, P. & Li, Y. & Zhu, N. & Dang, Z. (2013) Journal of Colloid and Interface Science 394, 564.

[135] Bookin, A.S. & Drits, V.A. (1993) Clays and Clay Minerals 41(5), 551.

[136] Bookin, A.S. & Cherkashin, V.I. & Dtirs, V.A. (1993) Clays and Clay Minerals 41(5), 558.

[137] Bellotto, M. & Rebours, B. & Clause, O. & Lynch, J. & Bazin, D. & Elkaïm, E. (1996) Journal of Physical Chemistry 100(20), 8527.

[138] Bourrié, G. & Trolard, F. & Refait, P. & Feder, F. (2004) Clays and Clay Minerals 52(3), 382.

[139] Evans, D.G. & Slade, R.C.T. (2006) *Structural Aspects of Layered Double Hydroxides*, In: Duan, X. & Evans, D.G. (ed.) Layered Double Hydroxides, Heidelberg: Springer-Verlag: Structure and Bonding 119, pp. 6, 22-23, 32.

[140] López-Salinas, E. & Garica-Sánches, M. & Montoya, J.A. & Acosta, D.R. & Abasolo, J.A. & Schifter I. (1997) Langmuir 13(17), 4748.

[141] Legrand, L. & Abdelmoula, M. & Génin, A. & Chaussé, A. & Génin, J.-M.R. (2001) Electrochimica Acta 46(12), 1815.

[142] Xu, Z.P. & Zeng, H.C. (2001) Journal of Physical Chemistry B 105, 1743.

[143] Shivaramaiah, R. & Navrotsky, A. (2015) Inorganic Chemistry 54, 3253.

[144] Newman, S.P. & Jones, W. & O'Connor, P. & Stamires, D.N. (2002) Journal of Materials Chemsitry 12, 153.

[145] Guerlou-Demourgues, L. & Delmas, C. (1994) Journal of Power Sources 52(2), 269.

[146] Guerlou-Demourgues, L. & Delmas, C. (1994) Journal of Power Sources 52(2), 275.

[147] Kukkadapu, R.K. & Witkowski, M.S. & Amonette, J.E. (1997) Chemistry of Materials 9(2), 417.

[148] Kaneyoshi, M. & Jones, W. (1998) Chemical Physics Letters, 296(1-2), 183.

[149] Vaysse, C. & Guerlou-Demourgues, L. & Demourgues, A. & Lazartigues, F. & Fertier, D. & Delmas, C. (2002) Journal of Materials Chemistry 12, 1035.

[150] Costa, D.G. & Rocha, A.B. & Diniz, R. & Souza, W.F. & Chiaro S.S.X. & Leitão A.A. (2010) Journal of Physical Chemistry C 114, 14133.

[151] Tredwell, W.D. & Bernasconi, E (1930) Helvetica Chmica Acta 13, 500.

[152] Turner, R.C. & Brydon, J.E. (1962) Science 136, 1052.

[153] Johnson, C.A & Glasser, F.P. (2003) Clays and Clay Minerals 51, 1.

[154] Boclair, J.W. & Braterman, P.S. (1999) Chemistry of Materials 11(2), 298.

[155] Boclair, J.W. & Braterman, P.S. (1998) Chemistry of Materials 10(8), 2050.

[156] Dean, J. A. (1999) *Lange's Handbook of Chemistry*, 15th ed., New York: McGraw-Hill, section 8.2.

[157] Miyata, S. (1983) Clays and Clay Minerals 31, 305.

[158] Parker, L.M. & Milestone, N.B. & Newman, R.H. (1995) Industrial & Engineering Chemical Research 34, 1196.

[159] Châtelet, L. & Bottero, J.Y. & Yvon, J. & Bouchelaghem, A. (1996) Colloids and Surfaces 111, 167.

[160] Ulibarri, M.Á. & Hermosín M.C. (2001) Layered Double Hydroxides in Water Decontamination. In: Rives, V. (ed.) *Layered Double Hydroxides: Present and Future*, Nova Science Publishers, New York, p. 288.

[161] Prasad, B.E. & Kamath, P.V. & Vijayamohanan, K. (2011) Langmuir 27, 13539.

[162] Manohara, G.V. & Kunz, D.A. & Kamath, P.V. & Milius, W. & Breu, J. (2010) Langmuir 26(19), 15586.

[163] Kumar, P.P. & Kalinichev, A.G. & Kirkpatrick, J. (2006) The Journal of Physical Chemsitry B 110, 3841.

[164] Hou, X.W. & Bish, D.L. & Wang, S.L. & Johnston, C.T. & Kirkpatrick, R.J. (2003) American Mineralogist 88, 167.

[165] Li, Q. & Kirkpatrick, J. (2007) American Mineralogist 92(2-3), 397.

[166] Marappa, S. & Radha, S. & Kamath, P.V. (2013) European Journal of Inorganic Chemistry 2122.

[167] Trave, A. & Selloni, A. & Goursot, A. & Tichit, D. & Weber, J. (2002) Journal of Physical Chemistry B. 106, 12291.

[168] Cuautli, C. & Ireta, J. (2015) The Journal of Chemical Physics, 142(9) http://scitation.aip.org/content/aip/journal/jcp/142/9/10.1063/1.4913570

[169] Bravo-Suárez, J.J. & Páez-Mozo, E.A. & Oyama, S.T. (2004) Quimica Nova 27(4), 574.

[170] Bravo-Suárez, J.J. & Páez-Mozo, E.A. & Oyama, S.T. (2004) Quimica Nova 27(4), 601.

[171] Mazeina, L. & Navrotsky, A. & Dyar, D. (2008) Geochimica & Cosmochimica Acta 72, 1143.

[172] Allada, R. & Navrotsky, A. & Berbeco, H. T. & Casey, W.H. (2002) Science 296, 721.

[173] Allada, R. & Pless, J.D. & Nenoff, T.M. & Navrotsky, A. (2005) Chemistry of Materials 17, 2455.

[174] Allada, R. & Peltier, E. & Navrotsky, A. & Casey, W.H. & Johnson, C.A. & Berbeco, H.T. & Sparks, D.L. (2006) Clays and Clay Minerals 54(4), 409.

[175] Miyata, S. (1980) Clays and Clay Minerals 28, 50.

[176] Theiss, F.L. & Ayoko, G.A. & Frost, R.L. (2013) Journal of Thermal Analysis and Calorimetry 112, 649.

[177] Rebours B. & dEspinoze de la Caillerie, J.-B. & Clause O. (1994) Journal of American Chemical Society 116, 1707.

[178] Costa, D.G. & Rocha, A. B. & Souza, W.F. & Chiaro, S.S.X. & Leitão, A.A. (2012) Journal of Physical Chemistry C 116, 13679.

[179] Leroux, F. & Besse, J.-P. (2001) Chemistry of Materials 13, 3507.

[180] Li, M. & Zhu, J.E. & Zhang, L. & Chen, X. & Zhang, H. & Zhang, F. & Xu, S. & Evans, D.G. (2011) Nanoscale 3(10), 4240.

[181] Kim, M.H. & Park, D.-H. & Yang, J.-H. & Choy, Y.B. & Choy, J.-H. (2013) International Journal of Pharmaceutics 444(1–2), 120.

[182] He, J. & Wei, M. & Li, B. & Kang, Y. & Evans, D.G. & Duan, X. (2006) *Preparation of Layered Double Hydroxides.* In: Duan, X. & Evans, D.G. (ed.) Layered Double Hydroxides, Heidelberg: Springer-Verlag: Structure and Bonding 119, pp. 89–119.

[183] Zhao, Y. & Li, F. & Zhang, R. & Evans, D.G. & Duan, X. (2002) Chemistry of Materials 14, 4286.

[184] Feng, Y. & Li, D. & Li, C. & Wang, Z. & Evans, D.G. & Duan, X. (2003) Clays and Clay Minerals 51, 566.

[185] Guo, S. & Li, D. & Zhang, W. & Pu, M. & Evans, D.G. & Duan, X. (2004) Journal of Solid State Chemistry 177, 4597.

[186] Songlin, W. & Shuyang, S. (2010) Qingdao Keji Daxue Xuebao, Ziran Kexueban 31(2), 2010 ,148-152

[187] Guodong, L. & Wenxia, L. (2010) Zhonghua Zhiye 31(10), 48.

[188] Songlin, W. & Jianlin, H. & Fushan, C. (2012) BioResources 7(1), 997.

[189] Schmidt, B. & Katiyar, V. & Plackett, D. & Larsen, E.H. & Gerds, N. & Koch, C. B. & Petersen, J. H. (2011) Food Additives & Contaminants, Part A: Chemistry, Analysis, Control, Exposure & Risk Assessment 28(7), 956.

[190] Dou, Y. & Xu, S. & Liu, X. & Han, J. & Yan, H. & Wei, M. & Evans, D.G. & Duan, X. (2014) Advanced Functional Materials 24(4), 514.

[191] Venderbosch, R.A.M. & Verlaan-Hooft, H.P.M. & Verlaan, J.P.J. & Talma, A.G. & Overbeek, R. *Layered double hydroxide-containing polymer compositions and applications*. World patent: WO 2010066642 A1.

[192] Winters, R. & Schomaker, E. & De Vos, S.C. (2009) *Production of filler-containing polymer compositions*. World patent: WO2009112441 A1

[193] Venderbosch, R.A. & Verlaan-Hooft, H.P. & Verlaan, J.P. & Talma, A.G. & Van Overbeek, R. (2010) International patent PCT/EP2009/066392. pp. 14–15.

[194] Lu, J. & Yan, D. & Wei, M. & Duan, X. (2010) CN 101775281 A (2010)

[195] Koehler, K. & Thiefes, A. & Tarrach, K. (2010) *Deep layered filters containing inorganic layered double hydroxides for purification of biological materials.* World patent: WO 2010017964 A1.

[196] Koehler, K. & Thiefes, A. & Tarrach, K. (2010) WO 2010017964 A1

[197] Tokarz, M. & Nilsson, J. (2007) Cellulosic product and process for its production. US patent: US 7303654.

[198] Mandal, S. & Mayadevi, S. (2008) Chemosphere 72, 995.

[199] Jun, L. & Dongpeng, Y. & Wei, M. & Duan, X. (2009) Method for preparing pressure-sensitive fluorescent color-changing material with intercalation structure from fluorescent bleaching agent 357 and hydrotalcite. Chinese patent: CN 101974323 A

[200] Wang, S. & Chen, F. (2011) Advanced Material Researh 174, 362.

[201] Beckham, G.T. & Biddy, M.J. & Chmely, S.C. & Sturgeon, M. (2014) US 201401073 A1 (2014)

[202] Möhmel, S. & Kurzawski, I. & Uecker, D. & Müller, D. & Geßner, W. (2002) Crystal Research and Technology 37, 359.

[203] Ditmars, D.A. (1990) Journal of Chemical Thermodynamics 22, 639.

[204] Zahra, C. & Zahra, A.M. (1996) Thermochimica Acta 276, 161.

[205] Stølen, S. & Grønvold, F. (1999) Thermochimica Acta 327,1

[206] Saketi, P. & Treimanis, A. & Fardim, P. & Ronkanen, P. & Kallio, P. (2010) Microrobotic Platform for Manipulation and Flexibility Measurement of Individual Paper Fibres. In: Proceedings of the IEEE/RSJ International Conference on Intelligent Robots and Systems, Taipei, Taiwan, 18–22 October 2010, pp. 5764–5766.

[207] Martin, A. (1951) Tappi Journal 34, 363

[208] Guo, X. & Zhang, F. & Evans, D.G. & Duan, X. (2010) Chemical Communications 46, 5197.

[209] Hänninen, T. (2011) *Studies on the ultrastructure of natural fibres and its effects on the fibre utilization*. Doctoral Dissertations 116/2011, Aalto University, School of Chemical Technology, Department of Forest Products Technology, Wood Chemistry, Unigrafia Oy, Helsinki, p. 40.

[210] Sirviö, J. & Nurminen, I. (2004) Pulp and Paper Canada, 105:8, T193.

[211] Gellerstedt, F. & Wågberg, L. & Gatenholm, P. (2000) Cellulose 7, 67.

[212] Benítez-Guerrero, M. & López-Beceiro, J. & Sánches-Jiménez, P.E. & Pascual-Cosp, J. (2014) Thermochimica Acta 581, 70.

[213] Socrates, G. Infrared and Raman Characteristic Group Frequencies, 3rd ed.; John Wiley & Sons, LTD: Chichester, SXW, England 2004.

[214] Lojewska, J. & Miskowiec, P. & Lojewski, T. &Proniewicz, L.M. (2005) Polymer Degradation & Stability 88, 512.

[215] Whiting, P. & Favis, B.D. & St. Germain, F.G.T. & Goring, D.A.I. (1981) Journal of Wood Chemistry and Technology 1, 29.

[216] Barré, S. & Chotard, T. & Benzeggagh, L. (1996) Composites Part A: Applied Science and Manufacturing 27A, 1169.

[217] Shen, C.H. & Springer, G.S. (1976) Journal of Composite Materials 10, 2.

[218] Zhou, J. & Lucas, J.P. (1995) Composites Science and Technology 53, 57.

[219] Kuang-Chung, T. and Drysdale, D. (2002) *Using cone calorimeter data for the prediction of fire* hazard. Fire Safety Journal 37: 697 – 706.

[220] Schartel, B. and Hull, T.R. (2007) Development of fire-retarded materials – Interpretation of cone calorimeter data. Fire and Materials 31: 327 – 354.

[221] Schartel, B.; Bartholomai, M. and Knoll, U. (2005) Some comments on the use of cone calorimeter data. Polymer Degradation and Stability 88: 540 – 547.

[222] Petrella, R.V. (1992). *The assessment of full-scale fire hazards from cone calorimeter data.* Journal of Fire Science 12(1): 14 – 43.

[223] Wang, M.; Wang, X.: Li, L. and Ji, H. (2014) *Fire Performance of Plywood Treated with Ammonium Polyphosphate and 4A Zeolite*. BioResources 9(3): 4934 – 4945.

[224] Lange, C.-E.; Lastusaari, M.; Reza, M.; Latifi, S.K.; Kallio, P. and Fardim, P. (2015) *In situ Hybridization of Pulp Fibres Using Mg-Al Layered Double Hydroxides*. Fibers 3(2): 103 – 133.

[225] Derkacheva, O. and Sukhov, D. (2008) *Investigation of Lignins by FTIR Spectroscopy*. Macromolecular Symposia 265: 61 – 68.

Carl-Erik Lange

Hybridisation of pulp fibres with LDH for applications in composites and lightweight fibrous foam

Fibre and cellulose technology

The dissertation concentrates on the pulp fibres that are hybridised with Layered Double Hydroxide (LDH) minerals in aqueous medium. The effects of LDH on pulp fibres' surface are studied by applying the hybrid fibres in thermoplastic composite and in lightweight fibrous foam. The chemical and physical properties of the prepared materials are discussed.

Åbo Akademi University Press | ISBN 978-952-12-3571-9